Earth-Science Reviews 238 (2023) 104336

Contents lists available at ScienceDirect

Earth-Science Reviews

journal homepage: www.elsevier.com/locate/earscirev

A dynamic 2000—540 Ma Earth history: From cratonic amalgamation to the age of supercontinent cycle

Zheng-Xiang Li [a,*], Yebo Liu [a,*], Richard Ernst [b]

[a] Earth Dynamics Research Group, School of Earth and Planetary Sciences, The Institute for Geoscience Research, Curtin University, GPO Box U1987, Perth, WA 6845, Australia

[b] Department of Earth Sciences, Carleton University, Ottawa, ON K1S 5B6, Canada

ARTICLE INFO

Keywords:
Full-plate reconstruction
Nuna
Rodinia
Supercontinent
Geodynamics
True polar wander
LLSVP
Subduction girdle
Superocean

ABSTRACT

Establishing how tectonic plates have moved since deep time is essential for understanding how Earth's geodynamic system has evolved and operates, thus answering longstanding questions such as what "drives" plate tectonics. Such knowledge is a key component of Earth System science, and has implications for wide ranging fields from core-mantle-crust interaction and evolution, geotectonic phenomena such as mountain building and magmatic and basin histories, the episodic formation and preservation of Earth resources, to global sea-level changes, climatic evolution, atmospheric oxygenation, and even the evolution of life. In this paper, we take advantage of the rapidly improving database and knowledge about the Precambrian world, and the conceptual breakthroughs, both regarding the presence of a supercontinent cycle and possible dynamic coupling between the supercontinent cycle and mantle dynamics, in order to establish a full-plate global reconstruction from 540 Ma back to 2000 Ma. We utilise a variety of global geotectonic databases to constrain our reconstruction, and use palaeomagnetically recorded true polar wander events and global plume records to help evaluate competing geodynamic models and also provide new constraints on the absolute longitude of continents and supercontinents. After revising the configuration and life span of both supercontinents Nuna (1600—1300 Ma) and Rodinia (900—720 Ma), we present a 2000—540 Ma animation, starting from the rapid assembly of large cratons and supercratons (or megacontinents) between 2000 Ma and 1800 Ma. This occurred after a billion years of dominance by small cratons, and kick-started the ensuing Nuna and Rodinia supercontinent cycles and the emergence of stable, hemisphere-scale (long-wavelength) degree-1/degree-2 mantle structures. We further use the geodynamicly-defined type-1 and type-2 inertia interchange true polar wander (IITPW) events, which likely occurred during Nuna (type-1) and Rodinia (type-2) times as shown by the palaeomagnetic record, to argue that Nuna assembled at about the same longitude as the latest supercontinent Pangaea (320—170 Ma), whereas Rodinia formed through introversion assembly over the legacy Nuna subduction girdle either ca. 90° to the west (our slightly preferred model) or to the east before the migrated subduction girdle surrounding it generated its own degree-2 mantle structure by ca. 780 Ma. Our interpretation is broadly consistent with the global LIP record. Using TPW and LIP observations and geodynamic model predictions, we further argue that the Phanerozoic supercontinent Pangaea assembled through extroversion on a legacy Rodinia subduction girdle with a geographic centre at around 0°E longitude before the formation of its own degree-2 mantle structure by ca. 250 Ma, the legacy of which is still present in present-day mantle.

1. Introduction

Establishing plausible global tectonic reconstructions is important for understanding the occurrence of a whole range of geotectonic phenomena including mountain building, magmatic and basin histories, and the related formation and preservation of Earth resources (Pehrsson et al., 2016). Such work also set the framework for Earth System studies such as global sea-level changes (Müller et al., 2013), climatic evolution (e.g., extreme climatic events such as Snowball Earth during Earth history; Cox et al., 2016; Hoffman et al., 1998; Li et al., 2004; Pu et al., 2022; Worsley and Kidder, 1991), atmospheric oxygenation (e.g., Campbell and Allen, 2008; Zhu et al., 2022), and the evolution of life

* Corresponding authors.
E-mail addresses: z.li@curtin.edu.au, zlicurtin@gmail.com (Z.-X. Li), yebo.liu@curtin.edu.au (Y. Liu).

https://doi.org/10.1016/j.earscirev.2023.104336
Received 7 July 2022; Received in revised form 26 January 2023; Accepted 27 January 2023
Available online 5 February 2023

(McMenamin and McMenamin, 1990). An advanced understanding of how tectonic plates have moved since deep time is also essential for understanding how Earth's geodynamic system has evolved and interacted with the plate tectonic system, i.e., the longstanding question of what "drives" plate tectonics (Anderson, 2001; Forsyth and Uyeda, 1975; Conrad and Lithgow-Bertelloni, 2004).

The recognition of the possible occurrence of a Precambrian supercontinent over 40 years ago (Bell and Jefferson, 1987; McMenamin and McMenamin, 1990; Nance et al., 1988) and subsequent rapid developments in the reconstruction of both the Neoproterozoic supercontinent Rodinia (e.g., Dalziel, 1991; Hoffman, 1991; Li et al., 2008a; Moores, 1991) and the Paleo-(?) to Mesoproterozoic supercontinent Nuna/Columbia (Evans and Mitchell, 2011; Meert, 2002; Pisarevsky et al., 2014a; Rogers and Santosh, 2002; Zhang et al., 2012b; Zhao et al., 2002) brought an explosion of knowledge in Precambrian geotectonic and palaeogeographic evolution. In particular, the rapid realisation of the likely cyclic occurrence of supercontinents in Earth history (Evans et al., 2016a; Nance et al., 1988), together with the seismic tomographic discoveries of both whole-mantle convection (van der Hilst, 2004; van der Hilst et al., 1997) and large lower mantle structures such as the large low-shear-velocity provinces (LLSVPs; Dziewonski, 1984), and the temporal and spatial linkages between supercontinent events and global plume episodes (Evans, 2003; Li et al., 2003, 2004; Li and Zhong, 2009), enabled the geoscience community for the first time to develop holistic global geodynamic models that link plate tectonics with global-scale mantle convection, first order mantle structures, and mantle plume generation (Li et al., 2008a; Li and Zhong, 2009; Maruyama, 1994; Zhong et al., 2007) with the latter being dramatically expressed in the Large Igneous Province record (Coffin and Eldholm, 1994; Ernst and Buchan, 2003). Although lithosphere-whole mantle coupled global geodynamic models are still in their early days and competing models exist (e.g., Burke et al., 2008; Dziewonski et al., 2010; Torsvik et al., 2008b; Torsvik et al., 2014), numerous subsequent geodynamic modelling (Zhang et al., 2010) and geochemical works (Doucet et al., 2020a; Doucet et al., 2020b; Gamal El Dien et al., 2019) have demonstrated that first-order mantle structure may indeed have coupled with the supercontinent cycle since 2 Ga. Li et al. (2019) even speculated the presence of a more complicated supercontinent-superplume (LLSVPs) coupling through the occurrence of intervening ca. 1.2 Ga superocean episodes.

Having a credible global full-plate reconstruction for the past 2 Ga has applications to all disciplines of Earth sciences. In addition to enhancing the understanding of how plate tectonics interacted with mantle dynamics through the past 2 billion years of Earth history, it is also critical for evaluating how the Earth's dynamic system evolved from a stagnant lid or plume/accretion-dominated system in perhaps the very early Earth, to a mobile-lid plate tectonic system as we see today (Brown and Johnson, 2019; Harrison, 2020; Holder et al., 2019; Korenaga, 2021; Kusky et al., 2021; Moresi and Solomatov, 1998; O'Neill and Roberts, 2018; Windley et al., 2021).

In this contribution, we present the first 2000—540 Ma global full-plate reconstruction. This interval starts from the time when the Earth appeared to have transitioned from a system with operative plate tectonics but most of the stable cratons we have today were still being amalgamated, to a system dominated by supercontinent (and possibly also superocean) supercycles. We will first describe our approaches, and then provide an update on the reconstruction of Precambrian supercontinents Nuna (Columbia) and Rodinia. This is followed by a documentation of our animation through a stage-by-stage description of the major events through the 2000—540 Ma Earth history. We then discuss possible geodynamic processes underlying this critical time of Earth history before a final conclusion section. Our work utilises the GPlates software (Williams et al., 2012; https://www.gplates.org), and builds on numerous previous Precambrian reconstructions (e.g., Kirscher et al., 2021; Li et al., 2008a, 2013; Merdith et al., 2017, 2021; Pehrsson et al., 2016; Pisarevsky et al., 2014a) but with more emphasis on the utilisation of various databases and global geodynamic considerations.

2. Approaches and databases used

Here we follow a similar multidisciplinary approach as in Li et al. (2008b), including utilising the latest version of the Global Palaeomagnetic Database (GPMDB; Pisarevsky et al., 2022), and various other geological databases as discussed below. For global palaeolongitudinal constraints, we generally follow an extended-orthoversion assumption (Mitchell et al., 2012) as in Li et al. (2019), and discuss the merits and limitations of some alternative models in sections *2.3* and *6.3*.

2.1. Palaeomagnetic data selection, and APWP/TPW considerations

Palaeomagnetism not only plays the most critical role in Precambrian plate reconstruction through providing palaeolatitudinal constraints and testing past continental connections through apparent polar wander path (APWP) comparisons (Evans and Pisarevsky, 2008), the documented (or hypothesized) true polar wander (TPW) events are also the essential evidence used for the preferred geodynamic model of supercontinent-superplume (LLSVP) coupling (Li et al., 2004; Li and Zhong, 2009) and the orthoversion model for palaeolongitudinal constraint (Mitchell et al., 2012) (see sections *2.3* and *6.3*).

In this work we adopt the poles selected by the 8th Nordic Palaeomagnetism Workshop 2017 as grades A or B poles (Evans et al., 2021) following the Van der Voo (1990) quality criteria, with a few additional new poles published in more recent years. All the poles are listed in Supplementary Material 1, which includes a palaeomagnetic pole list and time coverage for each major craton. There are a few poles that we decide to discard for the purpose of reconstruction due to contradiction with other more reliable results, and these poles are marked with light grey shade in the data table. For poles based on clastic sedimentary rocks, an inclination-shallowing correction (Kodama, 2009; Tauxe and Kent, 2004) was applied using a uniform flattening factor of 0.6 as adapted at the 2017 NORDIC Palaeomagnetic Workshop following King (1955) and Torsvik et al. (2012).

For the reconstruction of supercontinents Nuna and Rodinia, we generally first use the best geologically and palaeomagnetically constrained reconstruction of the core constituents of each supercontinent to construct their respective APWP, and then try to find an optimum position for the less constrained continental blocks based on geology, palaeomagnetism (through comparing available poles with the APWP of the core constituents), and kinematic considerations such as previous position of each continent before joining the supercontinent, and next data-constrained positions of such continents after the break-up of that supercontinent. The selected palaeomagnetic poles are given in Table 1. We use the weighted running mean-pole calculation method with spline smoothing (Wu et al., 2021) to generate the APWPs for reconstruction. In this method, the size of the A95 confidence oval, the overall Van der Voo (1990) quality (Q) factor, and the age precision and overlap with the sliding age window (totalling 30 million years) for the mean poles, are all taken into account in the weighted-mean calculation, with each mean pole coming with a relative quality factor of its own. The resulting weighted mean poles and spline-smoothed poles for Nuna and Rodinia are given in Table 2.

For transition times between supercontinents, we generally use palaeomagnetic poles to constrain the palaeolatitude of each continent, and kinematic considerations (including plate motion speed, feasibility of plate tectonic boundary conditions, interactions between continents along the pathway etc.), and geodynamic considerations (e.g., the role of subduction girdle and orthoversion assumption etc.; see sections *2.3*, *2.4*), to constrain their relative positions.

In this work we accept the occurrence of both normal true polar wander (TPW) — the rapid motion of the entire silicate Earth relative to the core and the rotation axis (Gold, 1955; Goldreich and Toomre, 1969), and a specific type of oscillatory TPW, called inertia interchange

Table 1
Selected palaeopoles for Nuna and Rodinia. Plat/Plon: palaeopole latitude/longitude; Clat/Clon: palaeopole latitude/longitude corrected for inclination shallowing with f = 0.6 unless otherwise marked (only applicable to clastic sediments); Rlat/Rlon: palaeopole latitude/longitude after rotated to present-day Laurentia coordinates (the rotation is made on Clat and Clon if they are available); A95: 95% confidence oval for palaeopoles; Q: quality factors of Van der Voo (1990). *Italic* entries are treated as outliers with reasoning given at table footnote, and excluded from the calculation of APWPs. The four-digit pole reference numbers listed under Reference/GPMDB-result# are those assigned to each data entry in the Global Palaeomagnetic Database (GPMDB; Pisarevsky et al., 2022).

Rock formation	Plat (°N)	Plon (°E)	Clat (°N)	Clon (°E)	Rlat (°N)	Rlon (°E)	A95 (°)	Q	Age (Ma)	Reference/ GPMDB-result#
Rodinia										
Laurentia										
Franklin LIP grand mean	6.7	162.1			6.7	162.1	3.0	6	727—721	Denyszyn et al. (2009)
Uinta Mountain Group	0.8	161.3	1.2	161.8	1.2	161.8	4.7	5	750—766	9290; age: Eyster et al. (2020)
Kwagunt Formation[a]	14.2	163.8	14.2	163.8	14.2	163.8	3.5	7	759—743	9981
Tsezotene Sills - combined result	1.6	137.8			1.6	137.8	5.0	6	780—776	5922
MEAN Wyoming "Gunbarrel" dykes (site-weighted mean of Tobacco Root B, Christmas Lake, Mt. Moran)	13.9	129.4			13.9	129.4	8.2	4	780—776	LULEÅ WORKING GROUP (Harlan et al., 1997; Harlan et al., 2008)
Baltica										
Hunnedalen Dykes	−41.0	222.0			−27.7	161.5	10.5	6	875—821	8299
Rogaland Igneous cx (old)	−45.9	238.4			−34.1	174.5	18.1	4	883—855	9280
Katav Formation, mean of 3 sections[b]	*35.7*	*169.9*			*46.9*	*104.9*	*11.4*	*5*	*900—700*	Pavlov and Gallet *(2010)* *(age estimated only)*
Bratton and Algon igneous rocks	5.0	249.0			14.6	193.1	3.9	4	927—905	909
Rogaland Igneous cx, unit-weighted mean of all sites[c]	*−43.2*	*207.9*			*−29.3*	*149.4*	*10.1*	*5*	*935—870*	*LULEÅ WORKING GROUP (*Brown and McEnroe, *2004*; Walderhaug et al., *2007)*
Bjerkreim-Sokndal layered intrusion[d]	*−35.9*	*217.9*			*−22.4*	*158.4*	*6.3*	*5*	*938—904*	*9570*
951—935 Ma Igneous Rocks (Sweden, Norway)	−2.6	239.6			8.6	182.4	5.8	7	951—935	9905
Blekinge dolerites (52,53,54b,55)	13.0	247.0			22.8	192.6	16.0	5	954—946	LULEÅ WORKING GROUP (Bylund, 1992; age: Söderlund et al., 2005; Söderlund et al., 2004)
971 Ma Blekinge-Dalarna Dykes	−27.0	230.4			−14.5	170.4	14.9	5	978—964	9906
Siberia (Aldan)										
Ust-Kirba Formation combined	8.1	2.6	0.3	359.4	−13.4	160.5	10.4	4	960—930	8936
Kandyk Formation combined	3.1	356.5			−11.8	156.7	4.3	5	1000—950	8935
Siberia (Angara-Anabar)										
Kitoi Cryogenian dykes	1.1	21.8			−2.3	158.0	5.6	6	762—754	9409
Turukhansk Fm	7.2	17.6			1.6	151.7	3.1	5	1000—950	9893
North Australia										
Johnny's Creek siltstones - B comp.	15.8	83.0	7.4	93.5	−1.5	165.7	13.5	6	790—730	9569
Western Australia										
Mundine Well Dykes - combined result	45.3	135.4			3.5	142.7	4.1	6	758—752	8561
Lancer borehole, Browne Formation[b]	*44.5*	*141.7*	*34.2*	*137.9*	*10.8*	*151.3*	*6.8*	*4*	*900—810*	*9314*
North China										
Hebei Dykes 775 Ma	−29.0	67.4			−6.1	128.5	5.4	6	780—770	9975
Huaibei 890 Ma sills	52.3	329.3			5.5	190.2	3.5	7	904—876	9483
N. China Sills	−28.2	141.9			29.6	184.1	10.4	6	945—920	9956
Wangshan Fm	26.1	320.3			31.6	182.3	5.2	6	950—890	9481
South China										
Upper Liantuo Formation - combined result[b]	*13.2*	*155.2*	*20.0*	*142.5*	*77.5*	*241.7*	*5.3*	*6*	*767—660*	Jing et al. *(2015)* *(includes data from* Evans et al., *2000)*
Lower Liantuo Fm[b]	*20.0*	*148.7*	*24.8*	*136.4*	*71.1*	*227.8*	*9.3*	*7*	*770—750*	*9972*
Chengjiang Formation	29.9	60.6	32.1	72.2	15.1	221.2	10.9	7	808—792	9982
Xiaofeng Dykes - C2 comp.	13.5	91.0			28.0	244.8	10.9	6	812—792	9117
Madiyi Formation	35.3	67.9	34.3	82.4	23.9	220.4	5.1	6	814—796	9928
Xiajiang Group (f = 0.6)	42.7	104.0	42.7	104.0	40.4	209.7	8.1	7	816—804	9973
Yanbian 'A' Dykes	45.1	130.4			56.1	193.3	19.0	6	824—818	Niu et al. (2016)
Tarim										
Qiaoenbrak Fm	6.3	197.5			0.7	136.2	8.6	5	715—635	9525
Beiyixi (Baiyisi) Fm	−17.7	14.2			−11.1	135.1	4.2	5	760—740	9330
Aksu Dykes	19.0	128.0			25.6	250.4	6.0	5	819—795	9144
Sailajiazitage Group	−23.5	37.0			−13.5	157.5	11.3	6	907—864	9899
India										
Malani Igneous Suite - combined result	69.4	75.7			4.5	154.2	6.5	6	771—752	9728
West Africa										
Manso Dykes	−28.3	177.6			−7.3	150.9	12.7	7	870—850	9968
Congo										
Luakela volcanics - A comp.	40.2	302.0			15.3	149.8	14.1	4	772—758	9352
Mbozi Cmplex	46.0	325.0			−1.9	145.6	6.7	4	773—713	7786
Gagwe and Kabuye Lavas	−25.0	273.0			42.6	227.3	9.2	4	802—788	7785
Svalbard										
Svanbergfjellet Formation	25.9	226.8			37.3	211.6	5.8	4	789—730	9655
Upper Grusdievbreen Formation	−1.1	252.6			3.0	226.1	6.2	5	811—789	9656
Lower Grusdievbreen Formation	19.6	204.9			37.7	184.9	10.9	5	850—811	9657
Nuna										
Laurentia										
Nain Anorthosite	11.7	206.7			11.7	206.7	2.2	5	1320—1290	2180

(*continued on next page*)

Table 1 (*continued*)

Rock formation	Plat (°N)	Plon (°E)	Clat (°N)	Clon (°E)	Rlat (°N)	Rlon (°E)	A95 (°)	Q	Age (Ma)	Reference/ GPMDB-result#
Pilcher, Garnet Range and Libby Fms	−19.2	215.3	−9.3	219.3	−9.3	219.3	7.7	6	1407—1362	9030
McNamara Formation	−13.5	208.3	−3.2	213.5	−3.2	213.5	6.7	7	1407—1395	9031
MEAN Rocky Mountain intrusions (3-study mean of Laramie anorthosite, Sherman granite, and Electra Lake gabbro)	−11.9	217.4			−11.9	217.4	9.7	5	1445—1415	LULEÅ WORKING GROUP (Harlan and Geissman, 1998; Harlan et al., 1994)
Purcell Lava	−23.6	215.6			−23.6	215.6	4.8	5	1450—1436	9037
Mistastin Pluton	−1.0	201.5			−1.0	201.5	7.6	4	1450—1400	2271
Snowslip Formation	−24.9	210.2	−18.8	213.0	−18.8	213.0	3.5	7	1463—1436	9038
Michikamau Intrusion - combined result	−1.5	217.5			−1.5	217.5	4.7	7	1465—1455	2274
Spokane Formation	−24.8	215.5	−17.9	218.2	−17.9	218.2	4.7	6	1470—1445	9039
St.Francois Mountains Acidic Rocks	−13.2	219.0			−13.2	219.0	6.1	6	1492—1460	8932
Tobacco Root Dykes - A combined	8.7	216.1			8.7	216.1	10.5	4	1497—1399	9291
Western Channel Diabase	9.0	245.0			9.0	245.0	6.6	5	1593—1587	2669
Cleaver dykes	19.4	276.7			19.4	276.7	6.1	6	1745—1736	9139
Jan Lake Granite - A comp.	24.3	264.3			24.3	264.3	16.9	3	1759—1757	Gala et al. (1995); age: Bickford et al. (2005)
Deschambault Pegmatites	67.5	276.0			67.5	276.0	7.7	5	1771—1761	8889
NE trending ECMB Diabase Dykes	20.4	265.8			20.4	265.8	4.5	6	1783—1776	9970
Dubawnt Group	7.0	277.0			7.0	277.0	8.0	6	1820—1750	2737
Greenland										
West Gardar Lamprophyre Dykes	3.2	206.4			5.4	197.1	7.2	5	1316—1273	2108
West Gardar Dolerite Dykes	8.7	201.7			11.3	192.8	6.6	5	1316—1273	2106
Victoria Fjord dolerite dykes	10.3	231.7			10.3	223.0	4.3	6	1384—1380	489
Midsommersoe Dolerite	6.9	242.0			6.0	232.9	5.1	5	1384—1380	99
Zig-Zag Dal Basalts	12.0	242.8			11.0	234.2	3.8	5	1384—1380	98
Melville Bugt diabase dykes	5.0	273.8			1.5	264.3	8.7	6	1638—1628	9495
Baltica										
Mashak Formation	1.8	193.0			−14.1	227.0	14.8	5	1385—1366	10,022
Lake Ladoga basalt, sill, dykes	15.2	177.1			5.4	220.1	5.5	6	1464—1440	9347
MEAN Tuna/Bunkris/Glysjön/Oje unit-weighted by study	28.3	179.8			15.2	229.2	13.2	4	1478—1460	LULEÅ WORKING GROUP (Bylund, 1985; Mulder, 1971; Piper, 1992; Piper and Smith, 1980; age: Söderlund et al., 2005)
Ragunda Formation	51.6	166.6			39.7	236.4	7.1	4	1519—1493	1320
Satakunta dyke swarm	29.3	188.1			12.3	236.2	6.6	6	1590—1565	9445
Åland dyke swarm	23.7	191.4			6.0	236.0	2.8	7	1590—1566	Salminen et al. (2016)
Hoting basic dykes[e]	*21.9*	*146.7*			*27.0*	*198.9*	*13.7*	*4*	*1638—1590*	*9473*
Quartz porphyry dykes	30.2	175.4			18.9	227.0	9.4	3	1641—1621	407
Sipoo Quartz Porphyry Dykes - An comp.	26.4	180.4			13.3	228.7	9.4	4	1643—1623	7765
Suomenniemi Dykes	27.8	171.7			18.7	222.7	7.9	4	1648—1632	9926
Häme dyke swarm	23.6	209.8			−1.3	251.3	14.7	5	1661—1633	9860
Turinge Gabbro-Diabase	51.6	220.2			22.3	268.8	4.8	4	1709—1697	9921
Volyn-Dniestr-Bug intrusions - Group E	*10.7*	*163.2*			*8.9*	*206.1*	*10.2*	*5*	*1734—1710*	*9422*
MEAN Ropruchey sill, 4 sites	39.1	217.0			11.2	262.4	8.6	5	1754—1748	LULEÅ WORKING GROUP (Damm et al., 1997; Fedotova et al., 1999; age: Lubnina et al., 2012)
Volyn-Dniestr-Bug intrusions	*26.5*	*169.1*			*18.9*	*219.9*	*3.9*	*7*	*1770—1740*	*9421*
Småland intrusives	45.7	182.7			28.4	241.7	8.0	7	1784—1769	9355
Hoting gabbro	43.0	233.3			11.8	275.5	10.9	6	1796—1776	9580
Shoksha Sandstones	39.7	221.1			10.8	265.7	4.0	7	1800—1750	8681
Kallax gabbro	49.0	209.0			22.5	260.6	3.9	5	1805—1794	10,003
Nottträsk gabbro	43.5	216.2			15.5	263.3	6.1	5	1812—1800	1331
Lake Ladoga, Mean intr. & dykes, A comp.	50.9	229.1			20.1	274.3	7.2	6	1819—1744	10,018
Siberia (Aldan)										
Ulkan granite[f]	*42.1*	*249.4*			*−25.0*	*−119.5*	*4.4*	*4*	*1729—1709*	*9500*
Elgetey Fm[f]	*7.1*	*183.5*			*18.7*	*347.3*	*13.2*	*7*	*1736—1728*	*9501*
Siberia (Angara-Anabar)										
Udzha-Chieress Intrusions	5.7	264.9			14.0	−140.2	6.3	5	1390—1370	9895
Sololi-Kyutingde intrusions	−33.6	73.1			−15.8	216.8	10.4	6	1497—1449	9318
North Anabar Intrusions	23.9	255.3			−6.0	−144.3	7.5	5	1500—1466	9553
West Anabar Intrusions	25.3	241.4			−11.4	−155.9	4.6	5	1505—1500	9552
Kuonamka Dykes	−6.0	54.0			4.0	190.4	19.8	5	1508—1498	8554
North Australia										
Derim Derim Sills	76.5	300.2			−3.7	205.0	15.0	6	1329—1312	9978
Mt.Isa Metamorphosed Dykes (IM)	−79.0	110.6			−6.7	204.0	8.4	4	1550—1500	7550
Balbirini Dolomite, upper part	−52.0	176.1			13.4	232.4	7.5	6	1592—1586	8724
Balbirini Dolomite, lower part	−66.1	177.5			1.9	224.2	5.7	6	1617—1606	8723
South Australia										
Blue Range beds & Pandurra Formation	−38.4	62.4			−9.4	204.6	3.5	5	1580—1300	9399
Gawler Range Volcanics	−60.4	50.0			−13.2	228.1	6.2	3	1590—1500	1962
Amazonia										
Nova Guarita dykes	−47.9	245.9			−7.0	−157.6	6.6	6	1422—1415	9361
Indiavai gabbro	57.0	69.7			−1.1	209.7	8.9	3	1423—1409	9367
Mucajai Complex[g]	*−38.2*	*0.1*			*1.5*	*278.0*	*12.6*	*5*	*1540—1520*	*9966*
Avanavero mafic rocks	−48.4	27.9			23.9	−83.8	9.2	6	1791—1786	9499

(*continued on next page*)

Table 1 (*continued*)

Rock formation	Plat (°N)	Plon (°E)	Clat (°N)	Clon (°E)	Rlat (°N)	Rlon (°E)	A95 (°)	Q	Age (Ma)	Reference/ GPMDB-result#
São Francisco										
Curaçá mafic intrusions and baked rocks	10.1	9.6			1.6	−107.9	15.4	6	1516—1500	9558
Pará de Minas Dykes	39.8	16.8			31.9	−110.5	17.0	5	1800—1785	9953
North China										
Yanliao mafic sills	−5.9	179.6			−1.5	199.7	3.6	6	1330—1316	9461
Tieling Formation	−11.6	7.1			9.3	−144.6	6.3	6	1458—1416	Wu (2005); age: Su et al. (2010)
Yangzhuang Fm (Wu + 05) - B comp.	17.3	214.5			0.5	241.2	5.7	6	1560—1437	9268
Yangzhuang Fm (Pei + 06) - C comp.	2.4	190.4			−0.2	213.3	11.9	6	1560—1437	9360
Luxi Dykes 1630 Ma	*20.8*	*182.5*			*19.4*	*216.9*	*8.3*	*5*	*1638—1630*	*9924*
Luxi Dykes 1680—1630 Ma combined[h]	−3.0	198.3			15.6	217.1	7.8	5	1680—1630	Cai et al. (2020)
Luxi Dykes 1680 Ma	*17.8*	*184.9*			*15.6*	*217.1*	*14.3*	*4*	*1685—1675*	*9925*
Taihang dykes (central zone)	47.9	275.2			15.6	297.7	4.0	7	1772—1766	9546
Yinshan Dykes - combined result	32.3	248.3			3.0	275.1	2.0	7	1772—1766	9544
Xiong'er Group	50.0	272.7			17.8	296.1	4.9	7	1790—1770	9548
India										
Lakhna Dykes	41.3	120.5			−20.6	209.1	20.5	6	1469—1463	Pisarevsky et al. (2013)
West Africa										
Tagragra d'Akka Dykes	87.4	44.7			−7.3	221.6	7.8	5	1400—1360	9980

[a] Corrected for inclination shallowing by f = 0.9 (Eyster et al., 2020).
[b] Excluded due to high age uncertainty.
[c] The original Rogaland Igneous cx pole is used because this mean pole deviates from most of other coaeval poles.
[d] Interpreted to be overprint (Walderhaug et al., 2007).
[e] Based on only four dykes. The magnetic age is derived from A-Ar age of the baked contact rock.
[f] Likely subjected to local rotations.
[g] Lacks field test and position coincides with Phanerozoic poles.
[h] The poles of 1630 Ma and 1680 Ma Luxi dykes overlap with each other and pass a common mean test. We combined those two poles.

true polar wander (IITPW) (Evans, 1998; Kirschvink et al., 1997), in Earth history. Recognition of TPW events during both Rodinia time (Li et al., 2004; Maloof et al., 2006; Niu et al., 2016) and Nuna and Pangaea times (see discussions in sections *2.3, 6.2 and 6.3*) is of particular importance, as it not only enables us to construct an APWP for Rodinia which would otherwise be considered too scattered a dataset (see section *3.1*), it also allows us to examine the mantle dynamics during supercontinent cycles (sections *2.3, 6.2 and 6.3*) and the validity of the extended-orthoversion hypothesis (Li et al., 2019, after Mitchell et al., 2012; see section *2.3*).

2.2. Geological databases for global reconstruction

Global palaeogeographic reconstructions need to consider all geological information (e.g., Fig. 1a of Li et al., 2008a). The best way to do so systematically is to have access to GIS-based global databases. Ideally, such an approach would allow researchers to use continuing or paired features between adjacent continents (e.g., long orogens, paired rift margins, segments of a shared large igneous provinces or LIPs etc.) across continents to examine their potential past connections in real time. However, there are currently severe limitations for such a database-based approach due to two major shortfalls. First, there is a shortage of GIS-based and uniformly covered and formatted global databases suited for such a purpose. The most systematic geological databases used for this work are (1) the IGCP 440 global pre-700 Ma geotectonic database in shapefile format (Li et al., 2008a), and (2) the global large igneous province (LIP) database in both shapefile and Excel table formats (after Ernst et al., 2021). Second, there is non-uniqueness in the interpretation of some geological features, in addition to accuracy limitations of the databases. For example, a sedimentary sequence with continental slope character could be interpreted by the database compiler as either the record of a passive margin, or the cover succession of a failed continental rift. A crustal extension-related unconformity could be interpreted by some as evidence for an orogen. A poorly dated orogen with upper age constrained by the age of the cover succession could lead to the orogen being shown on a reconstruction long after it ceased to active. Such limitations will gradually diminish with time as more and better global georeferenced databases become available.

*IGCP440 pre-700 Ma global geotectonic database (*Supplementary Material 2*).* This was a GIS-based database compiled by members of the IGCP 440's map committee (see attribute on The Geodynamic Map of Rodinia as appendix I of Li et al., 2008a). The database features interpreted tectonic facies for major crustal provinces between 1600 and 700 Ma, Paleoproterozoic orogenic belts, known or inferred Archaean cratons, and some 1600—700 Ma geological features such as basin record, major faults, intracratonic granitoids, and ophiolites. The data compilation stopped at 700 Ma as it was deemed that data after that time is irrelevant to the evolution of the supercontinent Rodinia, which was the focus of that IGCP project. In this work we utilise and display most features of that database in the 2000—700 Ma segment of the global full-plate animations, but simplified the display by having all variety of orogens (including metamorphic terranes) shown by the same colour (green).

*Neoproterozoic sedimentary facies point data (*Li et al., 2013*;* Supplementary Material 3 *for the database in shapefile format)*. This simple point data database for selected Neoproterozoic time windows between 825 and 540 Ma helps to fill the age gap of 700—540 Ma in the IGCP 440 database (Supplementary Material 2). It emphasises the sedimentary (including hiatus), paleoclimatic, igneous, and metamorphic spot records during the break-up of the supercontinent Rodinia.

*Global large igneous province (LIP) database (*Ernst et al., *2021;* Supplementary Material 4 *for shapefile database and Excel tables)*. The global LIP record not only can be used for reconstructing past continental connections (Ernst et al., 2013a; Ernst et al., 2008; Evans et al., 2016b), it also provides a key argument for either the geodynamic model of coupled supercontinent-superplume cycles (Li et al., 2008a; Li and Zhong, 2009) or the opposing view (Torsvik et al., 2008b). In section *6.3* we use the data to discuss some of the alternative geodynamic models.

LIPs are defined as large volume (>0.1 million km^3 or Mkm^3; frequently above 1 Mkm^3), mainly mafic (−ultramafic) magmatic events of intraplate affinity (based on tectonic setting and/or geochemistry) that occur in both continental and oceanic settings, and are typically either of short duration (<5 million years or Myr; often <2 Myr) or consist of multiple short pulses over a maximum of a few 10s of Myr (Ernst, 2014; Ernst et al., 2021). They consist of volcanic packages (flood basalts) and plumbing systems of regional dyke swarms (linear,

Table 2
Weighted mean poles for Nuna and Rodinia, and synthetic poles generated using spline smoothing as shown in Figs. 3 and 7. Lat/Lon: latitude/longitude; E95a/E95b: semi-major/semi-minor axes of error ellipses; ω: orientation of the semi-major axis; N: number of paleopoles in a time window of 30 Myr; Weight: the weight of each mean pole.

Weighted mean								Spline	
Age (Ma)	Lat (°N)	Lon (°E)	E95a (°)	E95b (°)	ω (°)	N	Weight	Lat (°N)	Lon (°E)
Rodinia								(Smoothing 3000)	
700	0.4	−39.7	21.4	20.2	−105.5	2	1.3	0.3	−39.2
710	−2.4	−30.8	20.4	15.8	−74.1	3	2.1	−2.7	−30.1
720	−5.3	337.6	24.6	13.9	−54.8	5	3.4	−4.9	−23.2
730	−5.4	339.1	21.7	11.8	−50.7	6	4	−5.2	−21.4
740	−3.9	335.6	15.6	9.5	−51.9	9	5.7	−4.2	−23.8
750	−4.2	334	14.5	9.3	−51	9	5.9	−3.9	−26
760	−3.5	331.4	13.8	8.8	−53.6	10	6.6	−3.3	−29.8
770	−4	327.4	12.5	8.7	−58.5	12	8.1	−3.8	−34.2
780	−8.1	−27.2	22.8	10.8	113.1	12	8.4	−10.1	−17.6
790	−26.4	44.4	21.2	10.6	91.2	12	8.6	−24.1	34.4
800	−27.6	42.2	13.6	11.2	−87	10	7	−28.6	46
810	−30.3	42.2	14.1	13	−63.8	10	6.6	−30.2	43.3
820	−30.2	39.3	16.6	14.8	−64.6	9	5.5	−32.9	38.3
830	−41.8	24	28.5	18.8	−49.1	5	3	−31.4	19.9
840	3.2	−16.9	36.1	17.9	159.1	3	1.8	−6.4	−7.6
850	12.8	341.8	24.8	15.2	−14.7	5	2.9	11.6	−19.1
860	14.4	341.4	22.8	14.9	−12.2	5	2.9	16.1	−18.9
870	15.7	−14.3	17.6	15.4	−46.7	5	2.9	15	−15
880	8.5	−11	20.8	14.5	−26.8	6	3.5	8.6	−10.1
890	−0.4	−2.7	25.7	16.8	158	4	2.3	−0.6	−3.3
900	−10.2	2	22	15.6	−37.9	4	2.2	−9.6	1.7
910	−15.3	3.3	19.1	14.1	−31.8	5	3	−14.6	2.4
920	−14.4	−1.6	22.5	13.6	146.9	5	3.2	−15.6	0.5
930	−16.6	1.6	18.1	12.6	−27.7	5	3.3	−15.6	0
940	−12.3	−3.3	16.6	10.7	139.6	8	5.2	−12.6	−3
950	−8.1	−6.8	17.2	10.8	144.7	8	5.2	−8.1	−6.7
960	−3	−9.6	17.9	11.8	142.6	7	4.4	−3	−9.7
Nuna								(Smoothing 10,000)	
1300	4.4	200.8	13.9	12.5	−21.8	5	3.6	4.3	−159.1
1310	2.8	201	12.2	11.1	−17.9	6	4.5	3.2	−159.3
1320	2.1	201.1	12.3	11.1	−18.3	6	4.5	2.1	−159.3
1330	1.7	201.2	12.7	11.5	−18.6	6	4.1	−0.1	−158.2
1340	−4.7	202.8	16.7	16.2	−32.6	3	1.9	−3.8	−153.9
1350	−8.7	215.6	18.2	16.1	−95.7	3	2	−5.9	−147
1360	−5.5	218.7	15	13.8	−0.1	5	3.4	−4.2	−140.7
1370	1	223.7	11.3	9.8	27.7	8	6.7	−0.5	−136.8
1380	1	223.6	11.2	9.7	26.7	8	6.8	1.2	−136.6
1390	1.1	−139.5	9.8	8.8	135.6	11	8.6	0.7	−140
1400	−1.7	−146.3	10.9	10.5	156.2	8	5.6	−1.3	−145.1
1410	−3.5	211.9	9.2	9.1	−117.3	10	7.4	−2.9	−148.2
1420	−2.9	210.8	9.9	9.6	26.5	9	6.6	−3.6	−148.6
1430	−4.7	213.6	9.6	9.1	35.5	12	8.8	−4.9	−146.6
1440	−6.9	216	9.9	8.9	12.3	12	8.9	−6.4	−144.4
1450	−6.7	216.7	8.7	7.5	19.2	16	11.9	−6.8	−143.3
1460	−6.2	216.8	8.7	7.4	22	16	12	−6.3	−142.9
1470	−5.3	217.8	9.2	7.8	25.5	14	10.5	−5.3	−142.1
1480	−4.4	219.1	12.8	9.3	25.2	11	7.7	−4.1	−141.5
1490	−2.3	−142.1	11.8	9.9	125.8	14	9.3	−2.9	−142
1500	−2.6	217.7	12.4	10.3	−120.5	13	9	−2.2	−142.3
1510	−1.4	217.7	13.3	10.9	−119.3	12	8.3	−1	−141.3
1520	1.2	221.9	18	14.4	−113.9	8	5.2	0	−139
1530	−0.2	−136.1	18.7	14.9	126.5	7	4.4	−1.3	−138.3
1540	−5.8	218	18.4	13.4	−97.1	5	3.2	−3.9	−139.9
1550	−5.8	218.3	18.7	13.6	−97.2	5	3.1	−4.2	−139.5
1560	−0.6	224.9	15.9	11.7	−113.9	7	4.6	−1.6	−135.8
1570	0.9	228.5	15.7	12.2	−118.7	6	4.2	1.6	−131.4
1580	5.6	233	14.1	11	−128.3	6	5	4.4	−128
1590	5.6	−127.1	14.6	11.4	127.7	6	4.7	5.9	−126.8
1600	6.4	−126	12.4	11.2	142.4	6	4.7	7	−127.3
1610	9.5	226.1	17.9	15.7	12.3	3	2.1	8.6	−128.4
1620	10	233	16.2	11.2	−71.2	7	4.9	9.9	−127.5
1630	10.7	−126.3	15.7	10.6	69.5	7	5.4	10.9	−126.1
1640	11.8	−124.5	17.2	10.7	66.7	6	4.8	11.4	−125.4
1650	11.6	−125.2	18.2	11.3	66.1	6	4.3	11.4	−126.6
1660	11.8	−130.5	25.3	16.3	61	3	2	11.5	−129
1670	9.1	−128.6	33.9	20.3	63.4	2	1.3	12.7	−129
1680	15.6	217.1	27.3	27.3	−109.6	1	0.7	15.9	−124.1
1690	21.6	248.1	38.4	19.3	−96.1	2	1.4	19.5	−113.1

(*continued on next page*)

Table 2 (*continued*)

Weighted mean								Spline	
Age (Ma)	Lat (°N)	Lon (°E)	E95a (°)	E95b (°)	ω (°)	N	Weight	Lat (°N)	Lon (°E)
1700	22.3	268.8	22.9	22.9	−0.1	1	1	21.6	−101.2
1710	22.3	268.8	22.9	22.9	−0.1	1	1	21.9	−92.9
1720	22.3	268.8	26.2	26.2	−0.3	1	0.7	20.5	−88.7
1730	19.7	−84.2	17.9	17.8	72.2	2	1.6	18.3	−87.4
1740	14.1	270.9	12.7	11.9	−122.8	5	3.9	17	−88.2
1750	19.9	−89.7	15.6	10.6	−176.6	7	5.4	18.2	−88.4
1760	19	−86.3	12.6	11.3	163.1	10	8.4	19.1	−86.9
1770	19.6	274	11.5	10.2	−27.9	11	9.6	19.6	−86.3
1780	20.2	272.9	10.4	9.1	−43.6	13	11.2	20.2	−86.9

radiating and a newly identified circumferential type; Buchan and Ernst, 2021), sill complexes, layered mafic-ultramafic (M-UM) intrusions, and crustal magmatic underplates. Those which do not reach the threshold of 100,000 km^2 are included as probable LIPs based on satisfying proxy parameters such as having mafic dykes which are typically at least 10 m in width (Ernst, 2014). With an increasing number of LIP events being discovered during Earth history, LIP data, and especially their regional dyke swarms, provide an efficient tool for constraining palaeocontinental reconstructions (Bleeker and Ernst, 2006; Ernst and Bleeker, 2010; Ernst et al., 2013a). Comparison of LIP time "barcodes" from different crustal blocks can reveal which were nearest neighbours and over what time span (Bleeker and Ernst, 2006). Reconstruction of coeval dyke swarm trends from different crustal blocks into giant linear, radiating and circumferential swarms, constrains the relative positioning of these blocks (Bleeker and Ernst, 2006; Buchan and Ernst, 2021).

Fig. 1 represents a global LIP barcode diagram updated from that of Ernst et al. (2021) for the interval of 2000 to 540 Ma. Grey bands in the background identify particular time periods with significant matches. A tabulation of these matches is provided in Table 3, and possible plume centres, speculated using radiating (and circumferential) dyke swarms and other evidence (Buchan and Ernst, 2021), is listed in Table 4. It is apparent from these tables that there is more of a concentration of globally widespread LIP events during Rodinia time of 900—700 Ma (Li et al., 2003; Li et al., 2008a) than for Nuna time of 1600—1300 Ma. In sections *3—5*, we honour some of the more confident LIP connections, but not all, because (1) such interpretations are often non-unique, for example, the possible presence of multiple plume centres at a similar age (Ernst and Buchan, 2002), and (2) our reconstruction tries to honour multiple independent lines of evidence as well as plate kinematic constraints. Nonetheless, by enabling the global LIP record to be linked with this (Supplementary Material 4 and reconstruction figures below) and alternative plate reconstruction models, future workers will be able to explore further the merits of both the various reconstructions and the competing geodynamic models (see section *6.3*).

We also utilised the global passive margin database of Bradley (2008) (Supplementary Material 5, in shapefile format), global orogen database of Condie et al. (2021) with minor modifications and in shapefile format (Supplementary Material 6), and global metamorphic database of Liu et al. (2022) to help define plate boundaries in our full-plate animations. We note, however, that some of the listed passive margins in the database may in fact represent the marginal slope of failed rift systems, for example, the late Neoproterozoic southeastern margin (present-day coordinates) of the Yangtze Block (Wang and Li, 2003).

2.3. Geodynamic constraints: introversion, extroversion, orthoversion, and palaeolongitude constraints

Introversion and extroversion are two opposing ways of supercontinent assembly: the former involves the closure of internal oceans generated during the break-up of the previous supercontinent (for example, the present-day Atlantic, Indian and the Southern oceans formed during the break-up of the supercontinent Pangaea), whereas the latter involves the previous supercontinent being turned inside-out to form the new supercontinent through closing the previous external superocean, and at the same time the internal oceans expand to form the new superocean (Murphy and Nance, 2003).

However, in practice, it is not easy to determine whether the closure of small oceans represent the closure of internal oceans as part of introversion, or that of oceans formed along active margins as part of a previous superocean. For example, the present-day Philippine Sea and Tasman Sea in the southwestern Pacific Ocean were formed due to subduction retreat along the margin of the former Pangaean external superocean, the Panthalassa Ocean. The hypothetical formation of a future supercontinent through the closure of the Pacific Ocean, a clear case of extroversion assembly, may be seen by some as an introversion assembly, because previous marginal seas like the Philippine Sea and the Tasman Sea (which may become the last sections of the Pacific Ocean to close due to their young ages) could be identified by some as the closure of "internal oceans". To address such ambiguity in distinguishing introversion assembly from extroversion, due to the difficulty in correct identification of genuine closure of internal oceans, Li et al. (2019) added the criterion of the survival of the old global subduction girdle, or the regeneration of a new one (for example, the present-day Pacific 'Ring of Fire', which existed as a subduction girdle since Pangaea assembly, is expected to survive if the next supercontinent assembles through introversion; Fig. 2 of Li et al., 2019) as another approach to distinguish introversion vs. extroversion supercontinent assembly.

In this study, we follow the general philosophy of Li et al. (2019) in having Rodinia assembled through introversion, and Pangaea through extroversion. However, we note that others (e.g., Martin et al., 2020; Murphy and Nance, 2003) interpreted otherwise. By following the geodynamic model of a dynamic coupling between the supercontinent and superplume (LLSVP) cycles (Li et al., 2008a; Li and Zhong, 2009; Zhong et al., 2007) and constrained by TPW and LIP records, our global reconstruction favours a weakened legacy degree-2 (degree-2 + degree-1) mantle structure for the early stage of both an introversion-assembled supercontinent (e.g., Rodinia) and an extroversion-assembled supercontinent (e.g., Pangaea). We will present a more detailed geodynamic discussion in section *6*.

How to assign palaeolongitude to supercontinents and palaeogeographic reconstructions in general is another challenge, as palaeomagnetism by itself is unable to provide absolute palaeolongitudinal information. Nonetheless, attempts have been made to control palaeolongitude indirectly through geodynamic assumptions (Mitchell et al., 2012; Torsvik et al., 2014). We will further discuss this topic in section *6.3*. Here we focus on models featuring a coupling between the supercontinent cycle and whole-mantle geodynamics (including lower-mantle features such as LLSVPs).

Following the principle of continents tending to be drawn to mantle downwelling regions or zones (geoid lows; Anderson, 1994; Zhong et al., 2007), Mitchell et al. (2012) proposed that a new supercontinent can assemble on the subduction girdle 90° away from the previous one

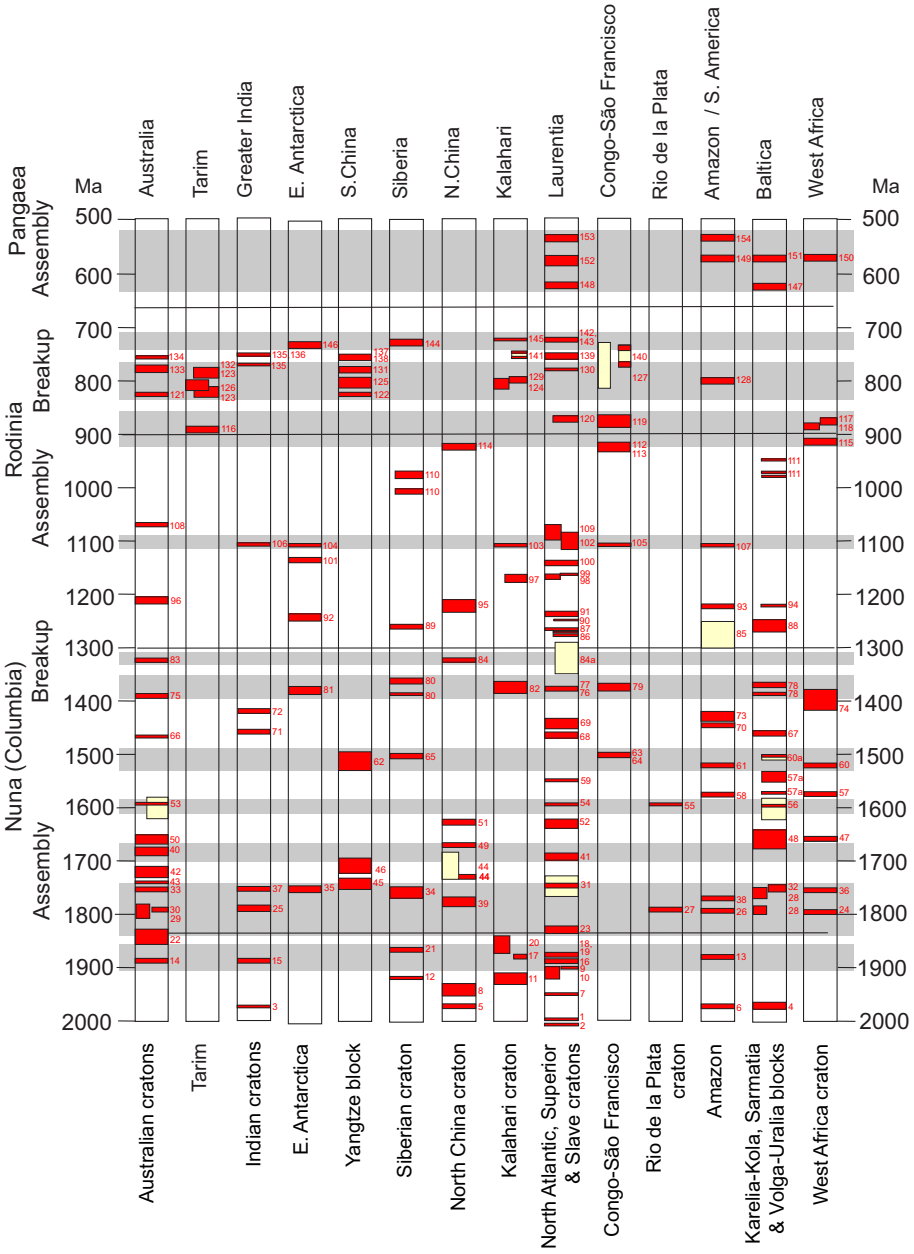

Fig. 1. An updated global LIP barcode diagram for the period 2010 Ma to 530 Ma based on Ernst at al. (2021). Beige boxes indicate events with large age uncertainty. Numbers correspond to LIP events and are explained below. Event names are shown in bold, with only new entries since Ernst et al. (2021) being given references. **1 = C, O Minto-Povungnituk-Eskimo [Superior craton] (1998 Ma), 2 = Kennedy** [Wyoming craton] (2010 Ma), 3 = Khajuraho (Jhansi) [Bundelkhand craton] (1970), 4 = **Pechenga-Onega** [Karelian craton] (1970 Ma), 5 = **Xiwangshan** [North China craton] (1970 Ma), 6 = **Moi Moi–Charlie-Lucie** [Amazonia] (1985—1975 Ma), 7 = **Mugford** [Nain portion, North Atlantic craton] (1950 Ma), 8 = **Xuwujia** [North China craton] (1960—1930 Ma), 9 = **Hearne** [Slave craton] (1900 Ma), 10 = **Frobisher Suite** M-UM event [Meta-Incognito block] (ca. 1920 Ma), 11 = **Hartley (Tsineng, Moshaneng)** [Kalahari craton] (1930—1910 Ma), 12 = **Angaul** [Siberian craton] (1915 Ma), 13 = **Maria-Carajas-Tucumã** [Amazonia] (1880 Ma), 14 = **Boonadgin** [Yilgarn craton] (1890 Ma), 15 = **Bastanar-Hampi** [Indian craton] (1890 Ma), 16 = **Ramah Group** [Nain portion, North Atlantic craton] (1890 Ma), 17 = **Mashonaland** [Kalahari craton] (1880 Ma), 18 = **Ghost-Mara River- Morel** [Slave craton] (1890—1870 Ma), 19 = **Circum-Superior** [Superior craton] (1885—1870 Ma), 20 = **Black Hills-Soutpansberg** [Kalahari craton] (1880—1840 Ma), 21 = **Kalaro-Nimnyrsky-Malozadoiskii** [s Siberian craton] (1870 Ma), 22 = Savannah (Kimberley) (1850—1830) [Halls Creek Orogen, Kimberley block] (Le Vaillant et al., 2020), 23 = **Sparrow-Uranium City-Christopher Island** [nw Laurentia] (1833—1818 Ma)., 24 = **Libiri** [West African craton] (1790 Ma), 25 = **Pebbair** [Dharwar craton] (1788 Ma), 26 = **Avanavero** [Amazonia] (1790 Ma), 27 = **Florida (Uruguayan)** [Rio de la Plata craton] (1790 Ma), 28 = **Ukrainian AMCG- Prutivka-Novogol** [Sarmatia] (1790—1750 Ma), 29 = **Hart (Carson-Mount Hay)** [Kimberley block, North Australian craton] (1810—1780 Ma), 30 = **Eastern Creek** [eastern North Australian craton] (1790-1780 Ma), 31 = **Kivalliq (Pitz-Nueltin, McRae, Wellington, Cleaver portions)** [n Laurentia] (1770—1730 peak 1750 Ma), 32 = **Aiski (Navysh)** [e Baltica] (1750 Ma), 33 = **Lunch Creek (north & south) / Mt. Isa** [North Australian craton] (1750 Ma), 34 = **Timpton** [Siberian craton] (1750—1770 Ma; (Gladkochub et al., 2022)), 35 = **Vestfold Hills-3** [Antarctica] (1750 Ma), 36 = **Tagragra of Akka** [Anti Atlas Inlier, West African craton] (1755 Ma), 37 = **Papilia** (Newer Dolerites) [Singhbhum craton] (1760 Ma), 38 = **Espinhaco** [Amazonian craton] (1770 Ma), 39 = **Xionger-Taihang** [North China craton] (1770 Ma), 40 = **Late Calvert (Sybella) (Willyama?)** [North Australian craton] (1690—1670 Ma), 41 = **Pelly Bay** [n Laurentia] (1700 Ma), 42 = **Fiery Creek (Oenpelli?)** [North Australian craton] (1730—1710 Ma), 43 = **Wonga** [North Australian craton] **(1740 Ma),** 44 = **Miyun** (1730 Ma) & **Damiao-Shachang** (1730—1680 Ma) [North China craton] (1730—1680 Ma), 45 = Wuding [Yangtze craton] (1740 Ma, Lu et al., 2020), 46 = Tongan [Yangtze craton] (1720—1700 Ma, (Lu et al., 2020)), 47 = **Zenaga** [Anti Atlas inliers, West African craton] (1660 Ma), 48 = **Hame** [Baltica] (1676—1640 Ma), 49 = **Laiwu** [North China craton] (1670 Ma), 50 = **Toole Creek (Dead Horse, Cobbold) & Bulonga** [North Australian craton] (1660—1655 Ma), 51 = **Taishan** [North China craton] (1630—1620 Ma), 52 = **Melville Bugt** (Greenland) [ne Laurentia] (1640—1630 Ma), 53 = **Gawler Range** [Gawler-Curnamona craton] (1590 Ma), 54 = **Mammoth-Western Channel (-Wernecke)** [w. Laurentia] (1590 Ma), 55 = **Tandil** [Rio de la Plata craton (1590 Ma), 56 = **Breven-Hallefors** [Baltica] (1600 Ma), 57 = **Korsimoro** [West African craton] (1575 Ma), 57a = Värmland & Åland-Åboland [Baltica] (1570–1540, 58 = **Mata Mata** [Amazonia] (1575 Ma), 59 = Ramshorn Creek [w. Laurentia] (1550 Ma, (Rogers et al., 2018)), 60 = **Essakane** [Amazonia] (1520 Ma), 60a = Brevik-Rjukan [Baltica] (1510–1500 Ma), 61 = **Kayser** [Amazonia] (1520 Ma), 62 = Dongchuan [Yangtze craton] (1530—1500 Ma, Lu et al., 2020), 63 = **Curaca-Chapada Diamantina** [São Francisco craton] (1500 Ma), 64 = **Humpata** [Greater Congo craton] (1500 Ma), 65 = **Kuonamka** [n Siberian craton] (1500 Ma), 66 = **Bangemall** [nw Australian craton] (1465 Ma), 67 = **Tuna-Trond Gota-Lake Ladoga** [n Baltica] (1460—1450 Ma), 68 = **Moyie** [w Laurentia] (1460 Ma), 69 = **Michael-Shabagamo** [e Laurentia] (1450—1425 Ma), 70 = **Betara** [Betara block] (1445 Ma), 71,72 = **Lakhna & Bandalimal)** [Bastar craton] (1460—1420 Ma), 73 = **Salto do Céu – Figuera Branca – Nova Lacerda** [Amazonia] (1440—1420 & 1380 Ma), 74 = **Bas Draa** [Anti Atlas inliers, West African craton] (1415—1380 Ma), 75 = **Biberkine** (Yilgarn craton) (1390 Ma), 76 = **Midsommerso-Zig Zag Dal** (Greenland) [ne Laurentia] (1385 Ma), 77 = **Hart River-Salmon River Arch** [w Laurentia] (1380 Ma), 78 = **Mashak** [e Baltica] (1385 Ma), 79 = **Kunene-Kibaran** [Greater Congo craton] (1380—1360 Ma),

80 = **Chieress (Severobyrrang)** [n Siberian craton] (1384 (1360 Ma)), 81 = **Vestfold Hills-4** [Antarctica] (1380 Ma), 82 = Pilanesberg [Kalahari] (1380—1360 Ma, #20 in Ernst et al., 2008), 83 = **Galiwinku-Derim Derim** [North Australian craton] (1320 Ma), 84 = **Yanliao** [North China craton (1320 Ma), 84a = Nain Plutonic Suite [Laurentia] (1350–1290 Ma), 85 = **Juscelândia-Serra dos Borges** [Brasilia belt] (1300—1250 Ma), 86 = **Harp** [Nain portion, North Atlantic craton] (1270 Ma), 87 = **Mackenzie** [Laurentia] (1272—1265 Ma), 88 = **CSDG (Central Scandinavian Dolerite Complex)** [Baltica] (1270—1250 Ma), 89 = **Sredne-cheremshan** [Siberian craton] (1260 Ma), 90 = **Mealy-Seal Lake** [e Laurentia] (1250 Ma), 91 = **Sudbury** [dykes] [e Laurentia] (1235—1238 Ma), 92 = **Vestfold Hills-5** [Antarctica] (1240 Ma), 93 = **Nova Floresta** [Amazonia] (1220 Ma), 94 = Protogine Zone [Baltica] (1220 Ma, #37 in Ernst et al., 2008), 95 = **Licheng** (1230 Ma) & **Yishui** (1210 Ma) [North China craton (1230—1210 Ma), 96 = **Marnda Moorn** [Yilgarn craton] (1210 Ma), 97 = **Lower Koras** [Namaqua belt, Kalahari craton] (1171 Ma, #42 in Ernst et al., 2008), 98 = **Thiselthwaite-Munn** [nw Laurentia] (1170 Ma), 99 = Gardar Late [Greenland, Laurentia] (1163 Ma, #43 in Ernst et al., 2008), 100 = **Abitibi-Corson** [c. Laurentia] (1150—1140 Ma), 101 **Bunger Hills** [Antarctica] (1130 Ma), 102 = **Keweenawan** [c Laurentia] (1115—1085 Ma), 103 = **Umkondo** (Africa) [Kalahari craton] (1112—1106 Ma), 104 = **Umkondo** (Antarctica) [Grunehogna craton] (1112—1106 Ma), 105 = **Huila (GN)-Epembe** [sw Congo craton] (1110 Ma), 106 = **Mahoba** [Bundelkhand craton] (1110 Ma), 107 = **Huanchaca-Rincon del Tigre** [Amazonia] (1110 Ma), 108 = **Warakurna** [c Australian craton] (1075 Ma), 109 = **Southwest Laurentia** (formerly Southwest Diabase Province) [sw Laurentia] (1100—1070 Ma), 110 = **Sette-Daban** [e Siberian craton] (1005, 975 Ma), 111 = Blekinge-Dalarna [Baltica] (980—920 Ma #54 in Ernst et al., 2008), 112 = **Bahia-Araquai** [São Francisco craton] (920 Ma), 113 = **Zadinian-Mayumbian (Gangil)** [Greater Congo craton] (924—912 Ma), 114 = **Dashigou (Sariwon)** [North China craton] (920 Ma), 115 = Oda [s West African craton] (915 Ma, (Antonio et al., 2021; Baratoux et al., 2019)], 116 = **Sailajiazitage** [Tarim craton] (890 Ma), 117 = **Iguerda-Taifast** [s West African craton] (870 Ma), 118 = **Manso** [n West African craton] (880 Ma), 119 = **Zambezi (Munali)** [Zambia, Congo craton] (880—860 Ma), 120 = **Glen Doe** (UK, Laurentia] (870 Ma, #58 in Ernst et al., 2008), 121 = **Gairdner-Willouran** [s Australian craton] (825 Ma), 122 = **Guibei** [South China block] (825 Ma), 123 = **Kuluketage** (**Qiganbualke**) [Tarim block] (820 & 780 Ma), 124 = **Rushinga-Bukoba** [Kalahari craton] (800 Ma), 125 = **Suxiong-Xiaofeng** [South China block] (800 Ma), 126 = **Aksu** [Tarim block] (810 Ma, #69 in Ernst et al., 2008), 127 = **Malagarazi-Bukoba** [Congo craton]; ca. 815—709 Ma, #70 in Ernst et al., 2008), 128 = **Niquelândia** [Brasilia belt] (790 Ma), 129 = **Gannakouriep** [sw Kalahari craton] (800 Ma), 130 = **Gunbarrel** [w. Laurentia] (780 Ma), 131, 132 = **Kanding** [South China block], **Kudi** [Tarim block] (780 Ma), 133 = **Boucaut** [s West Australian craton] (780 Ma), 134 = **Mundine Well-Keene** [West Australian craton] (755—750 Ma), 135 = **Malani** (India) [greater Indian craton] (755 Ma), 136 = **Malani (Seychelles)** [Seychelles] (755 Ma), 137 = **Shaba** [South China block] (755 Ma), 138 = **Ogcheon** [Korea, linked to South China] (755 Ma), 139 = **Mount Rogers** [e Laurentia] (755 Ma), 140 = **Roan** [Congo craton] (765—735 Ma), 141 = Damara-Kauka [Kalahari] (750 Ma #83 in Ernst et al., 2008), 142 = **Franklin (-Thule)** (Canada & Greenland portions) [n Laurentia] (716 Ma), 143 = **Kikitat** [Alaska] (715 Ma), 144 = **Irkutsk** [Siberia craton] (720 Ma), 145, 146 = **Mutare-Fingeren** [Kalahari & Grunehogna cratons] (720 Ma), 147 = **CIMP: Baltoscandian-Egersund** [Baltica] (615 Ma), 148 = **CIMP: 615 Ma pulse** (Long Range pulse) [e Laurentia] (615 Ma), 149 = **Precordillera** (S. America) (576 Ma), 150 = **CIMP: Ouarzazate** [West African craton] (580—560 Ma), 151 = **CIMP: Volyn, Seiland** [Baltica] (580—570 Ma), 152 = **CIMP 590—560 Ma pulse** (Grenville dykes, Sept Isle intrusion & Catoctin volcanics) [e Laurentia] (580 Ma), 153 = **Wichita** [sw Laurentia] (533 Ma), 154 = **Paraupebas-Piranhas** [Amazonian craton] (535 Ma).

through the closure of smaller oceans along the girdle instead of either the major internal oceans (introversion), or the previous external superocean (extroversion), a phenomenon termed orthoversion supercontinent assembly (Mitchell et al., 2012, 2021). Therefore, in an orthoversion assembly, both the bulk of the internal oceans and the bulk of the external superocean survive supercontinent assembly. Li et al. (2019) extended this concept by having each supercontinent forms 90° away from the previous one, regardless of whether it assembles through introversion, extroversion or orthoversion. We call this the *extended-orthoversion* model.

More recent geodynamic modelling (Huang et al., 2022) suggests, however, that introversion supercontinent assembly can easily occur at a similar location as the previous supercontinent, whereas an extroversion supercontinent assembly tends to occur on the other side of the globe ca. 180° away from the position of the previous one. We mark this non-orthoversion geodynamic model *180—180–0* because it would have both Nuna and Rodinia centred at 180°E, whereas Pangaea centred at 0°E.

There is yet no definitive proof for which of these models is correct or whether they could all occur in nature. In this paper we mainly discuss three scenarios: *Scenario Ia (0–90 W-0),* an extended-orthoversion model where each of the latest two supercontinents assembled 90° away from the previous one regardless whether they assembled through introversion, extroversion or orthoversion, with Nuna centred at 0°E, Rodinia at 90°W (Müller et al., 2022), and Pangaea at 0°E; *Scenario Ib (0–90E-0),* same as *Scenario Ia* except by having Rodinia centred at 90°E (Li et al., 2019); *Scenario II non-orthoversion (180—180–0)*: introversion 0° away, extroversion 180° away. Of course, there are other possible scenarios with any other possible longitudinal variation between successive supercontinents. All models need to be further tested using combined palaeomagnetism, geodynamic modelling, and other geological and geophysical means. Here we present *Scenario Ia* as our slightly preferred scenario (see animation in Supplementary Material 7), but also provide the full-plate animation for *Scenario Ib* (Li et al., 2019; Supplementary Material 8). We slightly prefer *Scenario Ia* over *Scenario Ib* because of the relatively more moderate plate motions required by the former (section *5.7*) and smoother transition from one supercontinent to the next following the extended-orthoversion model (section *6.3.2*, and Supplementary Materials 7, 8). In Supplementary Material 9 we highlight the occurrence of LIP events in time and space in both *Scenarios Ia* and *1b* animations. We will discuss the merits and shortfalls of these scenarios in section *6.3*.

2.4. Full-plate model construction

2.4.1. Reference frame and plate circuit

The plate reconstructions presented in our model are in essence describing the motions of rigid objects through time on the surface of a sphere using Euler's rotation theorem (McKenzie and Parker, 1967; Morgan, 1968). In common practice, the motion of one plate is often referenced to another plate (determined by geological and/or geophysical data), the motion of which is in turn relative to yet another plate until this circuit reaches the 'root plate' of the hierarchy. This hierarchical structure organising the Euler rotations are referred to as plate circuits. The motion of the root plate relative to an absolute reference frame (e.g., Earth spin axis) is then determined using methods such as palaeomagnetism. In doing so, the absolute motions of all plates can be restored through the translation of the plate circuit — see Domeier and Torsvik (2019) and Seton et al. (2012) for more detailed discussions. Such relative plate circuits with Africa as the root are common choices for plate models concerning the Mesozoic and Cenozoic (e.g., Matthews et al., 2016; Merdith et al., 2021; Müller et al., 2016; Seton et al., 2012; Torsvik et al., 2008a). The rationale behind this popular choice is: (1) the availability of oceanic spreading history surrounding Africa that allows all neighbouring continents to be reliably restored to their relative positions since Pangaea time, and (2) Africa has moved relatively little for the past 200 Ma relative to the mantle plume reference frame (Torsvik et al., 2008a). Due to the absence of pre-Jurassic oceanic lithosphere and pre-130 Ma hotspot tracks, pre-Mesozoic plate reconstructions (e.g., Domeier and Torsvik, 2014; Li et al., 2008a; Merdith et al., 2017) generally have a flatter plate circuit, i.e., more plates directly connect to an absolute reference frame instead of arranging almost all plates in a relative tree structure.

The structure of the plate circuit constructed in our model varies with

Table 3
Matching LIP events on multiple crustal blocks (as shown in Fig. 1).

LIP Timing	Participating Crustal Blocks
2010—1980	n Superior and Wyoming
1980—1960	Karelian, North China, Amazonian, Bundelkhand
1950—1960	North Atlantic, North China
1930—1900	Slave, Kalahari, Siberian, Meta-Incognito
1790—1780	Dharwar, West Africa, Rio de la Plata, Sarmatia, North Australian,
1770—1750	n Laurentia, e Baltica, Siberian, Antarctica, West African. Singhbhum, North China, Amazonian
1740—1690	North Australian, n Laurentia, North China
1670—1640	West African, Baltica, North China, North Australian
1640—1620	North China, n Laurentia
1590—1600	Gawler, w Laurentia, Rio de la Plata, Baltica
1575	West African, Amazonia
1520	West African, Amazonia
1500	São Francisco, Greater Congo, Siberian
1460—1420	Amazonia, Bastar, e Laurentia, Baltica, West Australian
1380	w Laurentia, Antarctica, Siberian, Greater Congo, Baltica, ne Laurentia, West African
1320	North Australian, North China
1270—1250	n Laurentia, s Siberia, e Laurentia, Baltica, North Atlantic, Brasilia belt
1240	e Laurentia, Antarctica
1210	Yilgarn, North China, Amazonia
1115 (−1085)	Laurentia, Congo, Amazonia, Kalahari, Bundelkhand, Gunehogna
1075—1090	Australian, sw Laurentia
920	North China, São Francisco, Congo
880—860	Congo, West African, Tarim
820—780	South China, West Austrlia, w Laurentia, Kalahari, Brasilia belt (Amazonian craton?), South Chian, Tarim
755	Greater Indian, West Australian, North China, South China, Congo
720	n Laurentia, s Siberian, Kalahari, Grunenhogna
615—550	South America, West Africa, Baltica, e Laurentia
535	sw Laurentia, South American (Amazonia)

the evolving stages of the supercontinent cycle. The plate circuit starts with a rather flat structure at 2 Ga, and becomes progressively more hierarchical as major continents, supercratons and supercontinents assemble, eventually leading to a fully relative structure during the tenure of each supercontinent. The fully relative circuit flattens again to varying degrees with the break-up of each supercontinent. Despite its incapability of constraining absolute palaeolongitude by itself (see sections *2.1*, *2.3, 6.3*), palaeomagnetism remains the only tool that can quantitatively restore the spatial relationship between a plate and the spin axis. For this reason, a palaeomagnetic reference frame is the most logical choice for any Precambrian plate reconstructions. The 2000—540 Ma full-plate model presented in this paper utilises a pure palaeomagnetic reference frame without TPW correction.

2.4.2. *Plate boundaries*

There are three principles guiding the implementation of plate boundaries in our model. The first is adding a plate boundary when there is evidence suggesting the presence of a plate boundary, which is the case for most of the continental arcs and rifts. Subduction zones play a major role in defining mantle structures (Li et al., 2008a; Li and Zhong, 2009; Maruyama, 1994; Zhong et al., 2007). In our full-plate model, the majority of the continental arcs are based on geological evidence (e.g., recognised orogens along ocean-facing continental margins; Supplementary Material 6), and active margins as discussed and shown in Pehrsson et al. (2016), Pisarevsky et al. (2014a) and Martin et al. (2020). The drawing of oceanic arcs has less constraints, but we normally add them when there is a need for a subduction zone but the facing continental margin either has a passive margin (Bradley, 2008) or has no clear orogenic record.

The second principle is adding a plate boundary when there is a geometrical or kinematical need for a plate boundary although clear geological support is lacking. For example, a mid-ocean ridge must be developed if two plates are moving apart even if there are no clear records of passive margins. The ridges implemented under this principle sometimes result in oceanic plates without any bordering continental crust. The motions of such plates are more artificial but the plates generally move toward the bounding active plate margins (subduction zones) when applicable. Similarly, when two plates move relative to each other dextrally or sinistrally, transform boundaries are required to accommodate such motions.

The third principle is geodynamic considerations. As predicted by the geodynamic model presented in this paper, a subduction girdle surrounding the supercontinent will form during and after the assembly stage. A modern example is the Pacific 'Ring of Fire' as a subduction girdle that existed since Pangaea assembly. Following this geodynamic consideration, we added some oceanic arcs and occasionally continental arcs in order to maintain a subduction girdle surrounding the supercontinent. The plate reconstruction of the superocean outside of the girdle is speculative, but we used the evolution of the Pacific Ocean since Pangaea time (the Panthalassa superocean) for guidance. We implemented the Mirovia-1 and -2 superoceans external to Nuna and Rodinia, respectively, to mimic the evolution of the Panthalassa superocean: it started with a simple three-plate scenario until the nascent Pacific plate grew out of the triple junction as the Panthalassa superocean got older and shrank into the present-day Pacific Ocean, accompanied by the formation of new triple junctions (see Matthews et al., 2016, for example).

3. A revised Nuna reconstruction and evolution history

The Paleo-(?) to Mesoproterozoic supercontinent Nuna (Hoffman, 1997) (Fig. 2), also known as Columbia (Rogers and Santosh, 2002), was first comprehensively reconstructed by Zhao et al. (2002) primarily through the cross-continental correlation of global 2.1—1.8 Ga orogenic belts, leading to the early belief that Nuna formed by ca. 1.8 Ga. Subsequent palaeomagnetic (Kirscher et al., 2019; Kirscher et al., 2021; Pisarevsky et al., 2014a) and geological work (Nordsvan et al., 2018; Pourteau et al., 2018; Thorkelson and Laughton, 2016; Thorkelson et al., 2001; Volante et al., 2020a; Volante et al., 2020b) demonstrated that Nuna completed its assembly at ca. 1.6 Ga, and broke up at ca. 1.3 Ga. The earlier, global 2.1—1.8 Ga orogenic events are now interpreted as recording the assembly of major cratons or supercratons/megacontinents prior to the final assembly of the supercontinent (Wang et al., 2021). Noting the debate regarding the naming of this Mesoproterozoic

Table 4
Locations of possible mantle plume centres determined from the LIP record (mainly radiating dyke swarms), most being shown in the animations (Supplementary Materials 7–9).

LIP	Age (Ma)	Lat.	Long.	Criteria	Block	Reference	Confidence
Paraupebas-Piranhas-Itabaiana event	535	0.0	−50.0	convergence of dykes	South America (ne)	Teixeira et al. (2019)	medium
Wichita LIP	550	32.5	−95.0	intersection of Wichita rift with Laurentian margin	Laurentia (s margin)	Hanson et al. (2013)	medium
CIMP (590—570 Ma) LIP-North American portion	580	45.2	−72.6	radiating swarm	Laurentia (e margin)	Ernst and Bell, 2010	high
CIMP (615 Ma) LIP- North American portion	615	46.4	−61.0	slight convergence to south of Long Range dykes	Laurentia (e margin)	Ernst and Bell, 2010	high
CIMP (615 Ma) LIP-European portion	615	60.0	5.0	convergence Egersund & Baltoscandian dykes (after correction for cratonward thrusting)	Baltica (w margin)	Ernst and Bell, 2010	medium
Irkutsk LIP	720	51.0	104.0	converging dykes at Irkutsk promontory	Siberia (s margin)	Ernst et al. (2016)	high
Franklin LIP	725	75.0	−120.0	radiating swarm	Laurentia (n margin)	Fahrig (1987)	high
Mundine Well LIP	755	−30.2	114.1	slightly radiating swarm, densest portion of swarm, aulacogen setting for dykes	Yilgarn (w margin)	Fig. 16 in Ernst and Buchan (2001)	medium
Gunbarrel LIP	780	50.0	−130.0	radiating swarm	Laurentia (w margin)	Park et al. (1995)	high
Gannakouriep LIP	790	−30.0	17.0	radiating swarm	Kaapvaal (sw margin)	Ernst and Buchan (1997)	medium
Gairdner-Willouran LIP	824	−36.4	140.2	approx. Extrapolated intersection of Gairdner swarm with southern edge of craton.	Australia (s margin)	Li et al. (1999)	high
Bahia event	920	−15.0	−37.5	radiating dyke swarm and mapped flow directions in dykes	Amazonia (e margin)	Correa-Gomes and Oliveira (2000); Evans et al. (2016b)	high
Dashigou LIP	925	33.7	118.1	radiating swarm	North China (s margin)	Peng et al. (2011)	high
Warakurna LIP	1070	−25.6	129.1	location of Giles Complex	Australia (central)	Wingate et al. (2004)	medium
Keweenawan LIP	1100	45.5	−87.5	Goodman Swell	Laurentia (central)	Buchan and Ernst (2019)	high
Umkondo LIP -Kalahari portion	1110	−20.6	22.2	intersection of Okavango extension zone with NW Botswana rift	Kalahari (nw margin)	Fig. 1 in De Kock et al. (2014)	high
Abitibi LIP	1140	46.0	−89.0	radiating swarm	Laurentia (central)	Fig. 9 in Ernst et al. (2018)	medium
Sudbury [dyke] LIP	1240	44.8	−75.9	aulacogen setting for swarm	Laurentia (se margin)	Fahrig (1987)	medium
Mealy event	1250	62.0	−35.0	based on reconstruction with CSDG pulses of Baltica	Laurentia (e margin)	Fig. 5 in Söderlund et al. (2006)	low
Mackenzie LIP	1270	71.0	−116.0	radiating swarm	Laurentia (n margin)	Baragar et al. (1996)	high
Central Scandinavian Dolerite Group (CSDG) event	1270	72.0	5.0	convergence with Mealy dykes in reconstruction. Clear radiating swarm from aeromagnetic data, but uncertainty in age and match with CSDG.	Baltica (nw margin)	Fig. 6 in Goldberg (2010)	medium
Yanliao LIP	1320	42.4	117.7	extrapolated trend of Datong dykes with craton margin	North China (ne margin)	Zhang et al. (2017)	medium
Derim-Derim-Galiwinku	1320	−11.0	135.0	radiating swarm	North Australia (n margin	Kirscher et al. (2021)	high
Bastar-Cuddapah event	1890	15.5	83.5	converging dykes of Bastar & Dharwar cratons	Indian (e margin)	Ernst and Srivastava (2008)	high
Curaçá-Diamantina event	1500	−11.0	−43.3	approx convergence of 1505 Ma dykes	São Francisco (nw margin)	Ernst et al. (2013b); Silveira et al. (2013)	medium
Kuonamka LIP	1501	69.4	125.2	convergence with 1505 Ma dykes of São Francisco craton in reconstruction with Siberia	Siberian (e margin)	Ernst et al. (2013b)	medium
Arnhem (ca. 1740—1670 Ma) event	1740	−9.7	140.6	placed at inferred break-up margin	North Australian (n margin)	Fig. 3 in Goldberg (2010)	medium
Timpton LIP	1770—1750	64.0	120.0	convergance of 1750 Ma dykes	Siberia (central)	Gladkochub et al. (2022); Gladkochub et al. (2010)	medium
Xionger-Taihang LIP	1780	34.0	112.0	link with Xiong'er rift system; radiating swarm	North China (south central margin)	Peng et al. (2008); see also Peng et al. (2022)	medium
Wiluna event	1843	−25.2	117.3	placed at inferred break-up margin	Yilgarn (nw margin)	Fig. 3 in Goldberg (2010)	medium
Circum-Superior LIP (Thompson centre)	1880	57.5	−95.0	radiating swarm; locus of high-Mg magmatism	Superior (nw margin)	Ernst and Bleeker (2010)	medium
Circum-Superior LIP (Chukotat centre)	1880	61.8	−75.3	locus of high Mg magmatism	Superior (ne margin)		medium

(*continued on next page*)

Table 4 (*continued*)

LIP	Age (Ma)	Lat.	Long.	Criteria	Block	Reference	Confidence
Ghost-Mara River-Morel LIP	1885	61.1	−117.3	possible convergence of Ghost swarm to SW, and possible extrapolated trend of 1900—1870 Ma Fishtrap Lake dykes	Slave craton (sw margin)	Fig. 3 in Buchan et al. (2010)	medium
Hartley-Tsineng (Waterberg-Olifantshoek) LIP	1920	−27.9	20.6	slight convergence of Tsineng swarm to west	Kalahari (w margin)	Goldberg (2010)	high
Kennedy LIP	2010	41.4	−104.5	rift parallel dykes, and ultramafic intrusions	Wyoming (se margin)	Cox et al. (2000); Summers et al. (1995)	medium

supercontinent (i.e., Nuna vs. Columbia; see Meert, 2012; Evans, 2013; Evans et al., 2016a), we follow the argument of Evans (2013) and use the name Nuna for the remainder of this paper.

3.1. Nuna's two-stage assembly, configuration, and break-up

The core components of Nuna, consisting of Laurentia, Baltica, Siberia, North China, Amazonia, and Australia-East Antarctica, are reasonably constrained both geologically and palaeomagnetically, with numerous recent reconstructions sharing many similarities (e.g., Evans and Mitchell, 2011; Kirscher et al., 2021; Li et al., 2019; Pisarevsky et al., 2014b; Wu et al., 2005; Zhang et al., 2012a). Fig. 3 illustrates palaeomagnetic evidence for the configuration of Nuna (Fig. 3a-b), its two-step assembly at ~1780 Ma (e.g., Evans and Mitchell, 2011; Wu et al., 2005; Zhang et al., 2012a) and ~1600 Ma (Kirscher et al., 2021; Pisarevsky et al., 2014b) (Fig. 3c-d), and its break-up after ~1300 Ma (Kirscher et al., 2021) (Fig. 3e). We use Fig. 3a to define the common APWP of both proto-Nuna (Fig. 3c inset for ca. 1780—1600 Ma; APWP is shown as dashed green line in Fig. 3a) using poles from Laurentia, Baltica and North China, and that of the completely assembled Nuna (Fig. 3d inset for ca. 1600—1300 Ma; APWP is shown with solid green line in Fig. 3) using poles from Laurentia, Baltica, Siberia and North China (Table 1). We then use the generated spline APWP, taking into account of the weight assigned to each of the weighted-mean poles, as a guide to place continents with three or fewer palaeopoles (e.g., Amazonia, Congo-São Francisco, India, and West Africa; Fig. 3b) within Nuna (Fig. 2). Continents with no palaeomagnetic constraints are placed in Nuna based on geological considerations. For example, Cathaysia of

Table 5
Euler rotations for reconstructing supercontinents Nuna and Rodinia to present-day Laurentia. Elat/Elon: latitude/longitude of the Euler poles; Eangle: the rotation angle of the Euler poles.

Rodinia				Nuna		
Craton/block/terrane	Elat (°N)	Elon (°E)	Eangle (°)	Elat (°N)	Elon (°E)	Eangle (°)
Greenland	61.8	−133.0	−11.0	61.8	−133.0	−11.0
Amazonia	11.6	−46.3	−107.1	53.9	−100.0	130.5
São Francisco	−25.7	152.0	209.1	1.9	40.5	−169.8
Río de la Plata	5.1	−50.7	−117.2	−15.4	23.0	−161.4
Baltica	75.8	−95.8	−59.2	47.5	1.5	49.0
Siberia (Angara-Anabar)	77.0	98.0	137.0	77.0	98.0	137.0
Siberia (Aldan)	77.3	112.6	159.1	77.3	112.6	159.1
India	47.4	155.1	148.2	1.1	159.3	207.1
Tarim	82.9	42.1	−241.4	55.2	−31.8	132.8
North China	33.1	76.8	70.6	33.7	17.3	39.0
Madagascar	27.2	124.9	143.7	−20.2	153.1	167.1
W. Africa	25.4	−23.4	−121.1	47.2	35.0	−169.1
Kalahari	13.7	−33.5	−160.7	5.3	45.0	−202.7
Congo	−22.7	166.7	259.3	18.0	60.0	−179.6
N. Australia	38.6	135.3	103.6	38.2	82.9	99.1
W. Australia	25.6	151.7	127.7	38.2	112.8	113.7
S. Australia	25.6	151.7	127.7	37.5	119.2	120.7
E. Antarctica	13.4	139.4	119.4	22.8	109.4	128.1
Dronning Maud Land	17.0	−19.5	−109.8	22.4	−134.6	188.1
Cathazia				53.9	158.4	−175.3
Yangtze				55.9	−160.3	171.9
Oaxaquia	17.1	−71.0	−89.8			
Chortis	22.2	−71.1	−110.9			
Paranapanema	5.9	−43.7	−100.4			
Parnaíba	9.9	−44.6	−107.1			
East Svalbard	50.2	−109.9	−34.5			
Rockall	−84.8	6.3	29.7			
Arabia	43.1	134.9	152.1			
Afif-Abas	37.5	132.8	160.0			
Lut (Iran)	39.6	131.2	146.4			
South China	54.2	158.1	−176.0			
Lhasa	40.0	146.8	172.3			
Hoggar	23.7	−58.6	−181.8			
Sahara	23.7	−58.6	−181.8			
Bayuda	23.7	−58.6	−181.8			
Rayner	11.4	118.7	109.8			

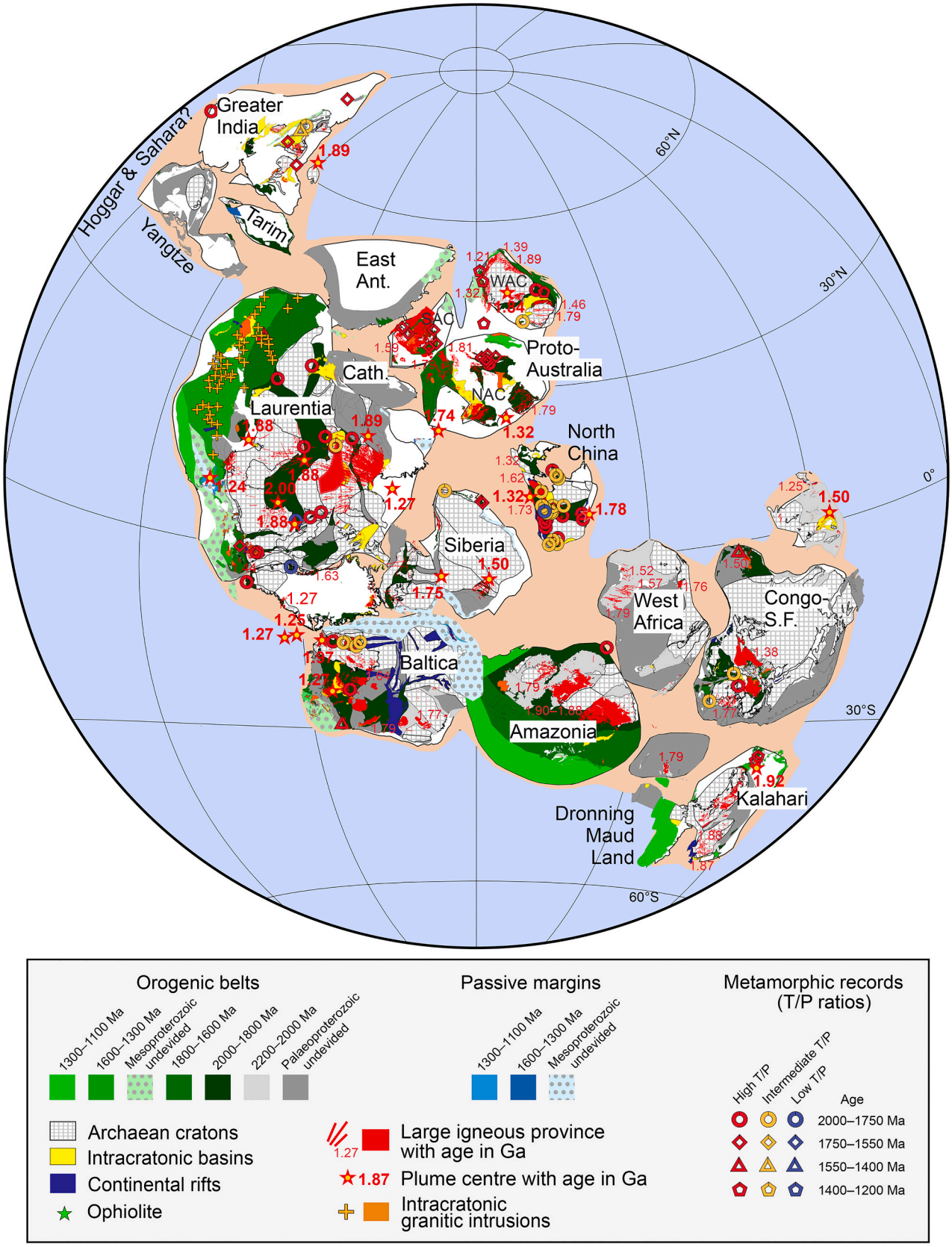

Fig. 2. A revised reconstruction of Nuna using both geological and kinematic constraints, and by matching palaeomagnetic poles with the common APWP for the core continents (Fig. 3). The Euler rotations for the reconstruction are given in Table 5. Lambert Equal Area Azimuthal projection with map centre at (15°N, 00°E) following the 1400 Ma reconstruction. Geotectonic features of 2000—1200 Ma are highlighted. Ant. = Antarctica; SAC = South Australian craton; WAC = West Australian craton; NAC = North Australian craton; Cath. = Cathaysia, South China; S.F. = São Francisco.

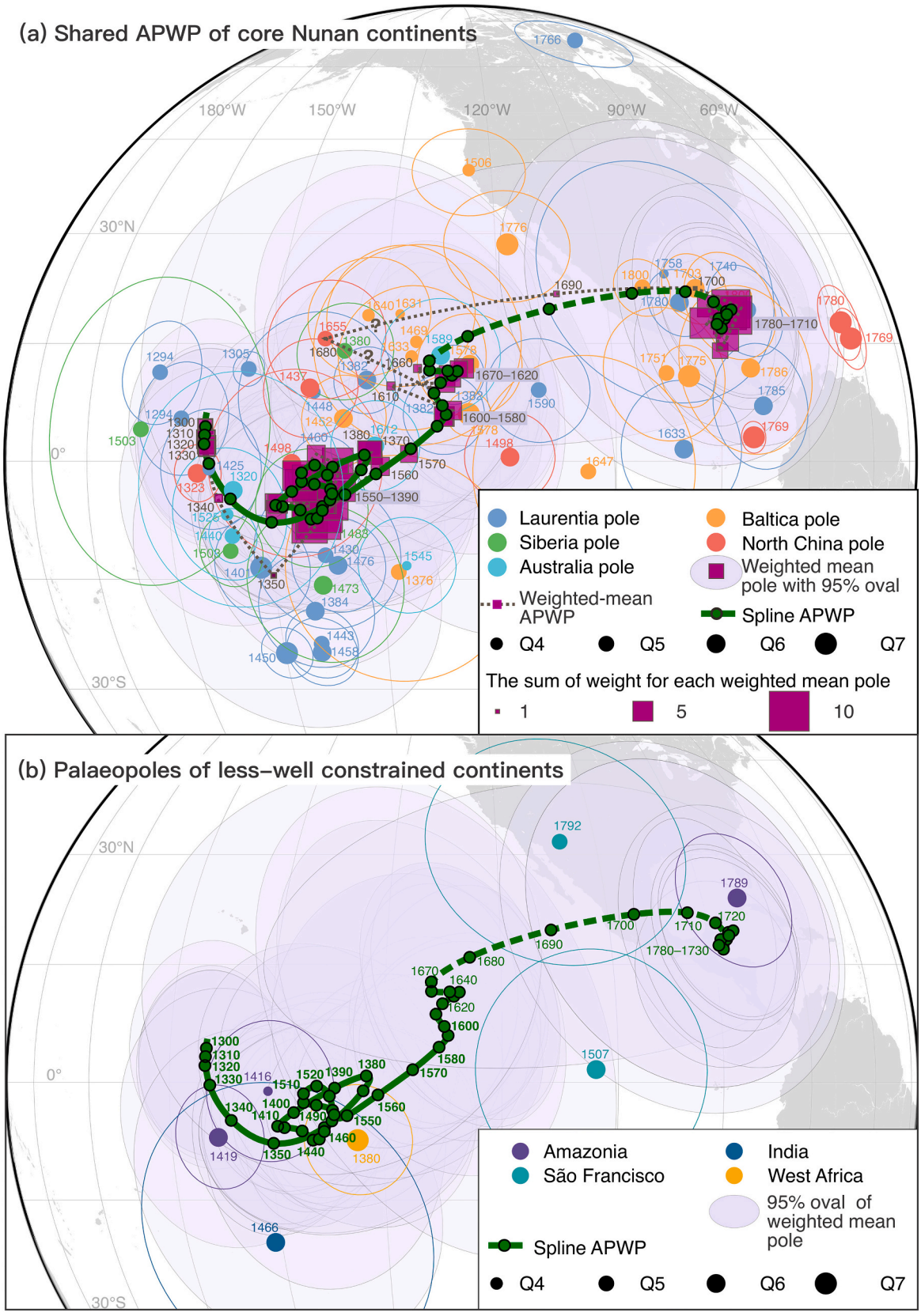

Fig. 3. Palaeomagnetic constraints on Nuna reconstruction. Palaeomagnetic poles are plotted on present-day geography. (a) Continents with more than three palaeopoles each, with Laurentia, Baltica and North China starting to share a common APWP from ca. 1780 Ma (Evans and Mitchell, 2011), whereas Australia and Siberia (which may have joined earlier — see (c) and *3.1*) poles joining this common APWP from ~1600 Ma. The weighted mean poles, their A95 error ovals, and the spline APWP, are also shown with only the solid APWP marking that of the fully assembled Nuna. (b) Reconstruction of continents with three or fewer poles against the APWP defined in (a). Note that the weighted mean and spline poles listed in Table 2 are recalculated using all poles shown in (a) and (b). (c) First phase (Phase-1) of Nuna assembly as illustrated by the merging together of poles from individual cratons prior to ca. 1780 Ma. (d) The second phase (Phase-2) of Nuna assembly

bringing Australia-East Antarctica and possibly India to join Laurentia by ~1600 Ma. (e) Palaeopoles diverge after 1300 Ma, signalling the break-up of Nuna (after Kirscher et al., 2021). Palaeopoles and corresponding A95s are colour-matched with the corresponding continents (see Table 1 for selected 1600—1300 Ma pole list). In (c)-(e), the spline APWP is based on grand weighted-mean poles as in Table 2. The sizes of all poles reflecting either their Q factors (for individual poles) or their weights (for weighted mean poles).

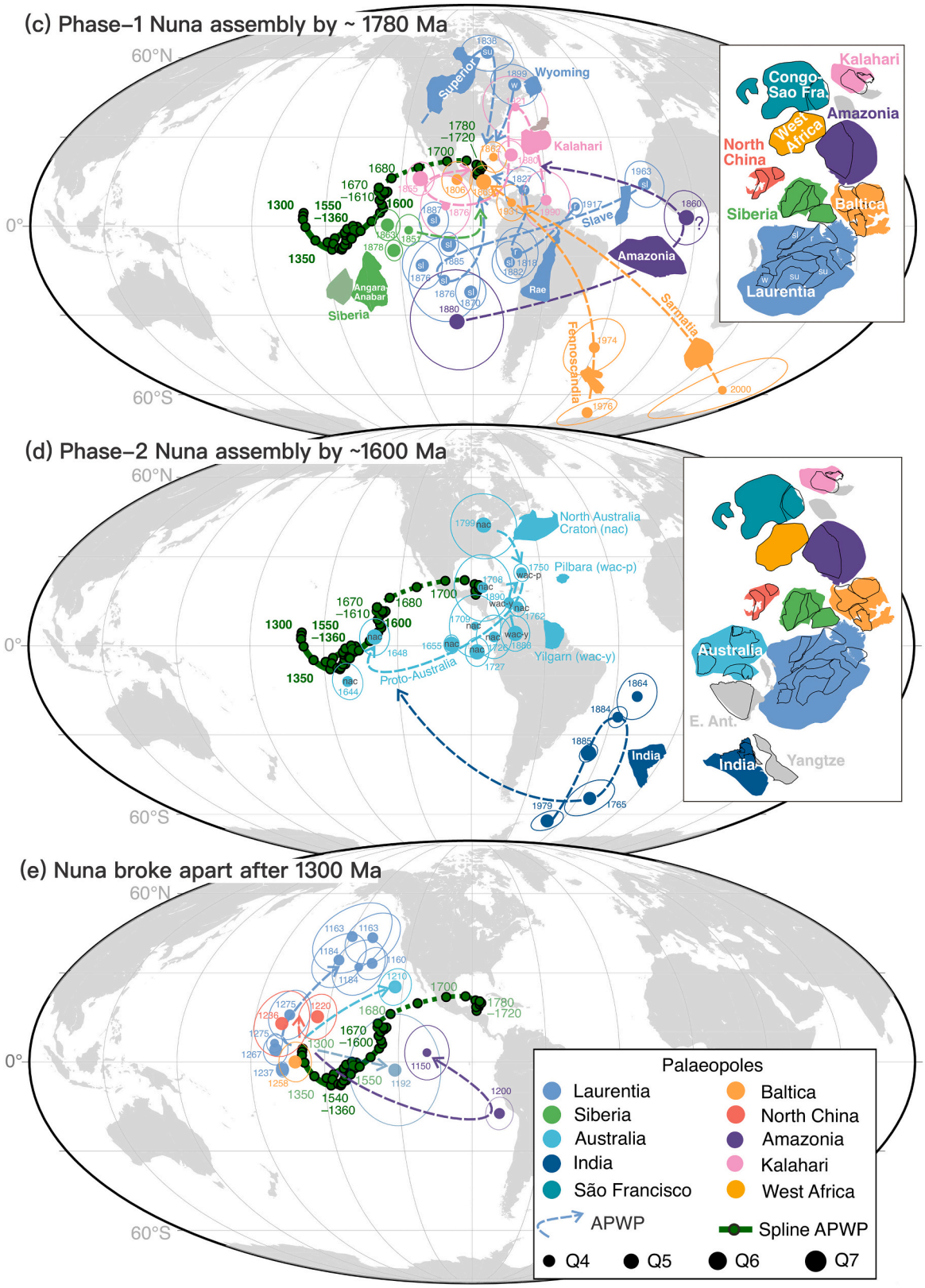

Fig. 3. (*continued*).

South China is placed against western Laurentia following Li et al. (2002), East Antarctica (part of the Mawson continent) is attached to North Australia, and Yangtze is placed close to India to allow an easy transit to its position in Rodinia.

Nuna's two-stage assembly and its configuration as in Fig. 2 are based on palaeomagnetic as well as geological evidence, including two generations of orogens dated at ca. 2.0—1.8 Ga and ca. 1.6 Ga representing the two stages of Nuna assembly (Figs. 2, 3, and Supplementary Material 7). Cratons involved in the first step (Phase-1) of Nuna assembly by ca. 1780 Ma (Zhang et al., 2012a) include Laurentia, Baltica, Siberia, North China and Amazonia, all with relatively good palaeomagnetic evidence (Fig. 3a-c). Siberia likely joined the Slave Craton by ca. 1840 Ma as shown by their 1880—1870 Ma palaeopole proximation in Nuna configuration (Fig. 3c), as noted by Evans and Mitchell (2011) and Zhang et al. (2012a). This is also consistent with geological evidence for a collisional event in southern Siberia (Donskaya, 2020) which could reflect its collision with the Slave Craton (Priyatkina et al., 2020). Likewise, the collision between the newly assembled Siberia and North China cratons likely occurred along the northern margin of the North China Craton (the Paleoproterozoic North Hebei Orogen of Kusky and Li, 2003, and Kusky et al., 2007; also called the Northern Margin Orogen by Wu et al., 2022) during 1.90—1.85 Ga (Kusky and Li, 2003; Kusky et al., 2016; Wu et al., 2022). Congo-São Francisco likely also joined proto-Nuna by that time as indicated by the rough fit of its two palaeopoles (with one being ca. 1.79 Ga) with the reference APWP in Fig. 3b. Kalahari and West Africa are inferred to have joined during Phase-1 Nuna

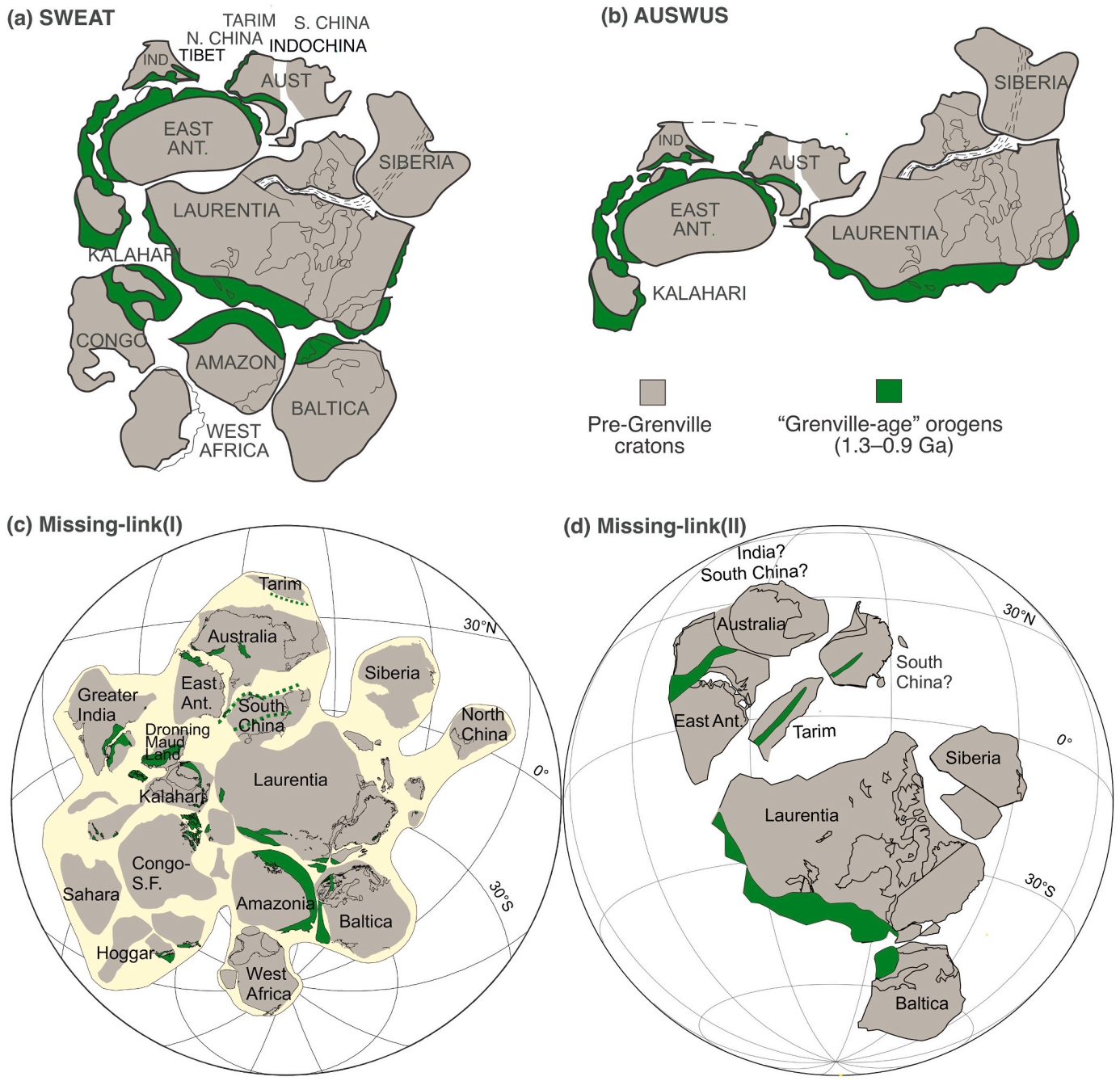

Fig. 4. Selected Rodinia reconstruction models from the literature: (a) Southwest U.S.–East Antarctica (SWEAT) connection (Dalziel, 1991; Hoffman, 1991; Moores, 1991), (b) Australia-Southwest U.S. (AUSWUS) connection (Brookfield, 1993; Karlstrom et al., 1999), (c) Missing-link connection-I (Li et al., 1995; Li et al., 2008a), (d) Missing-link connection-II (Wen et al., 2018).

assembly with Kalahari having numerous 1.9—1.8 Ga poles falling close to that of the other assembling cratons (Fig. 3c), whereas West Africa is only constrained by one 1380 Ma pole (Gong et al., 2021; Fig. 3b). The Phase-1 Nuna assembly occurred almost simultaneously with the assembly of these continents themselves (for example, Laurentia itself was generally believed to have assembled by ca. 1800 Ma; Evans and Mitchell, 2011; Hoffman, 2014; Swanson-Hysell et al., 2021; see section *5.1*) or soon after their individual cratonic assembly (e.g., Siberia; Donskaya, 2020).

Both palaeomagnetic (Kirscher et al., 2019; Pisarevsky et al., 2014b) and geological (Furlanetto et al., 2016; Nordsvan et al., 2018; Pourteau et al., 2018; Thorkelson and Laughton, 2016; Volante et al., 2020a; Volante et al., 2020b) evidence point to the collision of proto-Australia-East Antarctica with western Laurentia at ca. 1.6 Ga, signalling the completion of Nuna assembly with a proto-SWEAT (southwest U.S.-East Antarctica; Moores, 1991) configuration (Phase-2 Nuna assembly; Figs. 2, 3a and d inset). Fig. 3d also illustrates the assembly of proto-Australia through the collision of North Australia (nac), Yilgarn (wac-y) and Pilbara (wac-p) by ca. 1.75 Ga (Johnson, 2014), and that together, proto-Australia joined proto-Nuna by ca. 1.6 Ga (Kirscher et al., 2019). India (and possibly also Yangtze) may also have joined Nuna by that time, although India's position is only constrained by a single ~1466 Ma pole (Fig. 3b) and no prior pole is available until ~1765 Ma and older (Fig. 3d). Sedimentary provenance links between eastern Australia and western Laurentia also started to occur from ca. 1.6 Ga (Brennan et al., 2021a; Nordsvan et al., 2018; Verbaas et al., 2018) and terminated at ca. 1.3 Ga (Brennan et al., 2021a), supporting a ca. 1.6 Ga final assembly of Nuna and its ca. 1.3 Ga break-up.

3.2. Using LIP record to test Nuna configuration

There are some convincing cases of using the LIP record to restore past continental connections during Nuna time. One such case is the connection of North China with North Australia at 1320 Ma through matching the Yanliao LIP of North China with the Derim-Derim Galiwinku LIP of the North Australian craton (Zhang et al., 2017, 2022) for which there is also palaeomagnetic support (Kirscher et al., 2021; Wang et al., 2019), with a plume centre defined by the Galiwinku radiating swarm of the North Australian craton (Fig. 2).

Another such example is the long-lived connection between northern Laurentia and southern Siberia between 1800 and 720 Ma, supported by common LIP records of ca. 1770—1750, 1700, 1640, 1380, 1270—1260, and 720 Ma (Ernst et al., 2016). Arguably the most significant constraint is the 720 Ma match between the Franklin LIP in northern Laurentia and the Irkutsk LIP in southern Siberia, with a well-defined plume centre (on the basis of a robust Franklin radiating swarm). This 720 Ma event is also inferred to mark the timing of break-up of Siberia from Laurentia. It should be noted that some authors (e.g., Cawood et al., 2020; Pisarevsky et al., 2021) prefer a significant separation rather than a tight fit between northern Laurentia and southern Siberia.

The Baltica-Laurentia connection, as constructed using palaeomagnetic constraints (Fig. 3), is also supported by common LIP records between 1750 and 1250 Ma. Key matches include the 1770—1730 Ma (peak 1750 Ma) Kivalliq event (Pitz-Nueltin, McRae, Wellington, Cleaver portions) of northern Laurentia with the 1750 Ma Aiski (Navysh) event of eastern Baltica, the 1380 Ma Midsommerso-Zig Zag Dal event of Greenland with the 1385 Ma Mashak event of eastern Baltica, and the 1270—1250 Ma Central Scandinavian Dolerite Group (CSDG) event with adjacent 1270—1250 Ma events in eastern Laurentia (Fig. 5 in Söderlund et al., 2006) and the 1270 Ma Mackenzie event in northern Laurentia. Not all the matching ca. 1750 Ma and 1270—1250 Ma LIP records of the two continents are proximal, which could be caused either by the occurrences of more than one plume at a time, or by lateral migration of plume heads beneath crustal blocks (e.g., Bright et al., 2014).

Another, less well documented example, is the positioning of South Australia (Gawler craton) adjacent to NW Laurentia at 1590 Ma based on shared LIP records and with paleomagnetic support (Hamilton and Buchan, 2010; Rogers et al., 2018).

4. A revised Rodinia reconstruction

The reconstruction of Rodinia is much more contentious than that of Nuna due to poorer palaeomagnetic constraints (see a recent review by Evans, 2021). Here we first provide a brief review of some of the major Rodinia reconstruction models, then present a Rodinia reconstruction model updated from that of Li et al. (2008a) based on a new synthesis of palaeomagnetic results as well as other constraints.

4.1. A brief review of major Rodinia models and contentious issues

Early reconstructions of Rodinia were mainly based on the correlations of ca. 1.3—1.0 Ga ("Grenvillian") orogens and Proterozoic basins, particularly Neoproterozoic rift-to-drift margins (Dalziel, 1991; Hoffman, 1991; Moores, 1991). Salient features of those reconstructions include the so-called Southwest U.S.-East Antarctic (SWEAT) connection (Moores, 1991) and the inclusion of almost all known continents that existed during the Proterozoic (Hoffman, 1991; Fig. 4a). However, one key element of the original SWEAT hypothesis, that the Southwest U.S.-East Antarctic connection started from the Palaeoporterozoic and lasted until Rodinia's break-up during late Neoproterozoic, was challenged by both geological observations (e.g., Borg and DePaolo, 1994) and palaeomagnetic data (Pisarevsky et al., 2003a, 2014b; Wingate et al., 2002). To address those difficulties as well as later observations, alternative Rodinia reconstructions were made, including the Australia-Southwest U.S. (AUSWUS; Brookfield, 1993; Karlstrom et al., 1999; Fig. 4b), Australia-Mexico (AUSMEX; Wingate et al., 2002), Missing-link (I) (Li et al., 1995, 2008a; Fig. 4c), and Missing-link(II) (Wen et al., 2018; Fig. 4d) models. The AUSMEX and Missing-link(II) models were made primarily on certain palaeomagnetic considerations, but both lack the necessary counterparts for the Neoproterozoic rift-to-drift margin along the present-day western margin of Laurentia (e.g., Dalziel, 1991).

Other contentious issues regarding Rodinia include (1) the positions of continents beyond the SWEAT-related continents in Rodinia, (2) the question of whether all continents were part of the supercontinent (for example, Kroner and Cordani, 2003, argued that African, southern Indian and South American cratons were not part of Rodinia), and (3) the timing of Rodinia's assembly and break-up. In the IGCP 440 preferred model (Fig. 4c), the final assembly of Rodinia occurred around 900 Ma, and break-up did not occur until post-750 Ma (and more likely post-720 Ma) after ca. 850—820 Ma initial rifting (Li and Evans, 2011; Li et al., 2008a) based on both palaeomagnetic and rift-to-drift transition records. However, in a recently published full-plate reconstruction model (Merdith et al., 2021), Rodinia break-up started as early as ca. 850 Ma with the SWEAT connection broken apart by as early as 800 Ma.

4.2. A revised Rodinia reconstruction based on geological and palaeomagnetic records

We revised the Rodinia reconstruction (Fig. 5) based on an early model of Li et al. (2008a) and Li et al. (2013) using updated palaeomagnetic constraints and geological understandings. Major changes from the Li et al. (2008a) model include (1) a reshaped Australia before 650 Ma, taking into account of a 40° rotation between northern and southern Australian cratons during the late Neoproterozoic, and allowing for a later (post-750 Ma) break-up of Rodinia as indicated by some geological evidence (Li and Evans, 2011; Li et al., 2013), (2) a revised position of the Tarim craton, (3) revised positions of the India and Sahara cratons, (4) revised positions of Siberia and North China, and (5) revised position of the Congo-São Francisco craton (see detailed descriptions in *4.2.2*). A major factor that influenced these changes is the

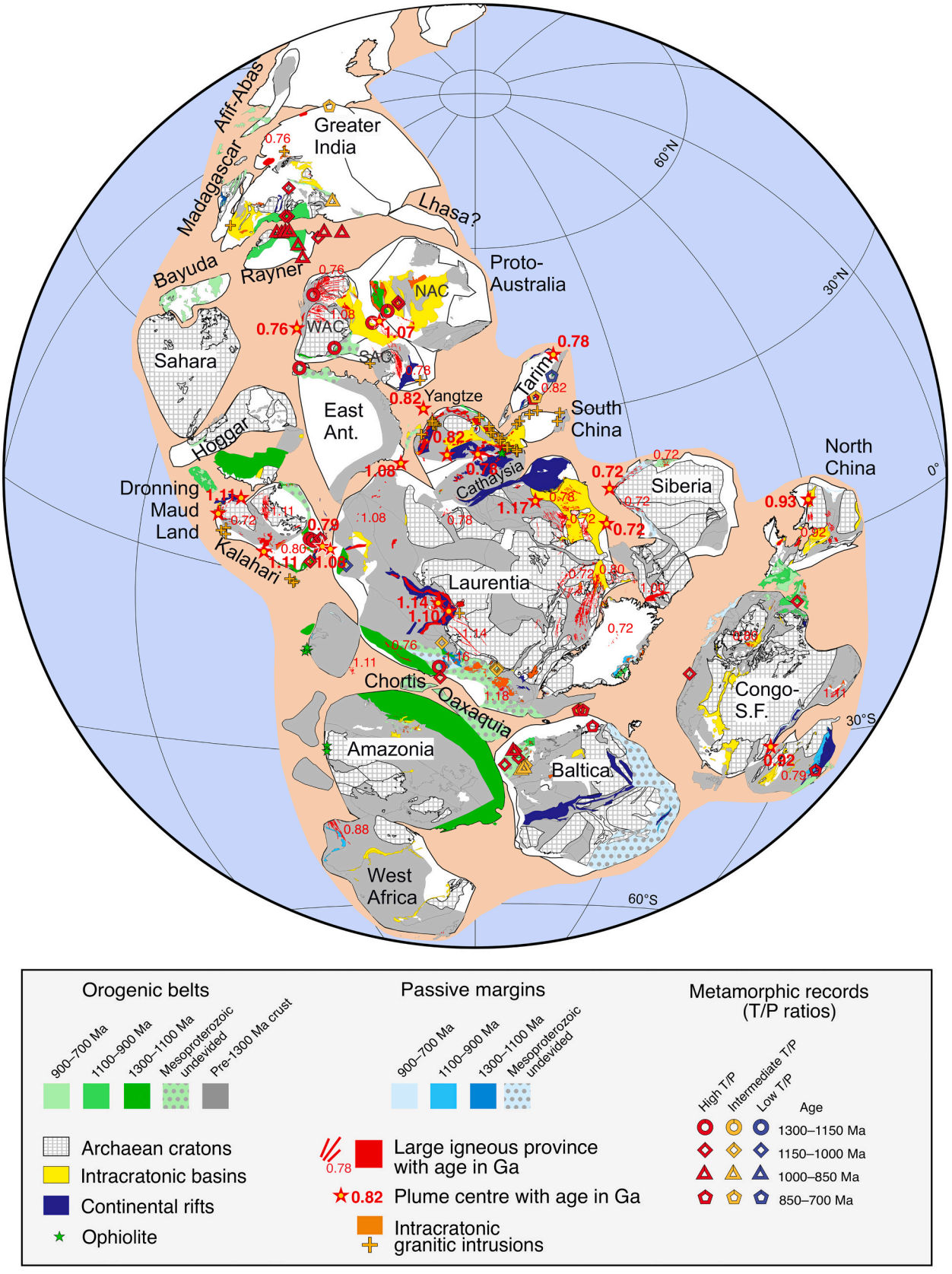

Fig. 5. A revised Rodinia reconstruction based on both geological connections and palaeomagnetism (Fig. 6). The Euler rotations for the reconstruction are given in Table 5. Lambert Equal Area Azimuthal projection with map centre at (20°N, 90°E) following the 850 Ma reconstruction. Geotectonic features of 1200—700 Ma are highlighted. Ant. = Antarctica; SAC = South Australian craton; WAC = West Australian craton; NAC = North Australian craton; Cath. = Cathaysia, South China; S.F. = São Francisco.

much improved, though still sporadic, palaeomagnetic dataset for the mid-Neoproterozoic time, which allowed us to re-evaluate the possible true polar wander (TPW) events during Rodinia time. We are able to use this new and fast moving APWP, based on data from continents with palaeopoles for at least two different ages, as a guide to constrain the relative positions of continents that only have single palaeopoles (e.g., India and West Africa; Figs. 6 and 7; see *4.2.1*). Geological considerations (Ernst et al., 2016; Li et al., 2008a), and transition to the position of each continent both prior to Rodinia's assembly and after its break-up, also provide valuable constraints.

Our Rodinia model (Fig. 5) is still a Missing-link model that features (1) the Cathaysia Block of South China being a part of Laurentia since the Paleoproterozoic (see geological arguments in Li et al., 2008b; Li et al., 2002; Yao et al., 2017) before joining the Yangtze Craton of South China by ca. 900 Ma during Rodinia assembly (Li et al., 2002, 2008a, 2009), (2) ca. 1000—900 Ma orogens and sutures between Australia-East Antarctica and Laurentia to account for the geological disconnections prior to 900 Ma (Borg and DePaolo, 1994) and palaeomagnetic evidence that argues against the existence of any SWEAT-like connection during 1200—1050 Ma (Pisarevsky et al., 2012; Wingate et al., 2002), (3) tectono-stratigraphic correlations of the rift-to-drift record (Brennan et al., 2021b; Li et al., 1995; Powell et al., 1994; Ross, 1991), and (4) mantle plume records of 825—720 Ma LIPs leading to the rifting and eventual break-up of Rodinia (Li et al., 1999, 2003, 2008a, 2022). The central location of South China in Rodinia, based on these evidences as well as our current palaeomagnetic analysis (see *4.2.1* below), has been challenged by numerous studies (e.g., Cawood et al., 2013; Chang et al., 2022; Merdith et al., 2021), but supported by others (Turnbull et al., 2021; Zou et al., 2021). Future verifications of the various competing Rodinia reconstruction models will critically depend on the availability of more high-quality palaeomagnetic poles from all major continents (see below).

4.2.1. *Palaeomagnetic constraints on continental connections and construction of the Rodinian APWP*

The recognition of TPW event(s) during Rodinia time (Li et al., 2004; Maloof et al., 2006) not only turned an otherwise "scattered" pole distribution into an advantage of enabling paired poles- or even APWP-matching for continental reconstruction, it also has geodynamic implications (Li et al., 2004, 2008a; Li and Zhong, 2009) (see section 6). In Fig. 6 we show the varying degree of palaeomagnetic constraints on our Rodinia model: from long-term APWP matching (e.g., the APWP matching between Siberia and Laurentia on the same configuration from Nuna time; Figs. 2, 3 and 6, including their paired palaeopoles for ca. 1050 Ma and ca. 750 Ma), matching of paired palaeopoles for the ca. 900—750 Ma Rodinia time (e.g., the pared ca. ca. 820 and ca. 800 Ma matching palaeopoles between South China and East Svalbard, and that of the ca. 800 Ma and ca. 750 Ma matching palaeopoles between Congo-São Francisco and Tarim; Fig. 6b-c), to constraints provided by single poles (e.g., India and West Africa).

The Liantuo Formation poles from South China (Fig. 6b) are notably discordant when compared with the 780—720 Ma pole cluster (Figs. 6b, 7). The Liantuo Formation has estimated rock ages ranging from as old as ~780 Ma (Lan et al., 2015; Park et al., 2021) to as young as 714 Ma (Lan et al., 2015) or even ~680 Ma as indicated by the youngest detrital zircons (Lan et al., 2015). The Liantuo poles plot close to the 645 Ma Nantuo pole of South China (7b; Zhang et al., 2013), making them less likely to be as old as 780 Ma (Li et al., 2013). Here we interpret that South China broke away from Rodinia by the time of Liantuo Formation deposition, estimated at an average of ~720 Ma. Therefore, the break-up of South China from Laurentia at ca. 720 Ma could also be linked with the proposed break-up of Siberia from Laurentia at 720 Ma in association with the Franklin-Irkutsk LIP/plume (Ernst et al., 2016; see Lu et al., 2022 for matching 720 Ma magmatic event in South China).

We illustrate in Fig. 7 the calculation of Rodinia weighted mean poles for the 900—750 Ma interval (Fig. 7a; note that although Rodinia break-up could have started later than 750 Ma, e.g., Li and Evans, 2011, there is only a single ca. 720 Ma Franklin pole from Laurentia plus two discordant and poorly dated Liantuo poles from South China for the ~720 Ma time), and the spline-smoothed APWP for Rodinia (Fig. 7b). The APWP (Fig. 7) shows the possible occurrence of at least two oscillating TPW events (e.g., that of ca. 860—820 Ma and that of ca. 800—780 Ma, each ca. 60—70°), if not also a smaller ca. 30° event at ca. 900—870 Ma. This modifies the originally proposed single ca. 90° TPW event between ca. 800 Ma and 750 Ma (Li et al., 2004), the two oscillating ca. 55° events during 805—800 Ma and 800—790 Ma respectively as proposed by Maloof et al. (2006), or one ca. 50° event during 820—800 Ma followed by a larger ca. 90° event during 800—780 Ma (Niu et al., 2016), to three possible oscillating TPW events: a ca. 30° event during 900—870 Ma, followed by two ca. 60—70° events during ca. 860—820 Ma and ca. 800—780 Ma respectively (Fig. 7).

We note the recent addition of two new Neoproterozoic palaeomagnetic poles from South China, one being the 832 Ma pole from Fanjingshan mafic sills (Fu et al., 2022), and the other being the pole from 790 to 770 Ma mafic sills (Chang et al., 2022). Although not included in the APWP calculations and the discussion above, neither poles negates our general APWP, TPW and paleogeographic interpretations. The 832 Ma pole with A95 = 8.6° plots on the edges of the 880—840 Ma and 780—750 Ma pole clusters, whereas the 790—770 Ma pole with A95 = 9.9° plots to the middle of the 820—790 Ma pole cluster (Fig. 7a). More Neoproterozoic palaeomagnetic poles with both high technical quality and precisely determined magnetisation age (Meert et al., 2020) are still urgently needed to test Rodinia reconstruction models and refine the likely multiple and rapid Neoproterozoic TPW events (Figs. 6, 7).

4.2.2. *Major changes from the 2008 IGCP 440 Rodinia model*

Australia's 40° intracontinental rotation during the Neoproterozoic. Li and Evans (2011) used a 40° intracontinental rotation between northern and southern Australian cratons during late Neoproterozoic (ca. 650—550 Ma) to reconcile the systematic mismatches of three sets of Australian Precambrian palaeomagnetic poles between ca. 1.8 Ga and 750—650 Ma, and account for the geologically enigmatic ca. 650—550 Ma Paterson-Petermann Orogen that runs across the Australian continent. The recognition of such an intracontinental rotation also allows at least the core part of Rodinia (e.g., Australia-East Antarctica and Laurentia) to remain relatively stable until at least ca. 750—720 Ma if not later, i.e., the tectonostratigraphically defined Rodinia rift-to-drift transition between 715 Ma and 650 Ma (Li and Evans, 2011; see Fig. 4 of Li et al., 2013). This is significantly different from the widely accepted pre-750 Ma break-up time (Li et al., 2008a; Wingate and Giddings, 2000).

Tarim's position. The initial location of Tarim adjacent to Australia's Kimberley craton was mainly based on geological correlations and its subsequent bioprovince connections to Australia and other Chinese cratons during the lower Paleozoic (Li et al., 1996, 2008a). In view of its close similarities to Neoproterozoic stratigraphic and magmatic events in South China, Lu et al. (2008) put Tarim adjacent to eastern Australia in Rodinia, joining South China to fill the gap between Australia-East Antarctica and Laurentia as in the Missing-link model (Li et al., 1995). Subsequent palaeomagnetic and geological correlation by Wen et al. (2017, 2018) revised this configuration into what we call here the Missing-link(II) fit by placing Tarim "below" South China (Fig. 4d).

In this study, we place Tarim in Rodinia through aligning a series of three Tarim palaeopoles at ca. 880 Ma, ca. 800 Ma and ca. 750 Ma with corresponding clusters of poles from other Rodinian continents (Figs. 6, 7), which place Tarim between northeastern Australia and South China (Figs. 5, 6, 7). This configuration shares some similarities with that of Lu et al. (2008). In our configuration, the present-day northwestern margin of Tarim faces the open ocean, allowing for the development of a Neoproterozoic active margin that hosts the mid-Neoproterozoic Aksu blue schists (Xia et al., 2019; Yong et al., 2013).

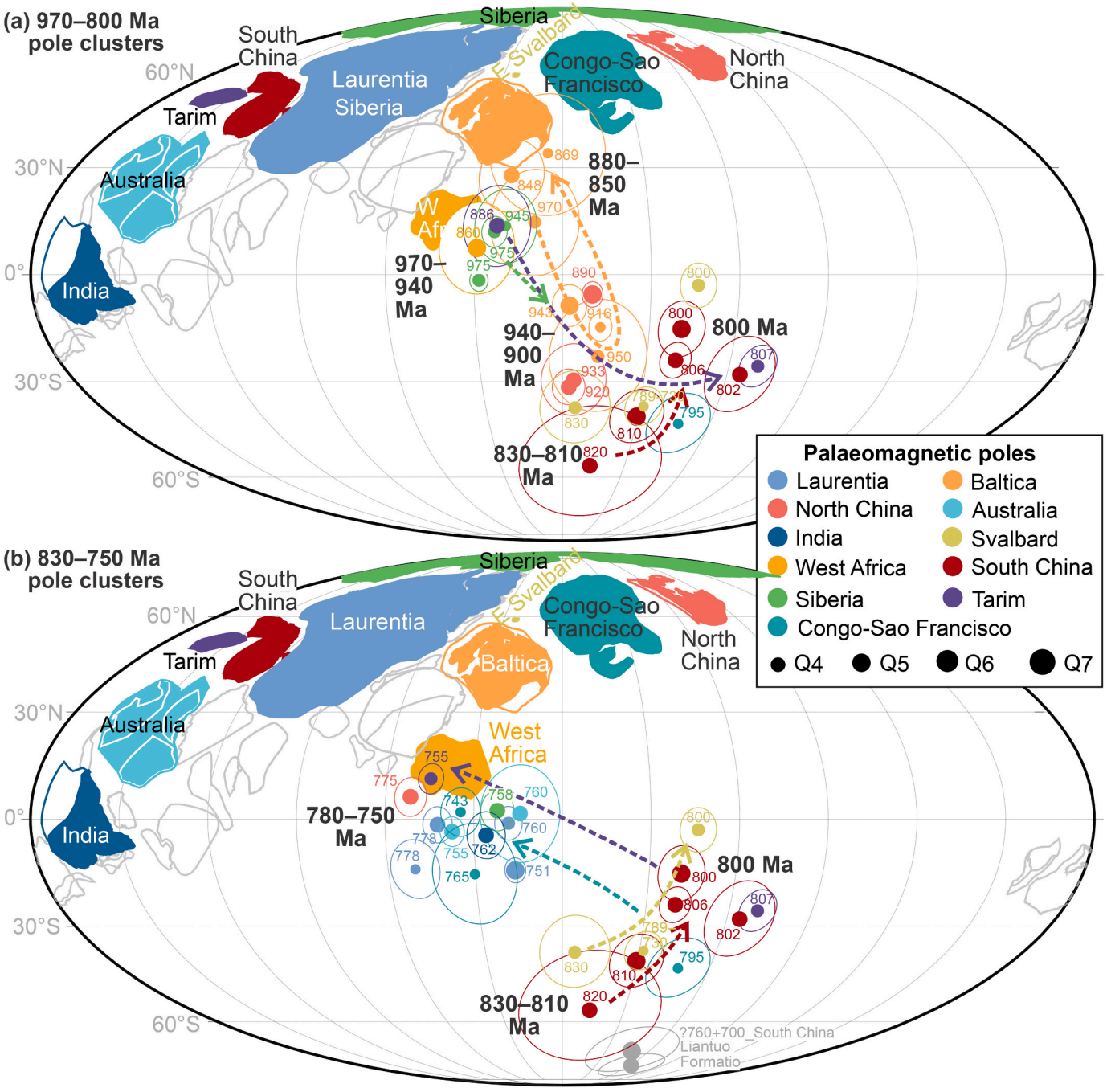

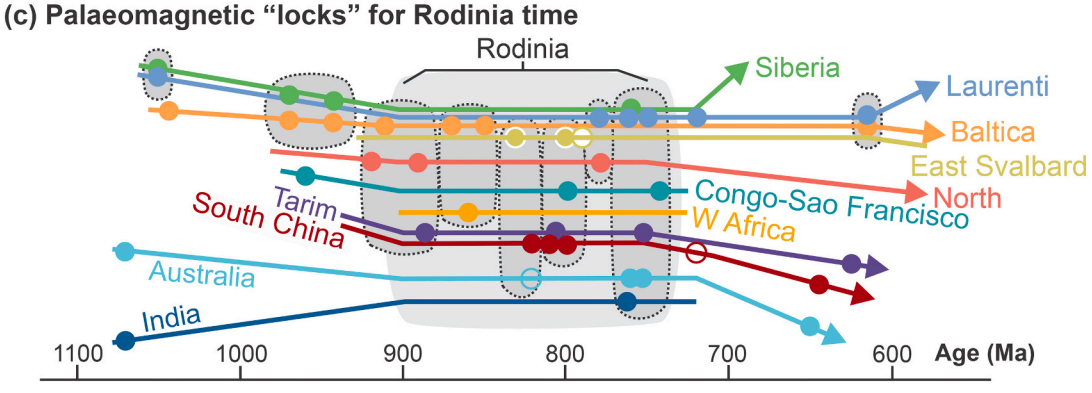

(caption on next page)

Fig. 6. Palaeomagnetic pole clusters shared by different continents during Rodinia time (900 to 750—700 Ma) (a, b, in present-day Laurentia coordinate) and cartoon illustration of the presence of palaeomagnetic "locks" formed by multiple poles from different continents of close ages (c). The most powerful constraints are provided by APWP matching between continents, for example, the ca. 820—800 Ma APWP matching between South China and East Svalbard, and the ca. 800—750 Ma APWP matching between Congo-São Francisco and Tarim (b). Ca. 970 and 945 Ma poles from Baltica and Siberia are also shown in (a) as they approached their Rodinia configuration by ca. 900 Ma. Only continents with selected palaeopoles are coloured, and poles and APWPs are colour-matched with the continents. See Tables 1 and 2 for pole list. The sizes of all poles reflecting either their Q factors (for individual poles) or their weights (for weighted mean poles). The position for East Svalbard generally follows that of (Niu et al., 2016), with the rationale that it stayed with Baltica in that position until the Paleozoic Caledonian Orogeny.

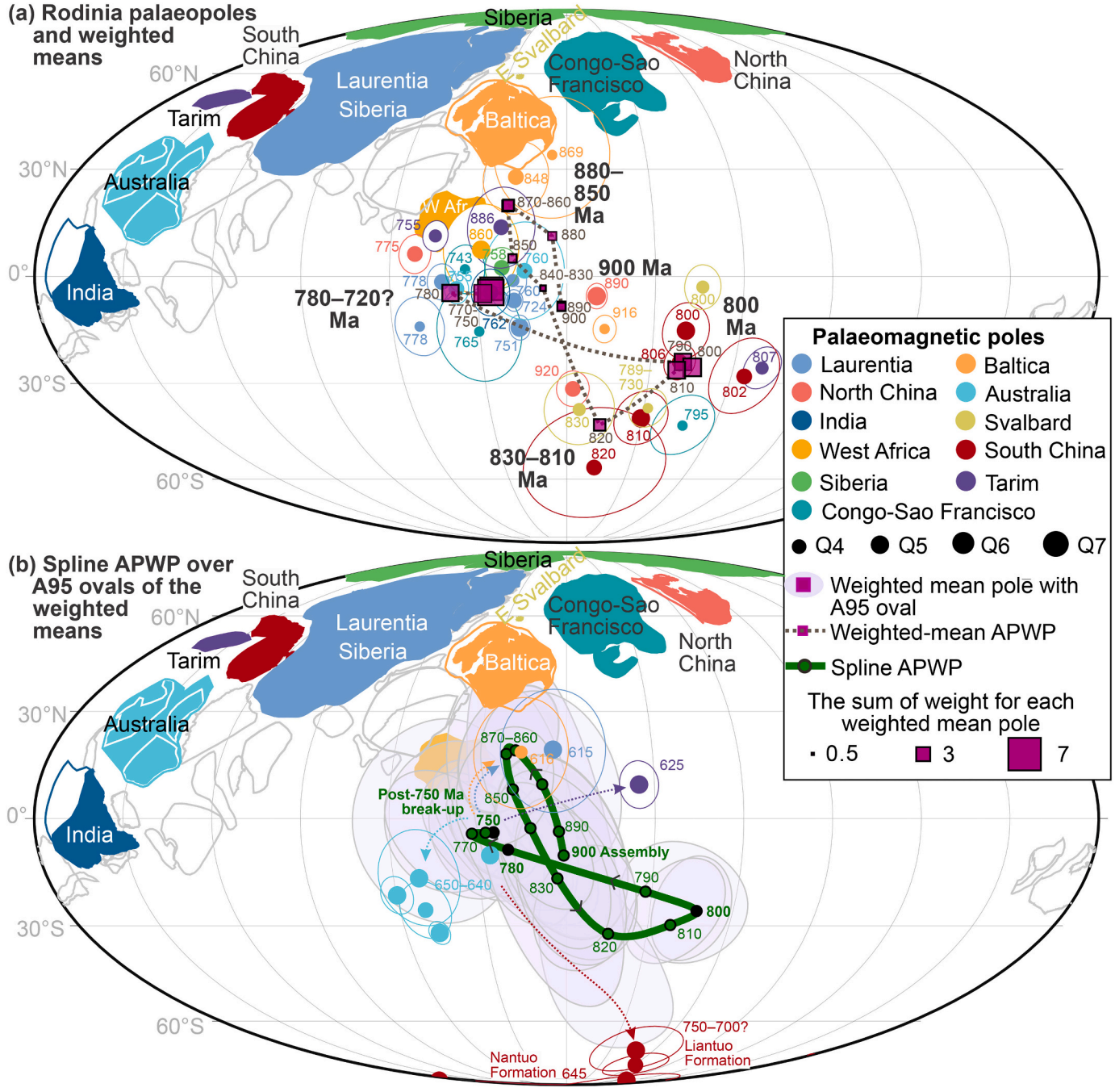

Fig. 7. Reconstruction of ca. 900—750 Ma Rodinian APWP using selected palaeomagnetic poles, with (a) showing the selected poles and their sliding window weighted means following (Wu et al., 2021), and (b) showing the A95 ovals of the weighted means, the spline APWP based on the weighted means, and the post-750 Ma scattering of palaeopoles reflecting Rodinia break-up after that time (though the break-up could have occurred as late as post-720 Ma (Li et al., 2013)). See Tables 1 and 2 for pole list. The sizes of all poles reflecting either their Q factors (for individual poles) or their weights (for weighted mean poles).

Positions of India and Sahara. India was placed in its Gondwana position relative to Australia-East Antarctica in the IGCP 440 Rodinia reconstruction (Li et al., 2008a) following that of the initial Rodinia reconstructions (Dalziel, 1991; Hoffman, 1991; Moores, 1991). To reconcile with the ca. 760 Ma Malani pole (Torsvik et al., 2001), India had to begin rifting away from Rodinia before 780 Ma in that model. In this study, we join India to Rodinia by ca. 900 Ma adjacent to northwestern Australia, honouring the Malani pole, along with the Archaean basement of Madagascar (Tucker et al., 2014) and possibly fragments of the Arabia shield (Figs. 5, 6, 7). This adjacency of India to NW Australia is also consistent with the Malani event in India being linked with the 755 Ma Mundine Well dyke swarm of western Australia (section 8.4.1 in Ernst, 2014). Note that the treatment of the entire Archaean basement of Madagascar as being an extension of India's Dharwar craton (Tucker et al., 2014) is at variance from the model of Collins (2006) which requires a Neoproterozoic suture between them. Two north African cratons, Sahara and Hoggar, which have Archaean basement fragments but no palaeomagnetic or strong geological constraints (Li et al., 2008a), are placed close to India to facilitate subsequent Gondwana assembly.

Positions of Siberia and North China. Whereas the relative position between North China and Siberia is similar to that of the IGCP 440 Rodinia reconstruction (Li et al., 2008a), Siberia's position relative to Laurentia is now better constrained by both palaeomagnetic (Figs. 3 and 6; Evans et al., 2016c) and geological (Ernst et al., 2016) evidence in a configuration similar to that first proposed by Rainbird et al. (1998) that possibly lasted from >1700 Ma till ca. 720 Ma. The position of North China is also supported by the ca. 900 Ma and ca. 770 Ma pole correlation (Figs. 6 and 7).

Position of the Congo-São Francisco craton. Congo-São Francisco is now placed against Greenland of Laurentia (Fig. 5) through matching its ca. 800 Ma and two ca. 750 Ma poles with the two respective pole clusters (Figs. 6 and 7). This is a drastic change from that of the IGCP 440 configuration (Li et al., 2008a), and is also in contrast with arguments that the Congo-São Francisco craton was never a part of Rodinia (Pisarevsky et al., 2003b).

5. A full-plate 2000—540 Ma global history: from cratonic amalgamation to the age of supercontinent cycle

In this section we summarise the global palaeogeographic evolution between 2000 Ma and 540 Ma as five major tectonic stages, covering two supercontinent cycles (Nuna and Rodinia) and highlighting some salient features. A full-plate global animation, displaying the selected databases, is provided in Supplementary Material 7. The palaeolongitudinal scenario presented here is that of the extended-orthoversion *Scenario Ia* (0–90 W–0). An alternative extended-orthoversion *Scenario Ib* (0–90E–0) is presented in Supplementary Material 8. For more detailed discussions regarding the two scenarios see sections *2.3* and *6.3*.

5.1. 2000—1800 Ma: The age of continental assembly before the start of the supercontinent cycle

The continents we see today are typically mosaics of Archaean cratons and younger orogens. Amongst orogens of varying ages, ca. 1.8 Ga orogens feature prominently, both in terms of their cumulative length (Condie et al., 2017) and a related peak in continental crustal growth (Condie, 2005) (Fig. 8). Those orogens played a dominant role in joining the many smaller Archaean cratons into larger continents, leading to the first proposition of the assembly of the supercontinent Nuna/Columbia by that time (Zhao et al., 2002).

We illustrate in Fig. 9 and in the animations (Supplementary Material 7) how >30 Archaean cratonic blocks might have assembled to form the majority of the Precambrian continental blocks as we know today, through a process not dissimilar to that depicted in Pehrsson et al. (2016). It should be noted that some of the cratons shown in our

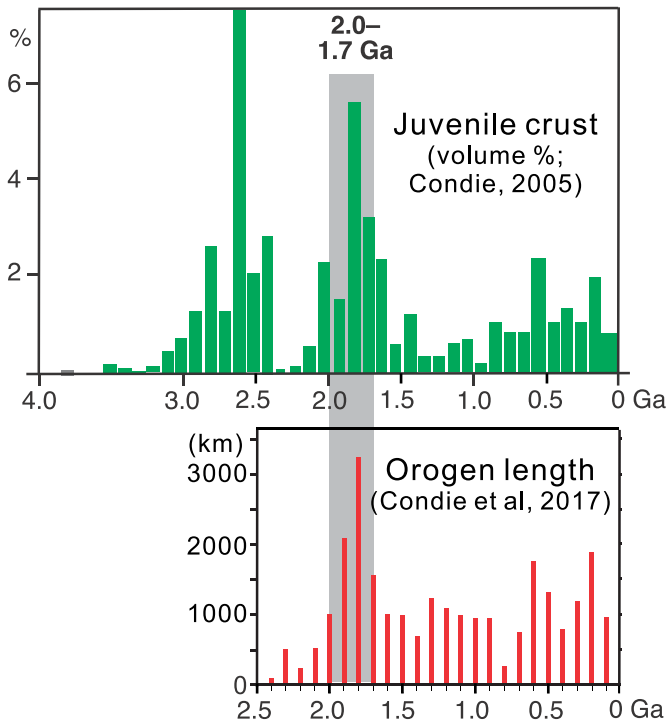

Fig. 8. Time variation of global total orogen length (Condie et al., 2017) and juvenile crustal addition (Condie, 2005), highlighting the importance of the ca. 1.8 Ga global orogenic events. See Fig. 9 and discussion in section *5.1* for the role of these orogens in the formation of the majority of the continental blocks we know today.

2000 Ma reconstruction (e.g., East Antarctica and Congo-São Francisco) (Fig. 9a) might have been oversimplified as coherent cratons at that time due to our lack of knowledge of their basement geology. In reality, each such craton might still consist of more than one continental piece at that time (Pesonen et al., 2021). There are also other Archaean continental pieces currently constituting Sahara that do not appear in our model until 900 Ma due to the lack of geological and palaeomagnetic constraints.

Our starting point at 2000 Ma (Fig. 9a) takes into account palaeogeographic considerations for earlier times, e.g., the Archaean "Vaalbara" (Kaapvaal together with Pilbara; Cheney, 1996; de Kock et al., 2009; Zegers et al., 1998) and "Zimgarn" (Zimbabwe together with Yilgarn; Smirnov et al., 2013) connections as well as global reconstructions (Liu et al., 2021). We also have the Amazonia, West Africa and Congo-São Francisco cratons together by ca. 2000 Ma following Pehrsson et al. (2016) and supported by the ca. 2 Ga orogenic belts between them (Fig. 9a). We adopt the interpretation of Tucker et al. (2014) to take all Archaean basement of Madagascar as an extension of the Dharwar craton of India. For cratons with little constraints, we place them in positions that can be easily transitioned into their better constrained positions in younger reconstructions. This applies to Yangtze and Tarim, both sharing similar ca. 1500 Ma magmatism of possible LIP type with India, with Yangtze and India also both recording ca. 1720 Ma magmatism (Lu et al., 2020; Fan et al., 2020). By having them placed nearby at 2000 Ma (Fig. 9a) and joined together by ca. 1800 Ma (Fig. 9c), it will allow Yangtze and Tarim to move into their Rodinia positions by 900 Ma (see *5.4*).

By ca. 1890 Ma (Fig. 9b) Siberia already completed its assembly (Donskaya, 2020) but Laurentia was only partially assembled (Hoffman, 2014; Swanson-Hysell, 2021). The West Australia Craton (WAC) consisting of the Pilbara and Yilgarn cratons, was assembled by 1950 Ma (Johnson et al., 2011). By 1890 Ma (Fig. 9b), the newly assembled WAC is placed together with India following the 1890 Ma LIP correlation

(Stark et al., 2019) and palaeomagnetic constraints (Liu et al., 2019).

This phase of global continental assembly peaked at around 1800 Ma (Zhao et al., 2002), when the majority of the smaller Archaean cratons have been (or are close to being) joined together to form the continental blocks that we are familiar with today (e.g., Laurentia). Nonetheless, the assembly of possibly the first stable supercontinent Nuna was not yet completed (Fig. 9c). From 1800 Ma, the Cathaysia Block of South China has been added against western Laurentia following the arguments of Li et al. (2002, 2008b) and Yao et al. (2017).

5.2. 1800—1600 Ma: The formation of the first stable supercontinent Nuna and superocean Mirovia-1

Palaeomagnetic analyses demonstrated that Nuna assembly did not complete until ca. 1600 Ma, although the ocean remaining between western Laurentia (present-day coordinate) and eastern Australia may not have been large after 1800 Ma (Kirscher et al., 2019; Pisarevsky et al., 2014a) (Fig. 10a-b). The presence of such an ocean before 1600 Ma is supported by tectonostratigraphic and sedimentary provenance analyses (Betts et al., 2016; Furlanetto et al., 2016; Gibson et al., 2017; Nordsvan et al., 2018; Thorkelson and Laughton, 2016). The closure of that ocean was recorded by the coeval and precisely dated ca. 1600 Ma Isa Orogeny in northeast Australia (Pourteau et al., 2018; Volante et al., 2020b) and the Racklan Orogeny in northwestern Laurentia (Furlanetto et al., 2013) (Fig. 10c).

In our animations we had North China joining proto-Nuna at ca. 1800 Ma adjacent to Siberia (Fig. 3c inset) partly because this is consistent with the palaeomagnetic record (Fig. 3a) as well as the orogenic record (Kusky and Li, 2003; Kusky et al., 2016; Wu et al., 2022; Fig. 9c). On the other hand, Wang et al. (2019) argued for a long-lived (ca. 1780—1320 Ma) connection between North China and North Australia in their Nuna configuration based on both palaeomagnetic and tectonostratigraphic/magmatic pulse correlations. Although both possibilities are currently feasible, we slightly prefer the model we adopt here because of the lack of ca. 1600 Ma orogenic record in either Siberia or North China side, which one would expect to see had North China joined Siberia during the ca. 1600 Ma final assembly of Nuna.

5.3. 1600—1200 Ma: Nuna and its break-up

Nuna maintained a relatively stable position during its lifespan with its geographic centre close to an equatorial position (Fig. 11). This is not dissimilar to that of Pangaea post ca. 270 Ma. The relative moderate counter-clockwise rotation that Nuna experienced around its geographic centre (Figs. 10c, 11) might represent a TPW event similar to that experienced by Pangaea after 250 Ma (Steinberger and Torsvik, 2008; see *6.3* for further discussion).

Early work on Nuna believed that the supercontinent broke apart sometime between 1400 and 1200 Ma (Pisarevsky et al., 2014a; Zhang et al., 2012a), but more recent work was able to more precisely define the break-up time of Nuna to soon after 1300 Ma (Kirscher et al., 2021; Wang et al., 2020a), which makes the lifespan of Nuna to be ca. 300 Myr. A ca. 1300 Ma break-up is further supported by the basin record of western Laurentia (Brennan et al., 2021a) and a global development of large-scale continental rifting during 1.4—1.3 Ga just prior to the break-up (Zhang et al., 2022).

5.4. 1200—900 Ma: Rodinia assembly through introversion?

Here we present a scenario in which Nuna finished its incomplete break-up by 1150 Ma (Figs. 11d, 12a; see *5.7* and Li et al., 2019 for discussion regarding Rodinia's incomplete break-up), and Rodinia was assembled from that point through an introversion process (Li et al., 2019). The introversion assembly process is here defined by the survival of both the circum-Nuna (at the same time also circum-Mirovia-2 superocean) subduction girdle from Nuna time as well as the Mirovia-1 superocean (Figs. 10c, 11, 12) (Li et al., 2019), which may differ from conclusions if one only looks at the life cycle of a particular ocean (e.g., the Iapetus Ocean for the assembly of Pangaea; Murphy and Nance, 2003) or that of an orogen (e.g., the Paleo- to Mesozoic orogens along southern Laurentia for the assembly of Rodinia; Martin et al., 2020). Note that we also follow the dynamic extended-orthoversion principle (Li et al., 2019, after Mitchell et al., 2012) here by having Rodinia assembled ~90° west of the location of Nuna.

Our reconstruction for ca. 1110 Ma is somewhat different from that of Choudhary et al. (2019) in that those authors had Kalahari, Congo, Amazonia, and India remained together (collectively termed Umkondia) at 1110 Ma based on matching an interpreted common LIP event. Further work is needed to examine the feasibility of such a configuration in view of other constraints, including the kinematic needs for all these continents to move from their Nuna positions to their Rodinia positions.

5.5. 870 Ma–750 Ma: Rodinia's rapid motions and early rifting

Following the revised Rodinia APWP (see *4.2.1* and Fig. 7), Rodinia experienced three episodes of oscillatory motion between 900 and 780 Ma along roughly the same longitudinal band: one during 900—870 Ma (Figs. 12d and 13a), one during 870/860—820 Ma (Fig. 13a-b), and one during 800—780 Ma (Fig. 13c-d). Such rapid and oscillating motions, if true, are best explained as representing inertia interchange true polar wander (IITPW) events, with a common axis of rotation close to the geographic centre of the predecessor supercontinent Nuna on the equator (see *6.3* for geodynamic explanations).

Although some models suggest early (e.g. 850—800 Ma; Merdith et al., 2021) break-up of Rodinia, no rift-to-drift transition time, as shown by tectonostratigraphic records, is older than 720 Ma (Powell et al., 1994; Preiss, 2000; Ross, 1991). Palaeomagnetic data (Figs. 6 and 7; *4.2.1*) also favour a post-750 Ma break-up. Here we adopt the thesis of Li et al. (2003, 2008a) that Rodinian intracontinental rifting, accompanied by bimodal LIP and SLIP magmatism, with some showing clear plume tectonostratigraphic or geochemical-petrological signatures (Li et al., 1999; Wang et al., 2007; Zhao et al., 1994), started as early as 860—850 Ma (Li et al., 2010; Shu et al., 2011). LIP magmatism became widespread after 825 Ma with global peaks at 825 Ma, 800 Ma, 780 Ma, 750 Ma (Li et al., 2003), and 720 Ma (Fahrig, 1987; Heaman et al., 1992). Due to the need to have South China breaking out by the time of the Liantuo Formation's deposition (we use a notional age of 720 Ma here; see discussion in 4.2.1), we started Rodinia's break-up at 750 Ma (Fig. 13e), noting that this is a compromise age which might be somewhat earlier than the real widespread rift-to-drift transition age (Li and Evans, 2011), but allows the model to accommodate the pre-720 Ma rift-related crustal extension.

5.6. 750—540 Ma: Rodinia break-up, snowball Earth, and the formation of Gondwana as the early stage of Pangaea assembly

Two major post-750 Ma episodes of break-up events occurred around Laurentia: the post-720 Ma separation of Siberia from Laurentia (Ernst et al., 2016; Gladkochub et al., 2019) (Fig. 14a), and the ca. 650—600 Ma diachronous opening of the Iapetus Ocean through the drifting-away of Amazonia (Robert et al., 2020) and Baltica (Cawood et al., 2016) from Laurentia (Fig. 14b-c). The post-615 Ma break-up of Baltica from Laurentia is supported by both palaeomagnetic evidence (Fig. 6) and by their matching LIP events at 615 Ma and 580—570 Ma (Fig. 1; Supplementary Materials 4 and 9). The ca. 720 Ma Rodinia break-up, accompanied by the Franklin LIP event and matching 720 Ma events in southern Siberia (Irkutsk LIP) and South China (the Hubei-Shaanxi magmatic province), coincides with the start of the Sturtian glaciation interpreted by some as representing the first Neoproterozoic Snowball Earth event (Cox et al., 2016; Hoffman et al., 2017; Lu et al., 2022; Pu et al., 2022). Causes for such catastrophic global glaciation are still debated, with popular factors including: (1) the enhanced effect of

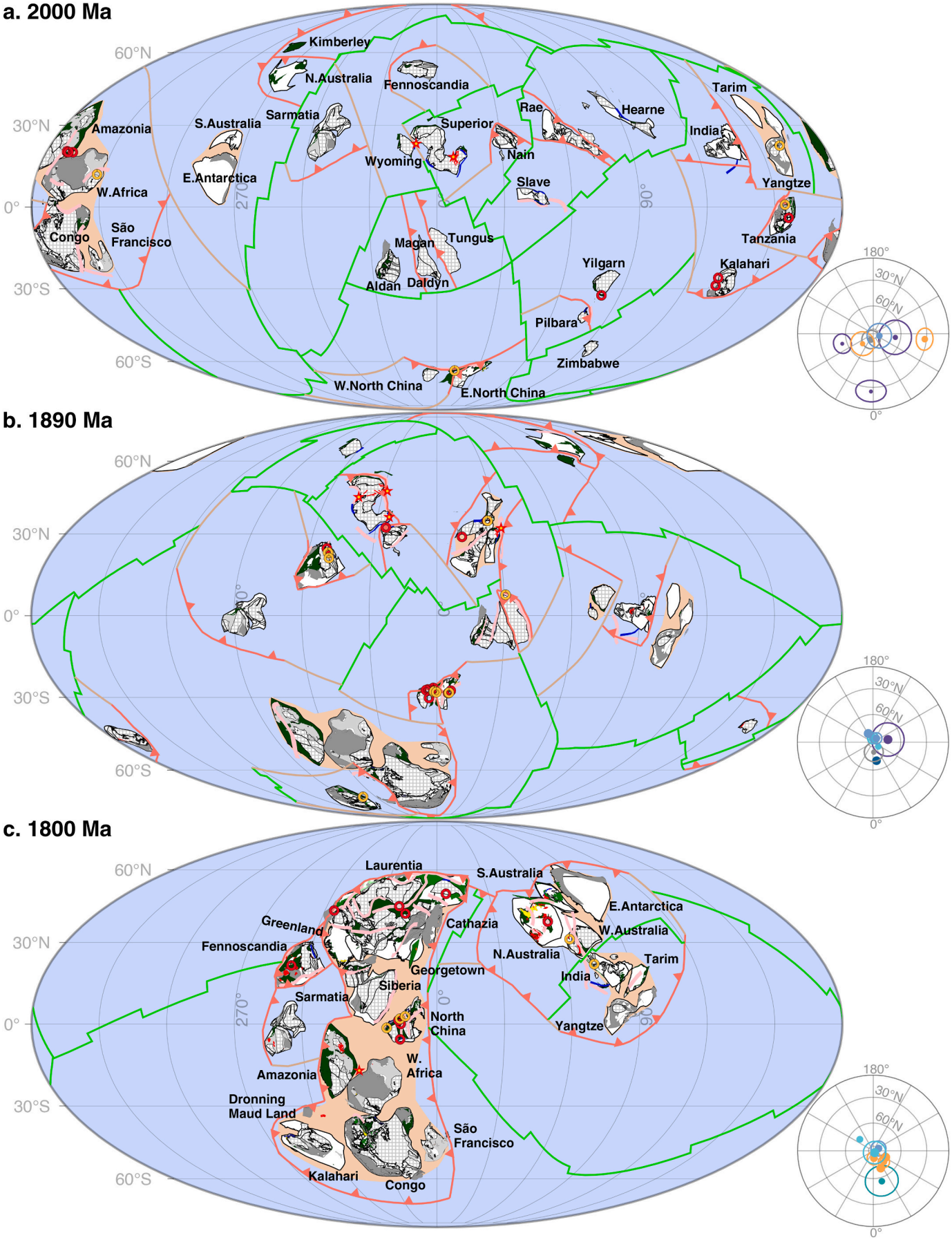
a. 2000 Ma
Kimberley
N.Australia
Fennoscandia
Sarmatia
S.Australia
Amazonia
Superior
Rae
Hearne
Tarim
India
Wyoming
Nain
E.Antarctica
Slave
Yangtze
W.Africa
São Francisco
Congo
Tungus
Magan
Tanzania
Yilgarn
Kalahari
Aldan
Daldyn
Pilbara
Zimbabwe
W.North China
E.North China
b. 1890 Ma
c. 1800 Ma
Laurentia
S.Australia
E.Antarctica
Greenland
Cathazia
W.Australia
Fennoscandia
N.Australia
Tarim
Georgetown
India
Siberia
Sarmatia
North China
Yangtze
W. Africa
Amazonia
Dronning Maud Land
São Francisco
Kalahari
Congo
60°N
30°N
0°
30°S
60°S
270°
0°
90°
180°

Fig. 9. Examples of 2000—1800 Ma reconstructions showing (a-b) early stage of craton assembly and (c) formation of most continental blocks we have today, coinciding with the first-stage assembly of Nuna (Fig. 3c). For this and Figs. 10-14: Mollweide projection with central meridian being 0°E. Relevant palaeomagnetic poles (with their A95s), and the spline-smoothed APWPs for Nuna and Rodinia (Figures are plotted for each time slice). Note that in both the animations (Supplementary Materials 7, 8) and Figures 10-14, as palaeomagnetic poles only appear within their given age ranges, the lack of palaeopole for a particular continent at a particular time does not necessarily mean that the continent's palaeolatitude is totally unconstrained as interpolated poles when applicable (not shown) were often used.

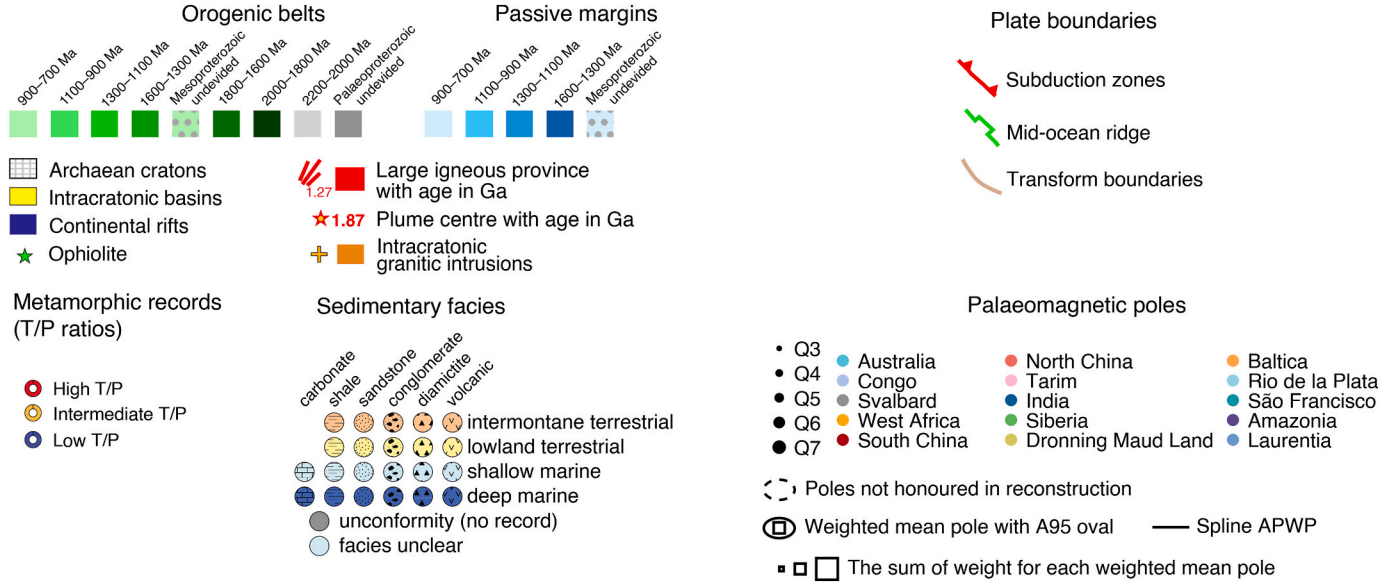

Fig. 9. (*continued*).

continental albedo due to the predominantly low to medium latitudinal positions of continents at the time and runaway ice-albedo feedback (Kirschvink, 1992; Worsley and Kidder, 1991), with the low-latitude distribution of continents attributed to TPW events as a consequence of supercontinent cycle (Evans, 1998; Li et al., 2004; Li and Zhong, 2009), and the expansion of the area of exposed terrestrial land caused by superplume-induced continental doming (Li et al., 2013); (2) equatorial silicate weathering, particularly of plume-induced mafic LIPs, during Rodinia break-up (Cox et al., 2016; Godderis et al., 2003; Goddéris et al., 2017; Lu et al., 2022; Pu et al., 2022); and (3) the enlargement of the area of shallow marine environment during the break-up of Rodinia in both continental rift basins and along passive margins to facilitate primary productivity and thus carbon burial (Hoffman et al., 1998; Knoll, 1991).

By 630 Ma, while Rodinia was still breaking apart (now mostly along the present-day southeast margin of Laurentia, i.e., the opening of the Iapetus Ocean), Earth experienced the second Neoproterozoic global glaciation (snowball Earth?) event termed the Marinoan event (Fig. 14b). This was also the time when Gondwana began assembling. By ca. 600 Ma (Schmitt et al., 2018) (Fig. 14c), West Gondwana was mostly assembled. Gondwana was fully assembled by ca. 540 Ma (Li and Powell, 2001; Meert, 2003) (Fig. 14d). In the interim at ca. 580 Ma occurred the short-duration and possibly local Gaskiers glaciation event, the final one of the Neoproterozoic (Pu et al., 2016; Youbi et al. 2021). The location and motion of South China during late Neoproterozoic follow that of Li et al. (2013) and Yao et al. (2014), and Tarim is placed close to South China due to their close tectonostratigraphic and bioprovince affiliations (Zhou and Chen, 1990).

5.7. *Plate velocity and number*

There is a wealth of data that can be extracted from full-plate models (see Zahirovic et al., 2015 for example). Here we simply extract the root-mean squared (RMS) velocity and the number of plates from our model and compare them with that from the model of Merdith et al. (2021), which is the only other published full-plate model that partly overlaps with the time span of our model. For simplicity, the Merdith et al. (2021) model is hereafter referred to as Mer2021. As the motion of the oceanic plates in our model does not have direct data constraint, for the plate velocity calculation we focus on plates that host continental crust (referred as continental plates hereafter).

The RMS velocities for our *Scenarios Ia* and *Ib* (Fig. 15a) are similar except for the 600—570 Ma period where the eastward motion of numerous continents in *Scenario Ib* result in a faster moving phase compared to *Scenario Ia*. We will focus our discussion below on our preferred *Scenario Ia* model. The overall man RMS of our model for 2000—540 Ma shares a similar value of 7—8 cm/yr as of the Mer2021 for the 1000—0 Ma interval (Fig. 15a). In details, the mean RMS of our model for 2000—1670 Ma is about the same as for the Mer2021 Phanerozoic model, but markedly lower for the 1670—1100 Ma interval, coinciding with the long-held speculation of subdued tectonism (dubbed the "boring billion") for the Mesoproterozoic (e.g., Cawood and Hawkesworth, 2014) possibly due to an introversion assembly of Rodinia (Li et al., 2019; Huang et al., 2022). The most striking contrast between our model and the Mer2021 model lies in the RMS velocity for the mid-Neoproterozoic: whereas our model features episodes of rapid motions with exceptionally high RMS values, the Mer2021 model gives RMS values close to that of the overall mean. These fast motions in our model are attributed to the proposed oscillating and rapid TPW events for Rodinia time based on our palaeomagnetic interpretation (see *4.2.1* and *6.3*) which were not considered in the Mer2021 model.

Another interesting trend is the change in global plate numbers with time, and a comparison of plate numbers between our model and the Mer2021 model for the overlap in Neoproterozoic time (Fig. 15c). According to our preferred model, pre-1800 Ma plate tectonics (Phase-1 assembly of Nuna) was characterised by up to 25, mostly small continental plates compared to the ~5 continental plates during the 1800—1600 Ma Phase-2 assembly of Nuna (see discussed in section *5.1*). In contrast, there were around 10 continental plates during Nuna to Rodinia transition at 1300—900 Ma, but this number increased to up to 16 at ca. 650 Ma after the break-up of Rodinia, which then decreases during the formation of Gondwana. The noticeably lower continental

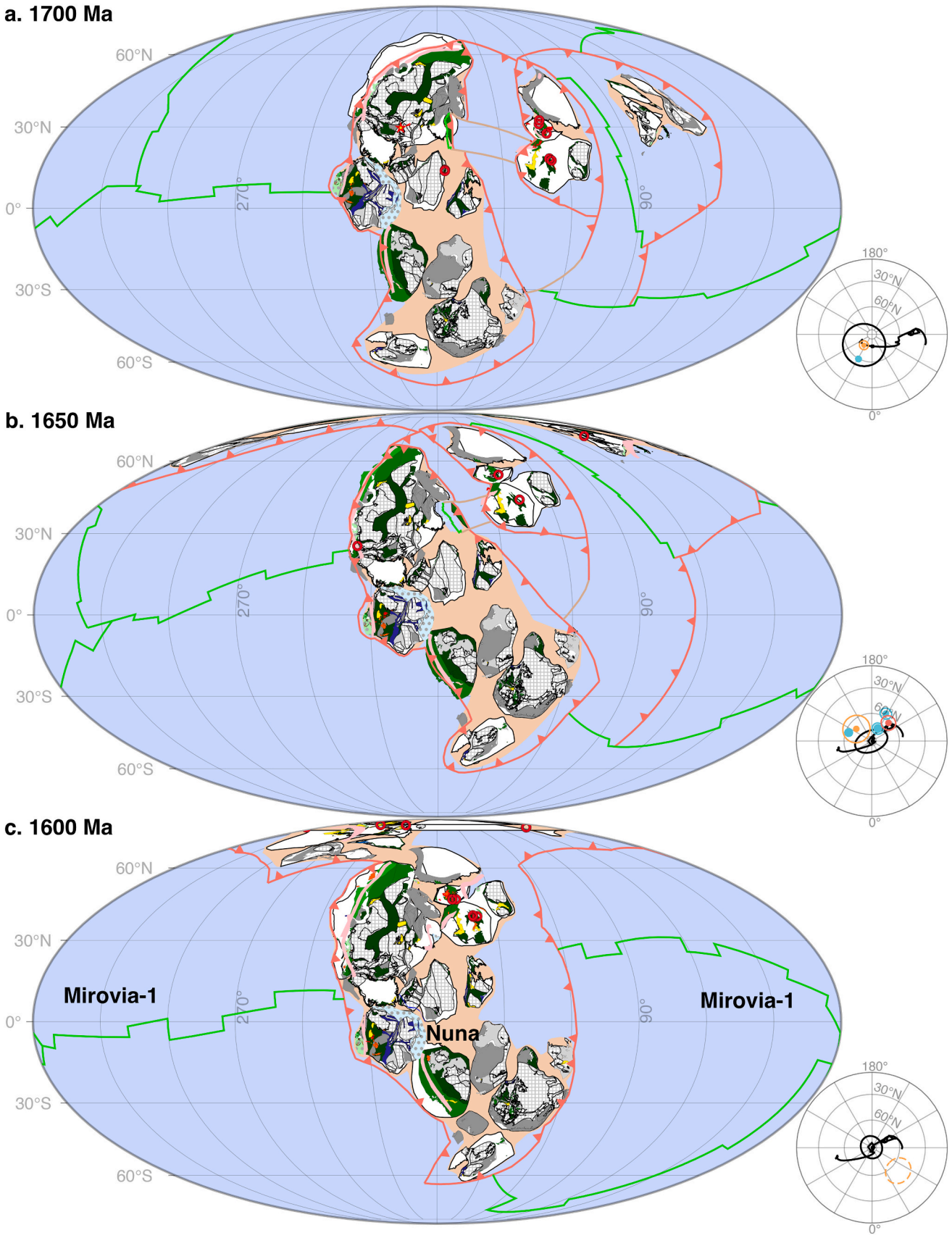

Fig. 10. 1700—1600 Ma reconstructions showing Nuna's final assembly by 1600 Ma.

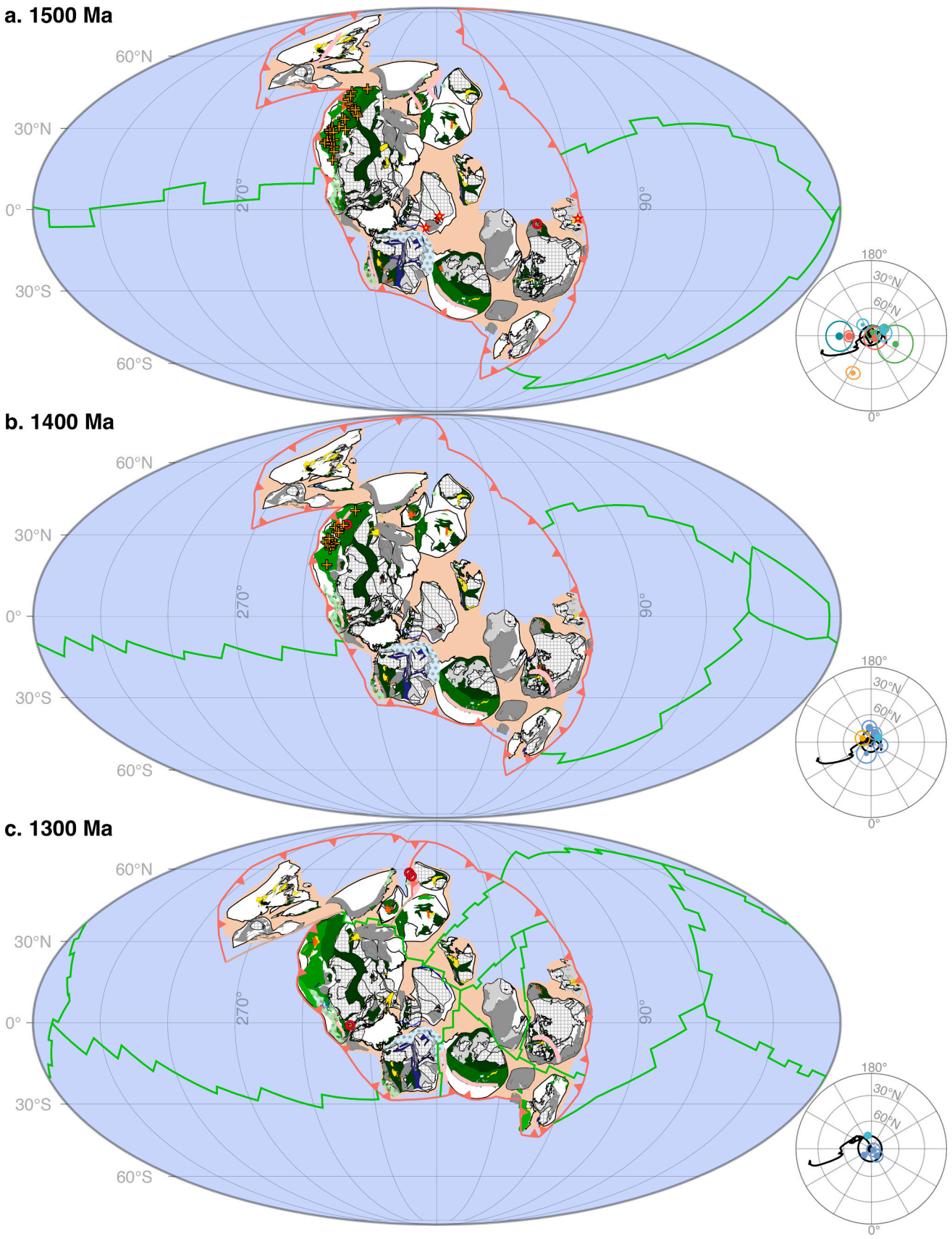

Fig. 11. 1500—1200 Ma reconstructions showing Nuna's moderate counter-clockwise rotation around an equatorial geographic central position since its full assembly at ca. 1600 Ma (Fig. 10c to a-c here), and its break-up after 1300 Ma (c-d).

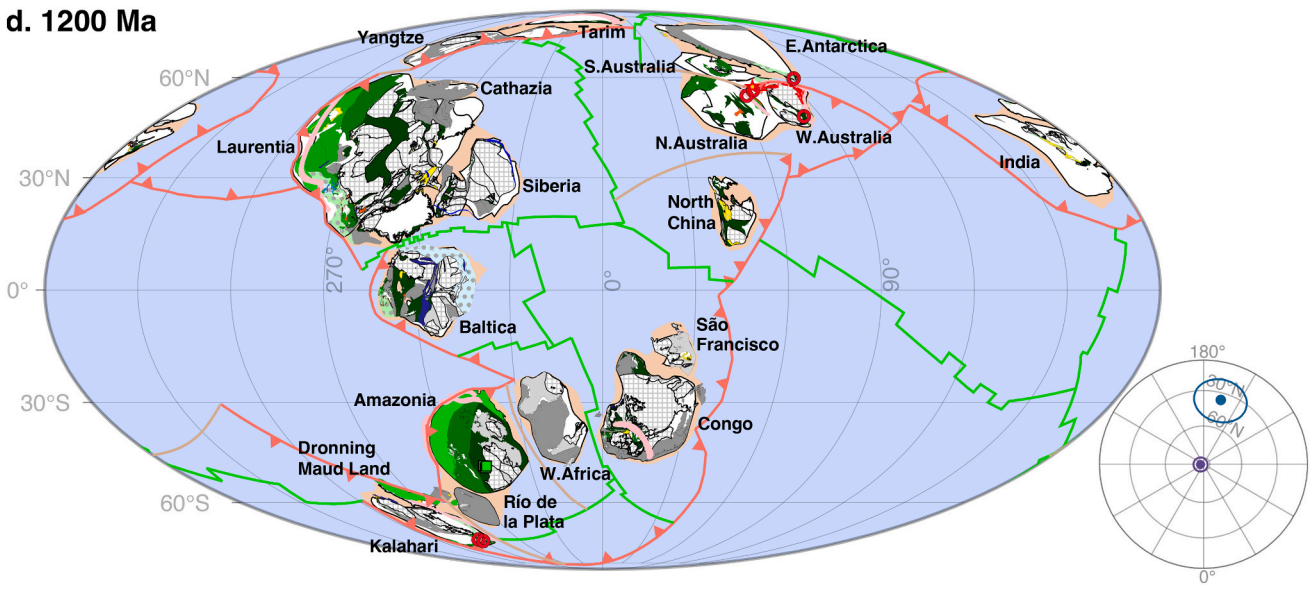

Fig. 11. (*continued*).

plate number after Nuna break-up than the number after Rodinia break-up can be interpreted as due to a more complete break-up of Rodinia after an introversion supercontinental assembly (Li et al., 2019). There are some obvious artificial signals in the plate number such as the simple four-plate configuration during the existence of Nuna and Rodinia, and the sudden step changes at the assembly and break-up points of supercontinents. Such signals resulted from the simplification of our full-plate model, mostly due to the lack of more precise constraints.

The number of plates in our model after 700 Ma is generally comparable to that of the Mer2021 model; however, the two models differ dramatically for the 900—700 Ma interval (Fig. 15c). This reflects the dramatically different reconstructions between the two models for that time interval, which largely coincides with the tenure of Rodinia in our model, whereas in the Mer2021 model Rodinia only had a transient presence.

6. An evolving dynamic system between 2000 Ma and 540 Ma: A transition from the age of supercratons to the age of supercontinents (supercycle plate tectonics), and using geodynamics to constrain palaeolongitude

6.1. Before 1800 Ma: The age of supercratons with smaller but more numerous mantle convection cells

It is now widely accepted that >60% of the continental crust we see today formed by the end of Archaean (ca. 2500 Ma) (Belousova et al., 2010; Dhuime et al., 2012; Windley et al., 2021), although whether subsequent crustal growth has been controlled by the supercontinent cycle is debated (Hawkesworth et al., 2013; Wang et al., 2020b) (Fig. 8a). Geodynamic modelling (Zhong et al., 2007) suggests that for an Earth consisting of many small subduction cells, as might have been the case during the early stage of plate tectonics from at least 3200 Ma (Cawood et al., 2018; Gamal El Dien et al., 2020; Windley et al., 2021), the small subduction downwellings tend to merge into large ones, dragging the small continental blocks to merge into larger continents (Fig. 16a-b). Geological (Bleeker, 2003; Gumsley et al., 2017) and palaeomagnetic (Liu et al., 2021) studies suggest that such processes likely dominated the Archaean–Paleoproterozoic time, featuring the formation and break-up of supercratons. Although a Pangaea-like supercontinent, such as the geologically speculated supercontinent Kenorland (Williams et al., 1991), is believed by some to have existed from >2.5 Ga until 2.1Ga (e.g., Aspler and Chiarenzelli, 1998; Williams et al., 1991), palaeomagnetic data indicate that any such supercontinent, if ever existed, could only have been a transient and unstable one between ca. 2.6 Ga and 2.4 Ga (Liu et al., 2021), with continents possibly moving relative to each other during that time while still remaining as a close cluster. An analogy for such a scenario would be a pack of ice blocks traveling together in a moving river, and we therefore call such a transient and unstable supercontinent an “ice-pack supercontinent”.

Whether a Pangaea-like stable supercontinent existed during the Archaean-Paleoproterozoic time has profound implications to mantle dynamics, mantle structure, and the magnitude and spatial distribution of heat flux across the core-mantle boundary (CMB) (Zhang and Zhong, 2011; Zhong et al., 2007) which in turn impacts the behaviour of the geomagnetic field (Amit and Olson, 2015; Hounslow et al., 2018; Zhang and Zhong, 2011) and possibly also the timing of inner core initiation (Mitchell et al., 2018). The model we adopt here implies that prior to the formation of the supercontinent Nuna between 1800 Ma and 1600 Ma (Figs. 3 and 10), there was no stable degree-1 or degree-2 mantle convection structures as in Fig. 16c-f. Instead, the mantle structure consists of either many small convection cells (Fig. 16a) or these plus a few larger convection cells associated with the occurrences of supercratons (Fig. 16b). Such mantle structures are generally less efficient in loosing heat from the CMB and the surface compared to mantle structures dominated by degree-1 and/or degree-2 mantle convection (Fig. 16c-d) (Zhang and Zhong, 2011; Zhong et al., 2007).

6.2. Post-1800 Ma: Coupled ca. 600 Myr supercontinent and superplume (LLSVP) cycles and longer superocean episodes during the age of supercycle plate tectonics

In our model, by ~1800 Ma, most continental blocks we know today had come together, and proto-Nuna was close to being assembled around Laurentia (Fig. 9c). The mantle structure at that time was probably close to that in Fig. 16b, featuring a growing superdownwelling under proto-Nuna. Nonetheless, a global-scale subduction girdle surrounding most emerging continents, which drives the eventual formation of degree-2 mantle structure (Fig. 16d) (Li et al., 2008a; Zhong et al., 2007), did not start to form until ca. 1700 Ma (Fig. 10a), and completed at ca. 1600 Ma when Nuna was fully assembled (Fig. 10c). We envisage that it was between 1800 Ma and 1600 Ma that Earth’s first stable global subduction girdle formed along with the formation of the first supercontinent over a mantle superdownwelling (Fig. 16c-d), which kick-started a new era of plate tectonics featuring the

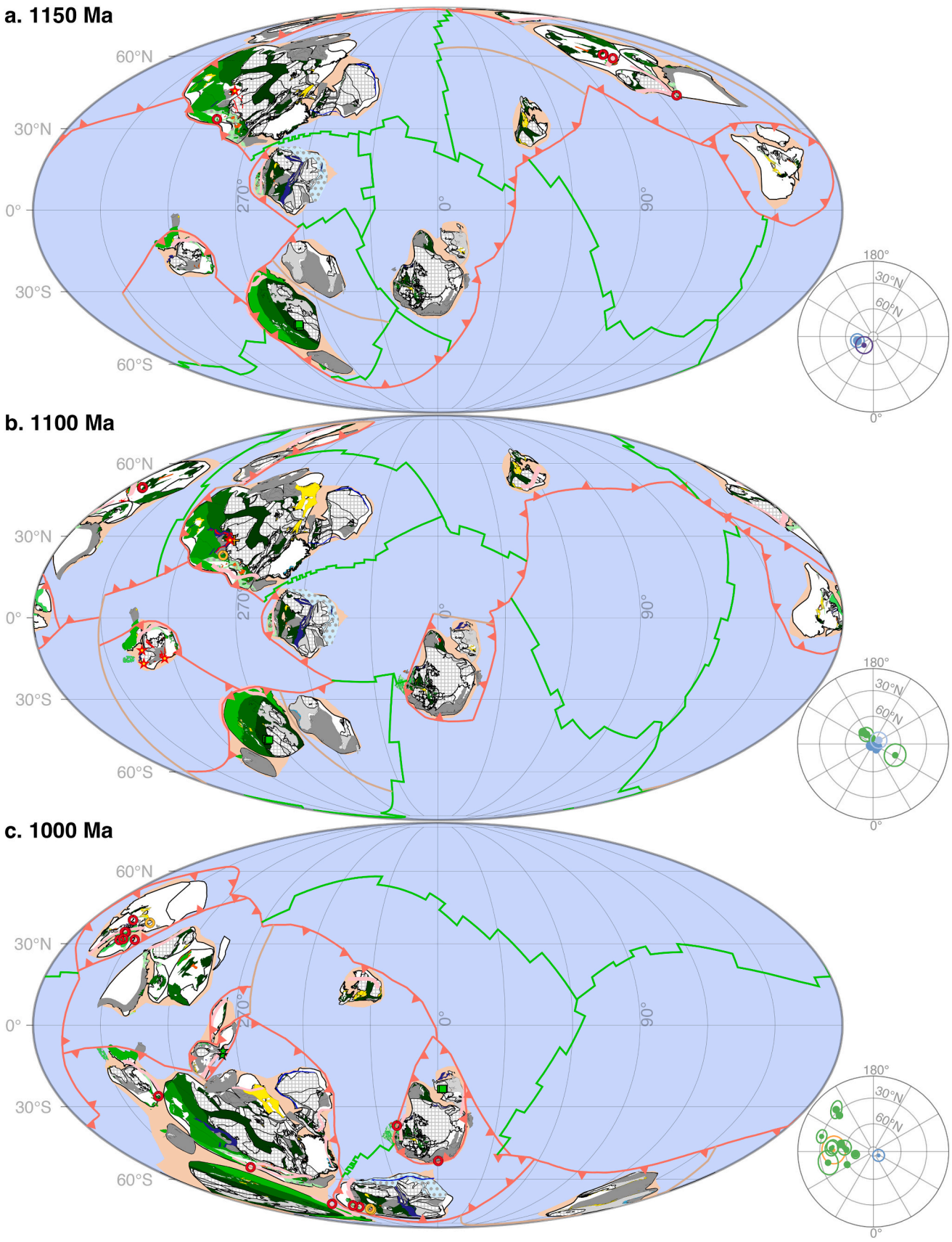

Fig. 12. 1150—900 Ma reconstructions showing Rodinia's introversion assembly confined within a long-lived subduction girdle.

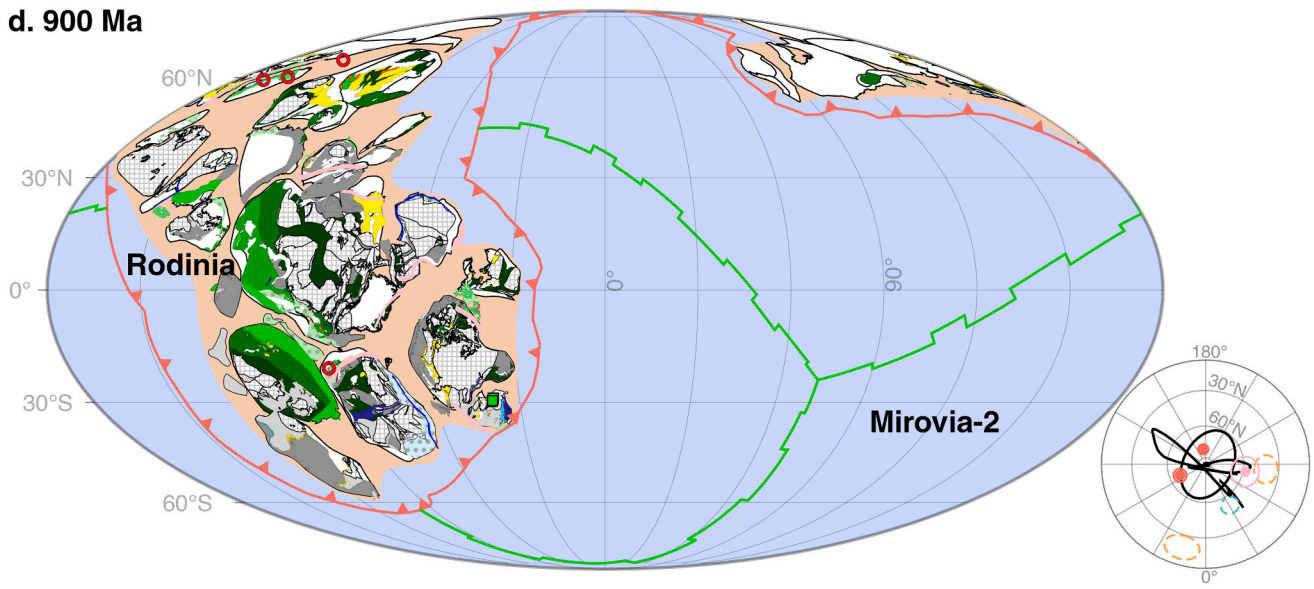

Fig. 12. (*continued*).

ca. 600 Myr cycle of supercontinent assembly and break-up, and the dominant occurrence of degree-1 and degree-2 long-wavelength mantle convection patterns (Li et al., 2019; Zhong et al., 2007).

In their dynamically coupled supercontinent-superplume cycle model (Li et al., 2008a, 2019; Zhong et al., 2007) (Fig. 16f), the location, geometry, and lifespan of LLSVPs are dynamically controlled by the evolving global subduction geometry during the supercontinent cycle. Supercontinents tend to assemble over a mantle superdownwelling, when the inherited or newly formed subduction girdle surrounding the supercontinent may not have formed a ring of dense rocks close to the CMB during the early stage of the assembly (Fig. 16c). As the subduction girdle fully develops, it would divide the lower mantle into two antipodal domains (a clear degree-2 structure), with one LLSVP remaining under the superocean, and another developing under the supercontinent some tens of million years after the formation of the subduction girdle, which would in turn initiate the break-up of the supercontinent (Li et al., 2003, 2008a) (Fig. 16d-e). If the supercontinent is not assembled in an equatorial position, the Earth's spin would lead to a TPW event that moves the breaking-up supercontinent, along with the antipodal LLSVPs, to the equator (Evans, 2003; Li et al., 2004) (Fig. 16d-f). Similar long wavelength geodynamic cycles are believed to have occurred during all three known supercontinent cycles: Nuna, Rodinia, and Pangaea. Although the dynamic coupling between the supercontinent cycle and lower mantle structure (e.g., the formation, lifespan and location of LLSVPs) was initially proposed based on palaeomagnetic TPW interpretations (Evans, 2003; Li et al., 2004; Li and Zhong, 2009), subsequent Earth-like geodynamic modelling work also reproduced such processes (Cao et al., 2021; Zhang et al., 2010; Zhong et al., 2007).

In our preferred model, we follow Li et al. (2019) in having Nuna's external superocean Mirovia-1 (Figs. 10c, 11a-c) surviving the Rodinia supercontinent assembly and returning to its full size again when Rodinia is fully assembled at ca. 900 Ma (the restored superocean is here termed Mirovia-2; Figs. 11, 12) as Rodinia assembled through introversion. However, Mirovia-2 (Figs. 12d, 13) gets consumed by an extroversion assembly of Pangaea (Fig. 14 and Fig. 2c-h of Li et al., 2019), and it was replaced by a new superocean, Panthalassa (Fig. 2c-g of Li et al., 2019). If correct, Mirovia would represent the longest-lived superocean in Earth history: spanning its first achievement of a superocean status at 1600 Ma (Mirovia-1; Fig. 10c), through a first wanning stage during Nuna's break-up until it regained its full size once again as Rodinia is fully assembled (Mirovia-2; Figs. 11, 12, 13). Mirovia-2 finally closed in two stages, first during the assembly of Gondwana (Fig. 14) and finally during the assembly and evolution of the youngest supercontinent Pangaea (the closure of the Tethys Ocean by the ca. 55 Ma closure of the Neo-Tethys between India and Eurasia; Fig. 2c-g of Li et al., 2019).

6.3. *IITPW events, implied mantle structure related to the supercontinent cycle, and longitudinal constraints on global reconstructions*

6.3.1. *Type-1 and type-2 IITPW events and related mantle structures during the Nuna and Rodinia supercontinent cycles*

As illustrated by Evans (1998, 2003), oscillatory IITPW events can occur when the axis of minimum moment of inertia (I_{min}, defined by the two antipodal LLSVPs) passes through the equator. We term IITPW when I_{min} passes through the geographic centre of an equatorial supercontinent (Figs. 16e and 17a) as Type-1 IITPW. Ca. 250—100 Ma oscillatory IITPW events around the geographic centre of Pangaea, identified by Steinberger and Torsvik (2008) and Torsvik et al. (2012), is an example of this type of IITPW (Mitchell et al., 2012). In our preferred reconstruction model (Supplementary Material 7) following the palaeomagnetic analysis as in Fig. 3, Nuna likely experienced such oscillating Type-1 IITPW events between 1700 Ma and 1300 Ma (Fig. 17d). We thus speculate that although the final oceanic closure to form Nuna did not occur until ca. 1600 Ma (Fig. 10), a degree-2 mantle structure with I_{min} intersecting central Nuna likely started to exist from ca. 1700 Ma. We envisage that the subduction girdle surrounding the assembling Nuna likely started to exist from ca. 1700 Ma (Fig. 10a) or even earlier, causing the formation of two antipodal LLSVPs on the equator (e.g., Fig. 17a). The continuation of such a mantle structure throughout Nuna's lifespan (Fig. 18a) would have allowed Type-1 IITPW to occur (Fig. 17d). There is geological evidence for the occurrence of mantle plume events during both the final assembly and the lifespan of Nuna. For example, the ca. 1590 Ma Gawler Range volcanic province in the South Australia Craton and the ca. 1550 Ma Croydon Volcanics in the North Australia Craton has been interpreted as products of a "migrating" mantle plume (Betts et al., 2009). The 1590 Ma plume head is also expressed in a matching LIP record in formerly attached NW Laurentia (Hamilton and Buchan, 2010; Rogers et al., 2018).

IITPW could also occur when a supercontinent assembles over a superdownwelling on the subduction girdle and yet the mantle structure is still dominated by a degree-2 structure inherited from the previous supercontinent cycle, and remains at an equatorial position (Fig. 17b) (Evans, 1998; Mitchell et al., 2012), here termed Type-2 IITPW.

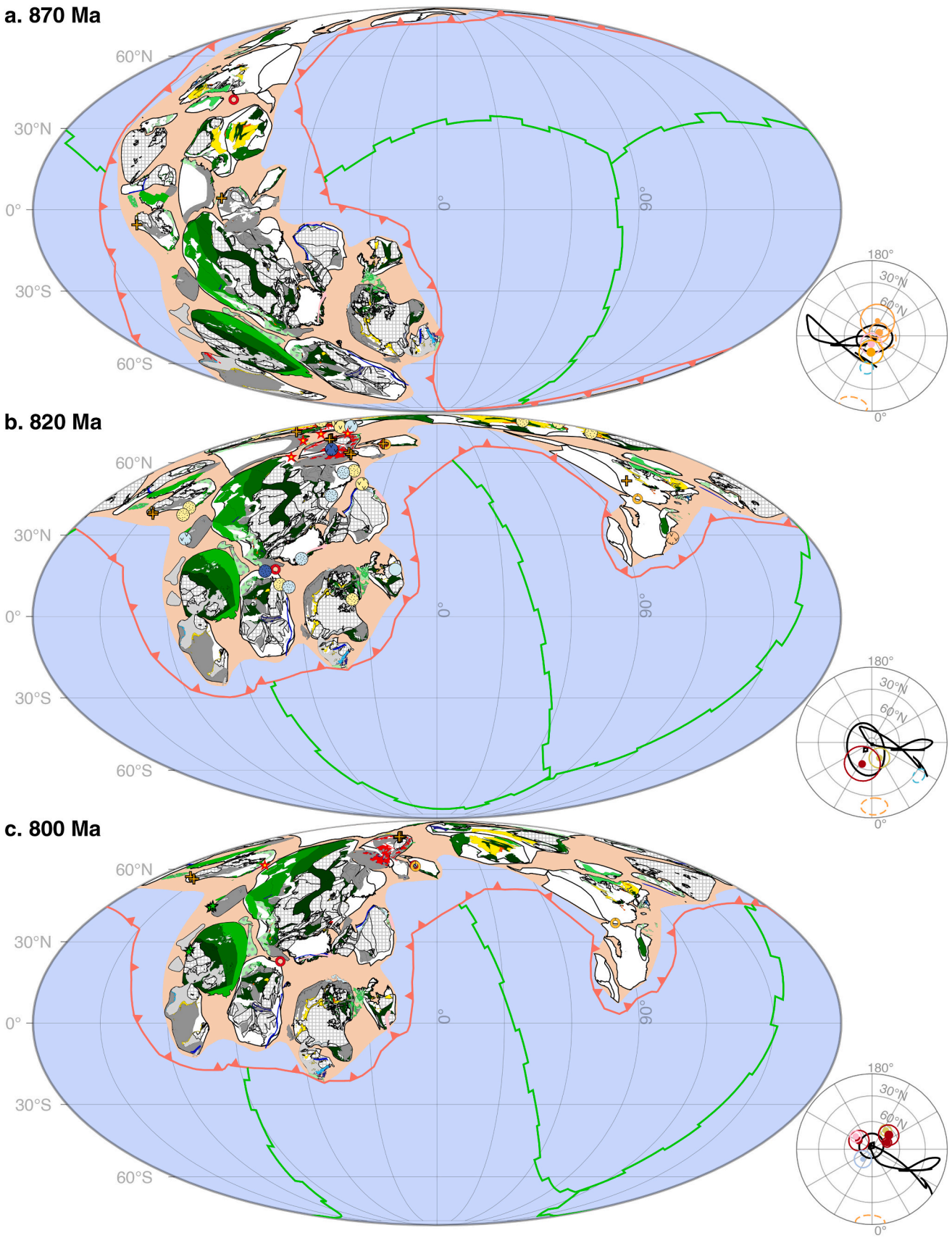

Fig. 13. 870—750 Ma reconstructions showing the rapid oscillating motion of Rodinia, interpreted to represent inertia interchange true polar wander (IITPW) events, and early rifting events within Rodinia.

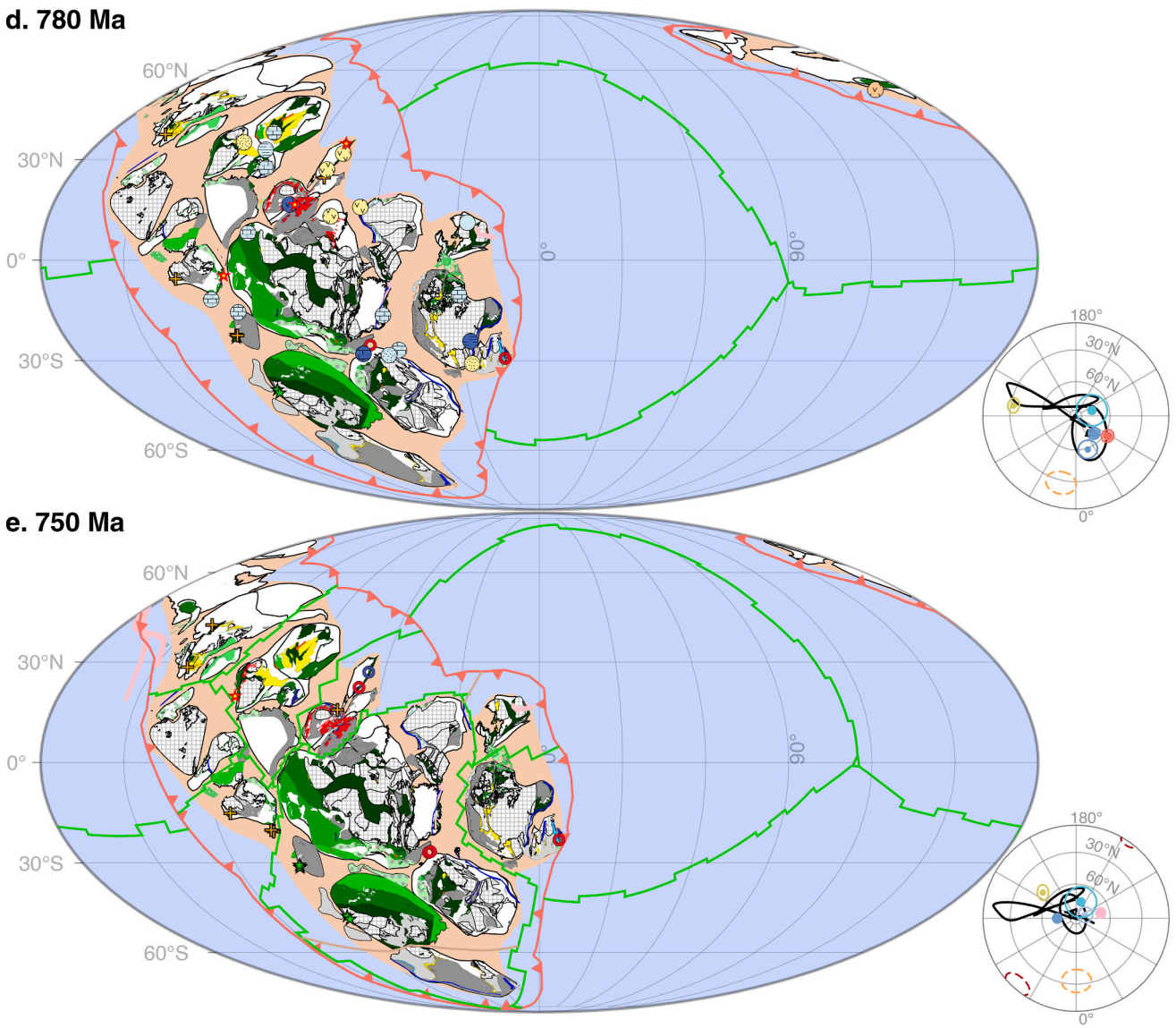

Fig. 13. (*continued*).

Rodinia's oscillatory motions during the early stage of its history (ca. 900—780 Ma; see sections *4.2.1* and *5.5*) around an equatorial axis close to the geographic centre of Nuna in our reconstruction (Fig. 17e) likely belong to this type of TPW. We interpret these episodes of Type-2 IITPW to have occurred around the I_{min} defined by the degree-2 mantle structure inherited from Nuna time. This interpretation implies that the assembly of Rodinia occurred on the previous subduction girdle (Figs. 12-13, and the legacy subduction girdle marked in Fig. 17b and Fig. 18c), and Rodinia did not have its own sub-supercontinent and antipodal LLSVPs developed (i.e., the Rodinia-centric antipodal LLSVPs; Fig. 16d,f and Fig. 18d) until close to 780 Ma. The cessation of such IITPW motion at ca. 780 Ma, when Rodinia was centred on the equator (Fig. 13d), probably indicates that the legacy Nuna degree-2 structure (Fig. 17b) had given way to a Rodinia-centric and equatorial degree-2 mantle structure by that time, during the prime stage of Rodinia rifting (Li et al., 2008a) (Fig. 16f, 17c and 18d-e). The ca. 780 Ma plume event is best expressed in western Laurentia by the 780 Ma Gunbarrel LIP (Harlan et al., 2003), and in South China by the Kangding event (Ernst et al., 2008; Li et al., 2003).

6.3.2. Longitudinal constraints by TPW record linked to conceptual geodynamic models

Constraining the longitude of global plate reconstructions remains a challenge. For the past 200 Ma, one can safely assume that the position (though not necessarily the shape) of the present-day African LLSVP largely reflects that of Pangaea before its break-up, and use a combined palaeomagnetic and LLSVP-linked hot spot reference frame, plus marine magnetic record, to constrain the palaeolongitude (Torsvik et al., 2014). However, more generally, for deeper geological time, other assumptions have to be made. Torsvik and others (Torsvik, 2019; Torsvik et al., 2014, 2016) argued that the LLSVPs observed in present-day Earth could have been there since at least the Neoproterozoic if not the start of mantle convection in very early Earth (Dziewonski et al., 2010), and we can thus use them (and their surface plume expressions) as a fixed longitudinal reference frame. However, combined palaeomagnetic and mantle plume records (e.g., Li et al., 2004) suggest that superplumes (LLSVPs) and supercontinents are dynamically coupled in both their occurrences, their geometry, and their geographic locations (Li et al., 2008a; Li and Zhong, 2009). Geodynamic modelling also demonstrates a strong dynamic coupling between LLSVPs and the location and evolution of supercontinents (Cao et al., 2021; Zhang et al., 2010; Zhong et al., 2007), making it unreliable to assume a stable and fixed lower mantle structure

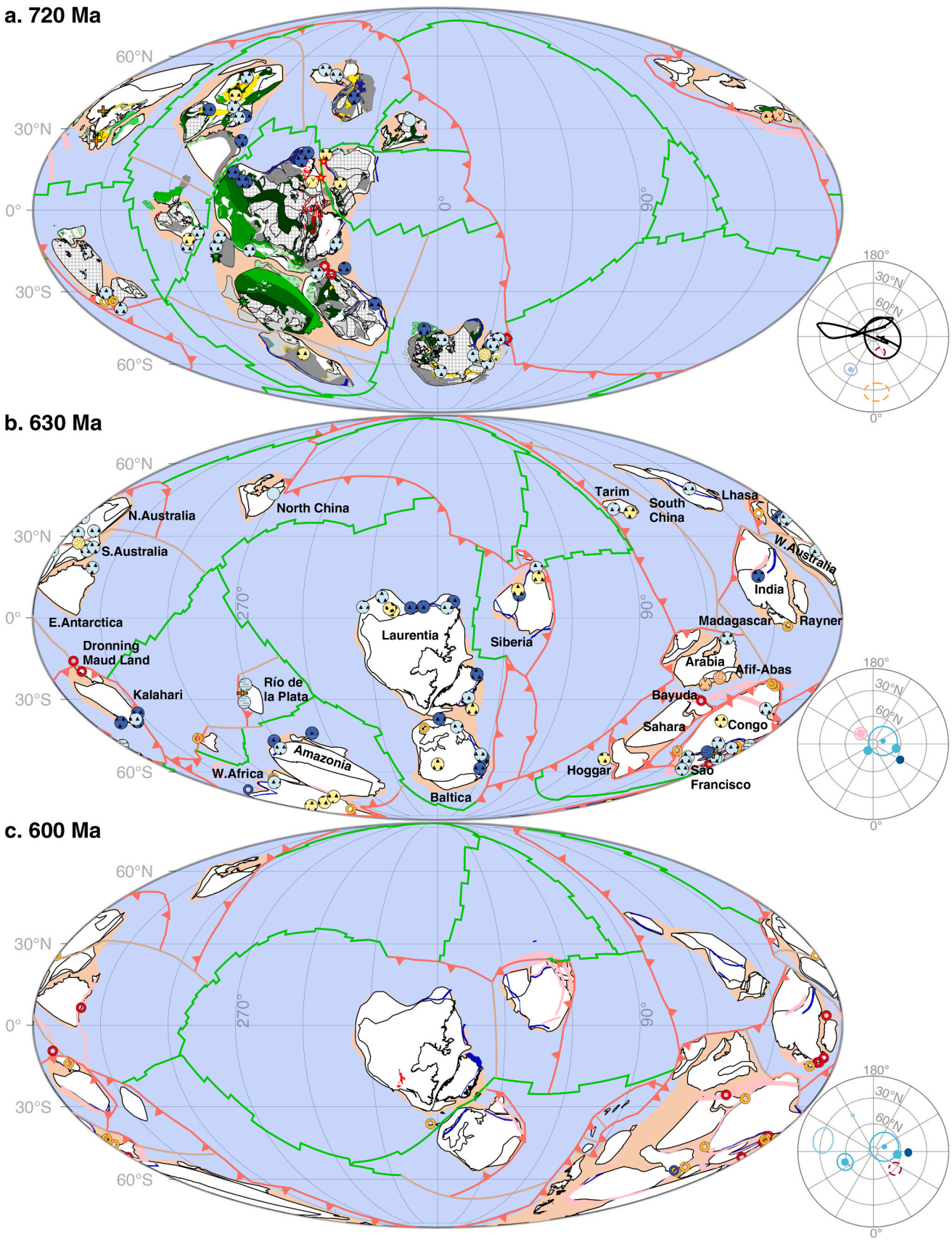

Fig. 14. 720—540 Ma reconstructions showing the break-up of Rodinia, snowball Earth events and the formation of Gondwana.

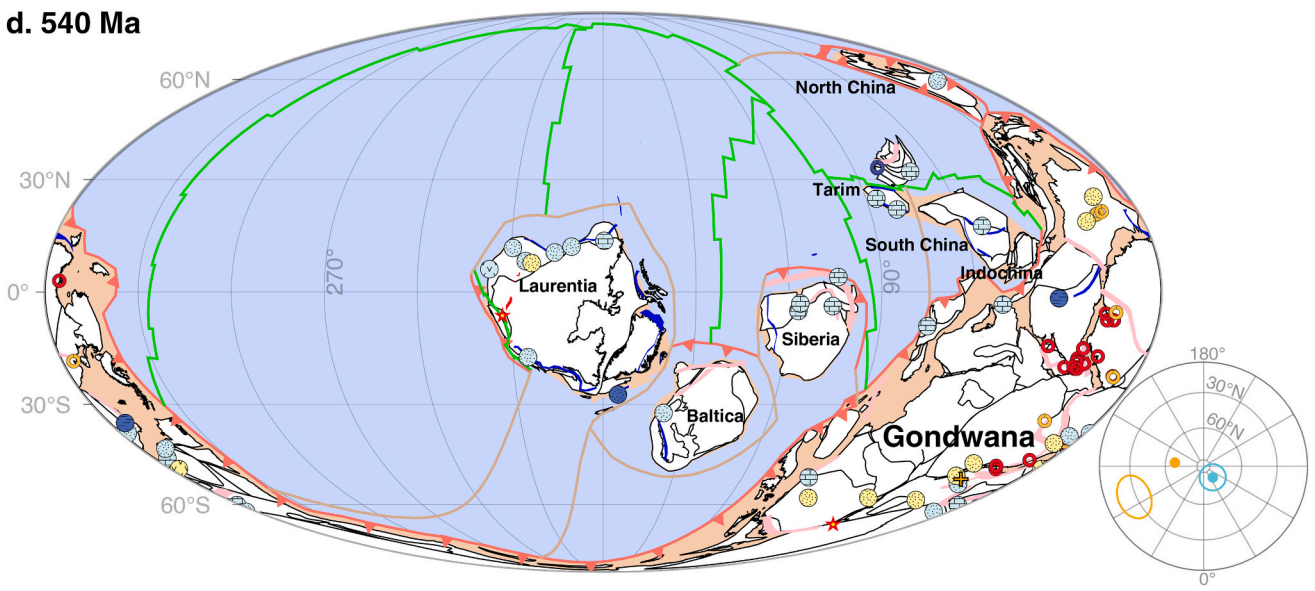

Fig. 14. (*continued*).

as a global reference frame for deep time.

Our *Scenario Ia* (the preferred scenario) features Nuna centred at 0°E, Rodinia at 90°W (Müller et al., 2022) and Pangaea at 0°E (annotated as Scenario 0–90 W–0; Fig. 18a-h and Supplementary Material 7). *Scenario Ib* following Li et al. (2019) features Nuna centred at 0°E, Rodinia at 90°E and Pangaea at 0°E (annotated as Scenario 0–90E–0; Fig. 18i-p and Supplementary Material 8*)*. Both follow the extended-orthoversion assumption which differs from the classic orthoversion model of (Mitchell et al., 2012). The latter only applies when the supercontinent assembles on the subduction girdle through closing small oceans along the girdle instead of either closing the previous superocean or closing the new internal oceans formed during the break-up of the previous supercontinent. In our extended-orthoversion model (Li et al., 2019), the new supercontinent assembles on the subduction girdle following the principle defined by Anderson (Anderson, 1994), regardless of whether the assembling process involved introversion (closure of the internal oceans and survival of the early subduction girdle and the previous superocean; Fig. 18a-c and i-k for the assembly of Rodinia) or extroversion (closure of the previous superocean; Fig. 18c-f and k-n for the assembly of Pangaea). In such scenarios, the legacy degree-2 structure from the previous supercontinent cycle would always be 90° away from that regenerated by the subduction girdle surrounding the new supercontinent (e.g., Fig. 18 between (a)-(c) and (d), and between (d)-(f) and (g)).

However, the situation would be very different if an introversion supercontinent involves a simple inward collapse of the internal oceans, leading to the new supercontinent assembling more or less at the same location as its predecessor (Fig. 19a-b), or an extroversion supercontinent assembly following an "inside-out" trajectory by closing the external superocean, leading to the formation of the new supercontinent on the opposite side of the Earth compared to its predecessor (Fig. 19b-c). We term this non-orthoversion scenario *Scenario II*.

The reconstruction scenarios as in Fig. 18 and that in Fig. 19 have rather contrasting consequences in terms of the resulting mantle structures, and potential possible TPW events and plume-induced magmatic events. With the extended-orthoversion scenarios (Fig. 18), a new supercontinent can be centred at any latitude along the subduction girdle when the global mantle structure is still dominated by the inherited degree-2 structure (Fig. 17b and Fig. 18c,k). This would permit type-2 IITPW (Fig. 17b,e) and the new supercontinent would only become stabilised in an equatorial position after a new, supercontinent-centric degree-2 structure is developed at the expense of the inherited degree-2 structure. The TPW motions would eventually align this new I_{min} axis on the equator and perpendicular to its predecessor during the break-up phase of the supercontinent, allowing for type-1 IITPW to occur afterward (Figs. 17c and 18d,g,l,o). Such scenarios also predict a delayed occurrence of plume magnetism over the newly assembled supercontinent as the new degree-2 structure would take a few 10s of million years to develop (Li et al., 2008a; Li and Zhong, 2009).

In contrast, if a supercontinent (e.g., Rodinia) is assembled through introversion in *Scenario II* (non-orthoversion; 180–180–0) as in Fig. 19a-b, the original degree-2 mantle structure is expected to partially survive during the assembly, and to be re-established quickly after the completion of the supercontinent assembly. In this case, one could expect type-1 IITPW throughout the assembly to the break-up phases of Rodinia. One would also expect to see continental plume magmatism from the very early stage of Rodinia assembly. If a new supercontinent (e.g., Pangaea; Fig. 19b-c) is assembled through extroversion on the opposite side of the globe, again the previous degree-2 mantle structure is expected to partially survive during the assembly, and will be re-established quickly after the completion of the supercontinent assembly (Fig. 19b-c). Therefore, again, type-1 IITPW is expected throughout the assembly to break-up phases of the new supercontinent (Fig. 19b-c), and continental plume magmatism is expected to start to emerge early.

Through comparisons of such model predictions with the palaeomagnetic and plume (LIP) records, we argue that the evidence favours the extended-orthoversion scenarios for Rodinia assembly (Fig. 18a-c and i-k) for two reasons. (1) Type-2 IITPW-like motions appear to have occurred both during the assembly stage of Rodinia (ca. 1100—900 Ma; Fig. 12, and Supplementary Materials 7 and 8) and during the early lifespan of Rodinia (900—780 Ma) around an equatorial I_{min} axis inherited from the Nuna supercontinent cycle (Figs. 7 and 16e, and Supplementary Materials 7 and 8). (2) Although continental rifting within Rodinia started as early as 860—850 Ma, plume magmatism did not become widespread until 825—720 Ma (see section *5.5* and Fig. 1).

Similar type-2 IITPW-like motions around a Rodinia-centric equatorial I_{min} axis during the assembly of Pangaea have been proposed (Mitchell et al., 2012; Van der Voo, 1994). We note the northward motion of Pangaea between 340 Ma and 270 Ma in the Phanerozoic reconstruction (Li and Powell, 2001; Merdith et al., 2021; Steinberger and Torsvik, 2008) (Fig. 17f-g), which could be seen as a type-2 IITPW motion around the potential legacy Rodinia degree-2 mantle structure. However, given the one-off nature of this motion, it can also be interpreted as a normal TPW event (Fig. 17g) although this does not change

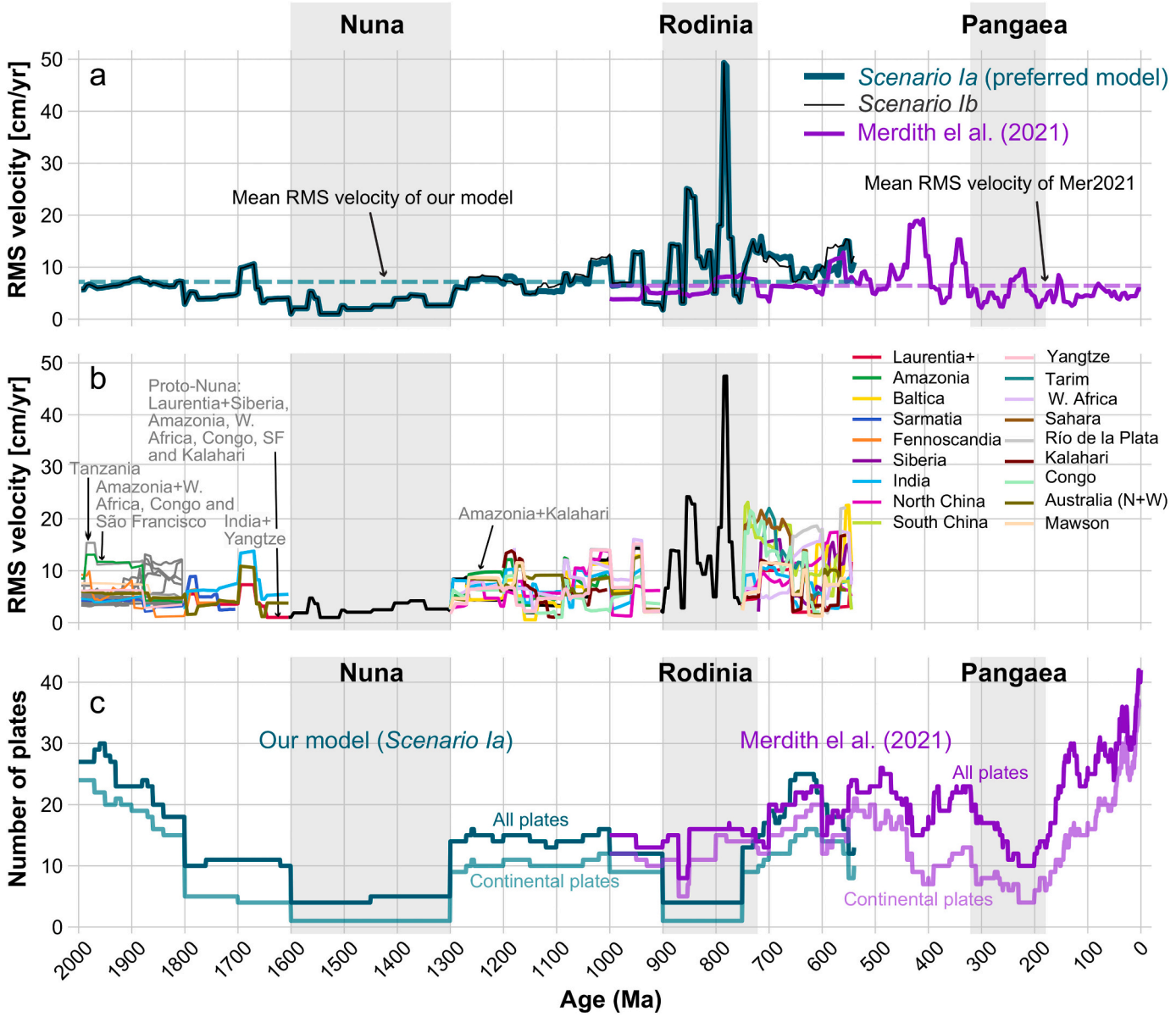

Fig. 15. Comparison of data extracted from our model and that of Merdith et al. (2021). (a) Root mean squared (RMS) velocity of plates hosting continental crust extracted at a 5 Myr step. (b) individual plate motion RMS for *Scenarios Ia*. Numerous small plates gave consistent low RMS of ~5 cm/yr for the 2000—1900 Ma interval, and such plates are not individually identified. (c) Changing number of plates with time. The plates that host any continental crusts are marked as continental plates.

the geodynamic implication of this motion. Plume/LIP activity was relatively scarce during the early stage of Pangaea tenure (noting the few 300—250 Ma events in Baltica and Asian continents along the northern end of Pangaea; Ernst et al., 2021; Supplementary Material 4 for shapefile database and Excel tables), and widespread plume/LIP events in Pangaea interior only started from ca. 200 Ma, making it comparable to the Rodinia record (Li and Zhong, 2009). Therefore, current data appears to favour the extended-orthoversion scenarios (Fig. 18 and Supplementary Materials 7, 8) over the non-orthoversion model (Fig. 19).

7. Conclusions

Since the three landmark papers over 30 years ago (Dalziel, 1991; Hoffman, 1991; Moores, 1991) that presented the community a testable model of a pre-Pangaea supercontinent Rodinia (McMenamin and McMenamin, 1990), the field of geotectonic research has transformed and expanded in numerous ways: from a post-550 Ma focus to considering Earth's entire geological history, and from compartmentalised and discipline-based focus to a broader science-question focus with a multidisciplinary and Earth system approach. Although details are still hotly debated, it is now widely recognised that the Earth has experienced three episodes of supercontinent assembly and break-up in a ca. 600 Myr interval after 2000 Ma. Together with a much improved seismic image of deep Earth, and palaeomagnetic and mantle plume/LIP evidence (along with theoretical validation by geodynamic modelling) for coupling between plate tectonics and mantle dynamics, it is now possible to explore how Earth's unique plate tectonic system has evolved through time as Earth's "surface" expression of an evolving geodynamic system.

In this study we utilise both geological (crustal ages, tectonic facies, metamorphic and orogenic records, passive margins, late Neoproterozoic facies, and large igneous events (LIPs); Supplementary Materials 2—6) and geophysical information (palaeomagnetism;

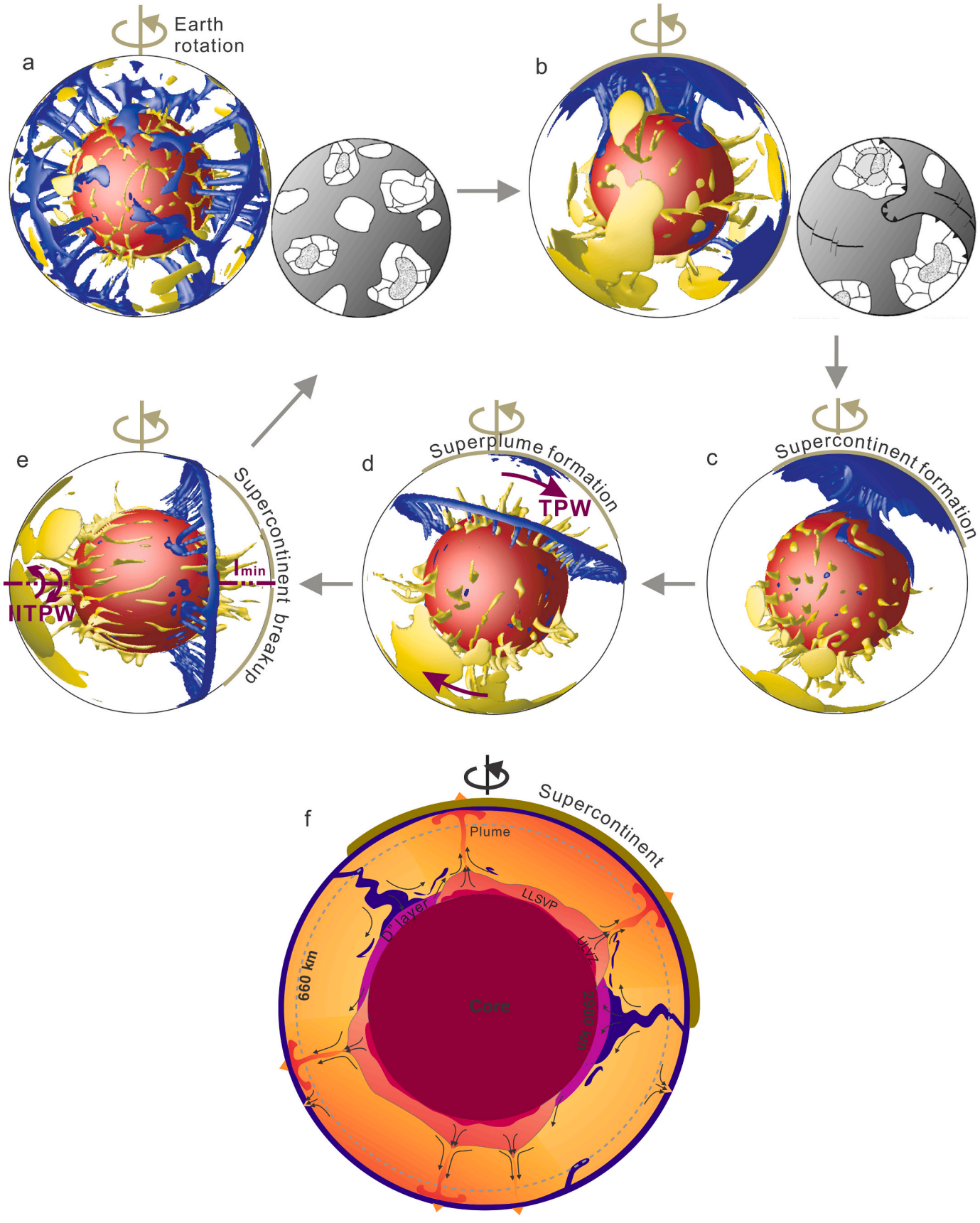

(caption on next page)

Fig. 16. Schematic mantle convection patterns in relation to evolving tectonic systems from the Archaean time (after Li and Zhong, 2009; Zhong et al., 2007). (a) Archaean time with many cratons and smaller-scale convection cells. (b) The occurrence of multiple supercratons during Archaean–Paleoproterozoic time, featuring reduced number and larger mantle convection cells. (c) The start of the supercontinent cycle since the Paleoproterozoic, featuring supercontinent assembly over a mantle superdownwelling. (d) Circum-supercontinent subduction girdle eventually turns the sub-supercontinent superdownwelling as in (c) into a superupwelling (also called superplume, which includes the lower-mantle seismic LLSVP, not explicitly shown here), which triggers the break-up of the supercontinent. (d)-(e) If the axis of Earth's minimum moment of inertia (I_{min}), the long axis of a prolate geoid defined by the two antipodal superupwellings (superplumes), does not intersect the equator, Earth's spinning force would cause the entire silicate Earth to rotate as a true polar wander (TPW) event of up to 90° (d), bringing I_{min} (along with the antipodal superupwelling and the breaking-up supercontinent) onto the equator (Evans, 2003; Li et al., 2004) (e). Once at the equator, oscillating inertial interchange true polar wander (IITPW) may then occur around I_{min} (Evans, 1998; Kirschvink et al., 1997) (e). (f) A conceptual model of a circum-supercontinent subduction girdle producing two antipodal LLSVPs, with the supercontinent eventually breaks apart largely driven by the sub-supercontinent superupwelling (Li et al., 2008a; Li and Zhong, 2009). See *6.3* for further discussion. The small grey cartoon Earth models in (a) and (b) isare from Bleeker (2003). Note that LLSVPs in the lower mantle are not exclipitly shown in cartoons (a)-(e).

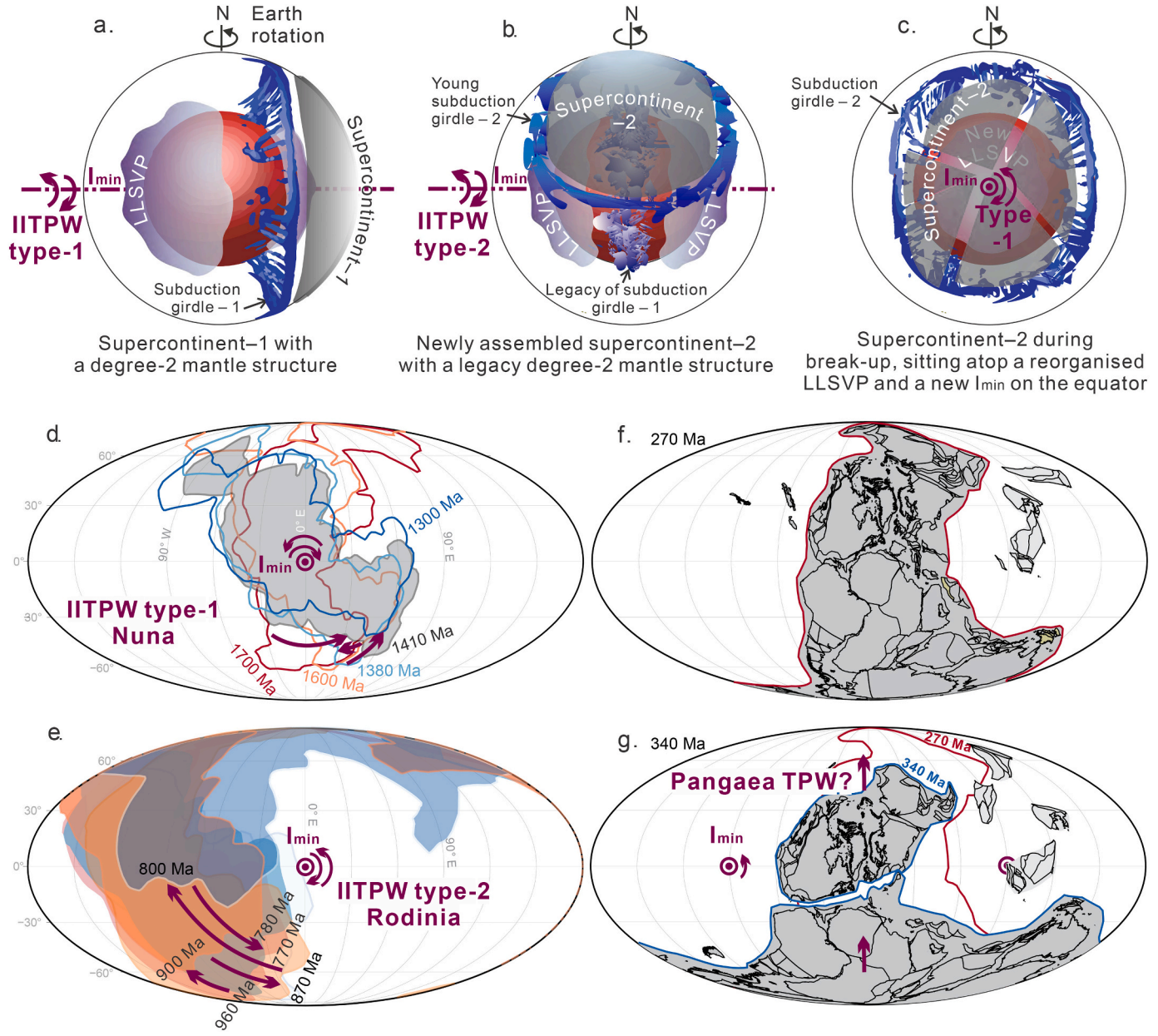

Fig. 17. Two scenarios of IITPW occurring during the supercontinent cycledriven by the reorganization of mantle structure (a-c), likely examples of Type-1 IITPW during Nuna time (d), example of Type-2 IITPW during Rodinia time (e), and a possible normal TPW event during Pangaea time between 340 Ma and 270 Ma (f-g: modified after Merdith et al., 2021). The rotating outline of Nuna and Rodinia are marked with ages in (d) and (e), respectively (note that the assembly of Nuna was not yet completed but was close at 1700 Ma), with arrows indicating TPW events.

Supplementary Material 1; see Pisarevsky et al., 2022), as well as geodynamic considerations, to provide two plausible models demonstrating how the many small continental cratons formed in Archaean time might have gradually gathered into larger continents, and eventually started

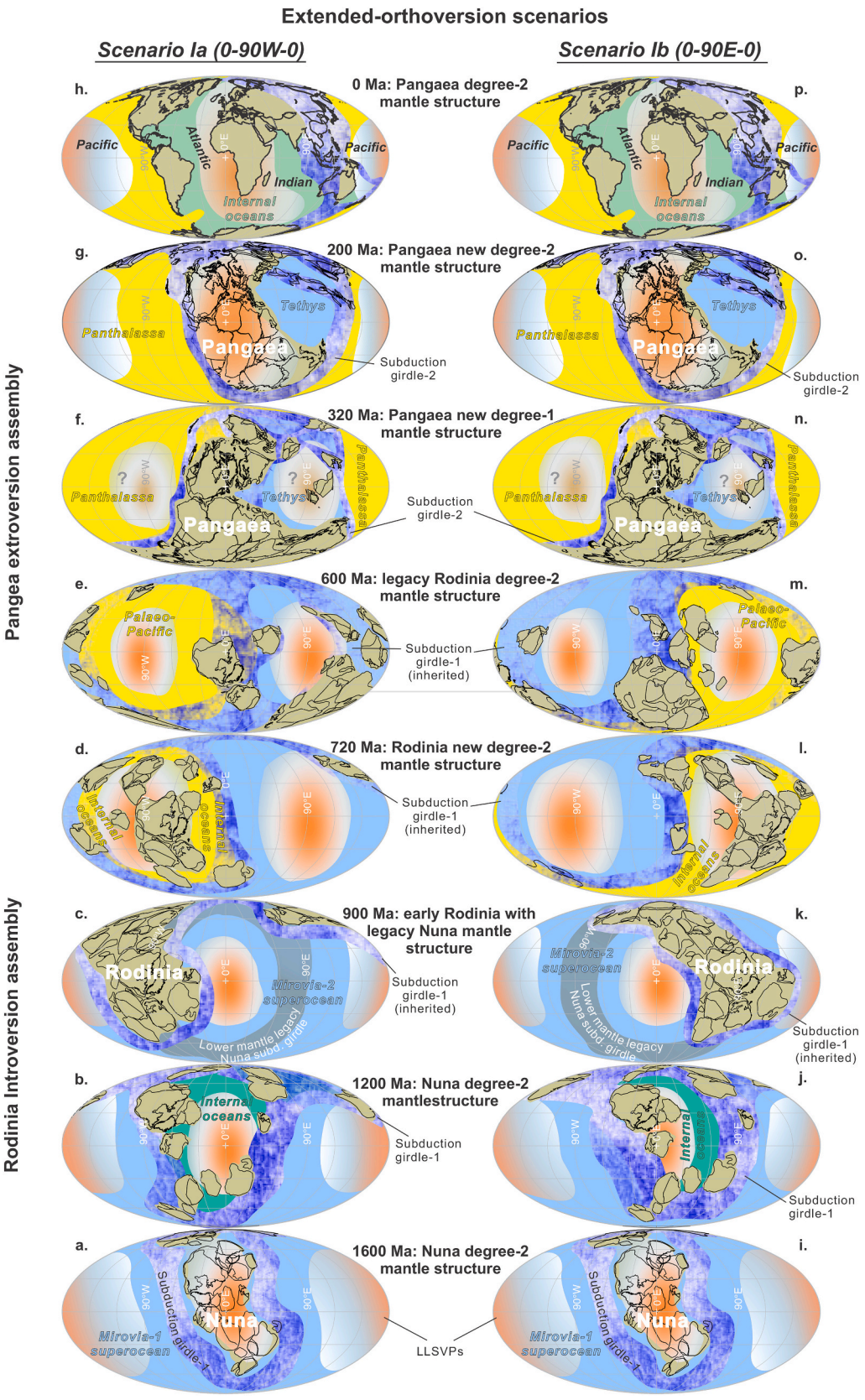

Fig. 18. Cartoons illustrating the implications of two alternative scenarios based on the extended-orthoversion geodynamic assumption where a 90° longitudinal change occurs between supercontinents and associated mantle structures (e.g., LLSVPs, and the I_{min}s as defined by the two antipodal LLSVPs). (a-h) *Scenario Ia* where Nuna is centred at 0°E, Rodinia at 90°W, and Pangaea at 0°E (0–90 W-0). (i-p) *Scenario Ib* where Nuna is centred at 180°E, Rodinia at 90°E, and Pangaea at 0°E (0–90E-0).

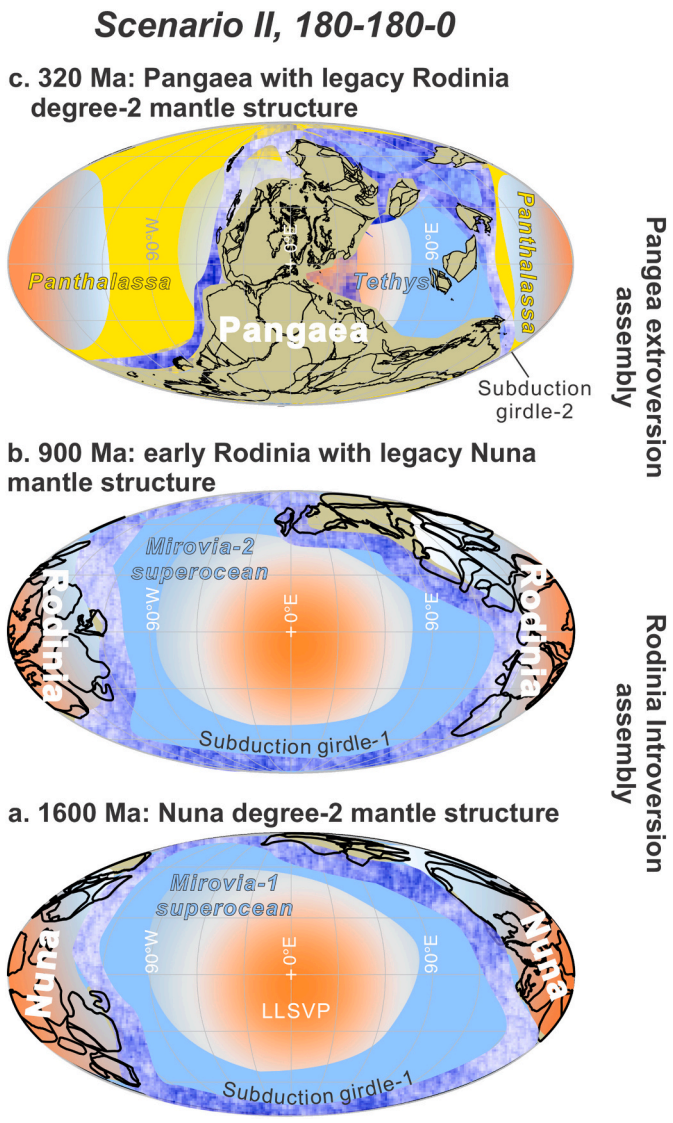

Fig. 19. Cartoons illustrating the implications of a non-orthoversion geodynamic scenario. Nuna was centred at 180°E, Rodinia assembled through introversion to the same longitude as Nuna, and Pangaea assembled through extroversion and centred at 0°E (180—180–0). Here the introversion supercontinent assembly occurs through a simple inward collapsing of the internal oceans with the new supercontinent assembling on the same position of the ancestor supercontinent, thus retaining much of the existing mantle structure. The extroversion supercontinent assembly occurs on the opposing side of the Earth through an in-side-out trajectory, and the weakened existing degree-2 mantle structure gets restored during the tenure of the supercontinent.

the supercontinent cycle after 2000 Ma, signifying the geodynamic transformation from dominantly multiple small-scale convection cells into hemispheric-scale convection patterns (Zhong et al., 2007). We start with a revision to the configuration and evolution histories of supercontinent Nuna (Columbia), possibly the first stable supercontinent (Fig. 2), and then Rodinia (Fig. 5) using palaeomagnetic and geological constraints. Both Nuna and Rodinia appear to have experienced a two-stage assembly: ca. 1800 Ma and ca. 1600 Ma for Nuna (Figs. 9c and 10c), and ca. 1000 Ma and ca. 900 Ma for Rodinia (Fig. 12c-d). In our preferred 2000—540 Ma global full-plate animation (Figs. 9—14, and Supplementary Material 7), we illustrate how an incomplete Nuna break-up after 1300 Ma (into ~10 continental blocks) might have reassembled into Rodinia through an introversion process, featuring the survival of both the Nuna superocean and the subduction girdle, followed by a more complete break-up of Rodinia after 720 Ma into >13 continental blocks before an extroversion assembly of Gondwana by ~540 Ma as the first stage of Pangaea assembly.

Palaeomagnetic data and latitude-sensitive palaeoclimatic indicators provide constraints for the palaeolatitude of continental blocks through time, but it remains a challenge to provide palaeolongitudinal constraints for pre-Cretaceous reconstructions. In this work we utilise a combination of geodynamic model predictions and palaeomagnetic and LIP records to evaluate the likelihood of some alternative palaeolongitudinal models. Through recognizing two different types of inertia interchange true polar wander (IITPW) (type-1 and type-2; Fig. 17a-c) during Nuna time (Fig. 17d) and the 960—780 Ma period of the Rodinia time (Fig. 17e), respectively, in conjunction with the LIP record during supercontinent cycles, we are able to assign significantly more confidence on the extended-orthoversion model (Fig. 18, *Scenario Ia* and *Ib*; see Figs. 9—14 and Supplementary Materials 7 and 8 for reconstructions) over *Scenario II* (Fig. 19) and the fixed-LLSVP model promoted by other workers (Dziewonski et al., 2010; Torsvik, 2019; Torsvik et al., 2014, 2016).

Being perhaps the first full-plate global palaeogeographic reconstruction back to 2000 Ma, our model will no doubt have much room for improvement in almost all aspects, but it does provide a testable global geotectonic and geodynamic framework for future research. Improvements will come through further geodynamic modelling and improved geophysical (e.g., palaeomagnetism) and the whole spectrum of geological datasets. The datasets we employed here are valuable collections, and can be analyzed in more detail to further test the validity of our reconstructions and together, be applied to a wide range of Earth System studies (e.g., sea-level changes, extreme global climate events, global supermountain events and atmospheric oxygenation, and biological evolution etc.; Li et al., 2013; Zhu et al., 2022). There is nonetheless an urgent need for more systematically collected and global uniformly formatted spatial geoscience databases for the entire Earth history. Such databases will facilitate more systematic, big-data and machine-learning-based, global geotectonic and geodynamic reconstruction and analyses.

Funding

Z.X.L and Y.L acknowledges Australian Research Council Laureate Fellowship grant to Z.X.L. (FL150100133). R.E. Acknowledges support of the LIPs – Industry Consortium (www.supercontinent.org), with industry funding matched by Canadian NSERC grant CRDPJ 523131-17.

Declaration of Competing Interest

The authors declare the following financial interests/personal relationships which may be considered as potential competing interests: Zheng-Xiang Li and Yebo Liu reports financial support and administrative support were provided by Curtin University. Richard Ernst reports financial support and administrative support were provided by Carleton University. Zheng-Xiang Li and Yebo Liu reports financial support was provided by Australian Research Council. Richard Ernst reports financial support was provided by Canadian NSERC. Zheng-Xiang Li is a co-guest editor of the BigDataLi special issue.

Data availability

All data are shared as online Supplementary Materials.

Acknowledgements

We are grateful to Sergei Pisarevsky for assisting with the palaeomagnetic data compilation, for an early attempt to reconstruct the paleogeography, and for ongoing discussions. Lei Wu is acknowledged for assisting with an early attempt of calculating the APWPs for Nuna

and Rodinia, and Josh Beardmore for proofreading. The APWP calculation code by Wu et al. (2021), and a modified Python version of that code based on the translation by Simon Williams, were used for the APWP calculation. Andrew Merdith and Matthew Domeier are thanked for technical advises on full-plate reconsruction. All members of the Earth Dynamics Research Group at Curtin University are thanked for regular science discussions and support. GPlates developed by the EarthByte research group has been used for making global reconstructions. Comments from two anonymous reviewers and editor Tim Kusky helped to improve the manuscript. This is a contribution to IGCP 648: Supercontinent cycles and global geodynamics.

Appendix B. Supplementary data

Supplementary data to this article can be found online at https://doi.org/10.5281/zenodo.7567623

References

Amit, H., Olson, P., 2015. Lower mantle superplume growth excites geomagnetic reversals. Earth Planet. Sci. Lett. 414, 68–76.
Anderson, D.L., 1994. Superplume or supercontinents? Geology 22, 39–42.
Anderson, D.L., 2001. Top-down tectonics? Science 293, 2016–2018.
Antonio, P.Y.J., Baratoux, L., Trindade, R.I.F., Rousse, S., Ayite, A., Lana, C., Macouin, M., Adu, E.W.K., Sanchez, C., Silva, M.A.L., 2021. West Africa in Rodinia: high quality paleomagnetic pole from the~ 860 Ma Manso dyke swarm (Ghana). Gondwana Res. 94, 28–43.
Aspler, L.B., Chiarenzelli, J.R., 1998. TwoNneoarchean supercontinents?Evidence from the paleoproterozoic. Sediment. Geol. 120 (1—4), 75–104.
Baragar, W., Ernst, R., Hulbert, L., Peterson, T., 1996. Longitudinal petrochemical variation in the Mackenzie dyke swarm, northwestern Canadian Shield. J. Petrol. 37 (2), 317–359.
Baratoux, L., Söderlund, U., Ernst, R.E., Roever, E.D., Jessell, M., Kamo, S., Naba, S., Perrouty, S., Metelka, V., Yatte, D., 2019. In: New U–Pb Baddeleyite Ages of Mafic Dyke Swarms of the West African and Amazonian Cratons: Implication for Their Configuration in Supercontinents Through Time, Dyke Swarms of the World: A Modern Perspective. Springer, pp. 263–314.
Bickford, M., Mock, T., Steinhart Iii, W., Collerson, K., Lewry, J., 2005. Origin of the Archean Sask craton and its extent within the Trans-Hudson orogen: evidence from Pb and Nd isotopic compositions of basement rocks and post-orogenic intrusions. Can. J. Earth Sci. 42 (4), 659–684.
Bell, R.T., Jefferson, C.W., 1987. In: An hypothesis for an Australia-Canadian connection in the Late Proterozoic and the birth of the Pacific Ocean, Proceedings of Pacific Rim Congress 87. The Australian Institute of Mining and Metallurgy, Gold Coast, Queensland, pp. 39–50.
Belousova, E.A., Kostitsyn, Y.A., Griffin, W.L., Begg, G.C., O'Reilly, S.Y., Pearson, N.J., 2010. The growth of the continental crust: constraints from zircon Hf-isotope data. Lithos 119 (3), 457–466.
Betts, P.G., Armit, R.J., Stewart, J., Aitken, A.R.A., Ailleres, L., Donchak, P., Hutton, L., Withnall, I., Giles, D., 2016. Australia and Nuna. Geol. Soc. Lond., Spec. Publ. 424 (1), 47–81.
Betts, P.G., Giles, D., Foden, J., Schaefer, B.F., Mark, G., Pankhurst, M.J., Forbes, C.J., Williams, H.A., Chalmers, N.C., Hills, Q., 2009. Mesoproterozoic plume-modified orogenesis in eastern Precambrian Australia. Tectonics 28.
Bleeker, W., 2003. The late Archean record: a puzzle in ca. 35 pieces. Lithos 71 (2—4), 99–134.
Bleeker, W., Ernst, R., 2006. Short-lived mantle generated magmatic events and their dyke swarms: the key unlocking Earth's paleogeographic record back to 2.6 Ga. In: Hanski, E., Mertanen, S., Rämo, T., Vuollo, J. (Eds.), Dyke Swarms – Time Markers of Crustal Evolution. Taylor and Francis/Balkema, London, pp. 3–26.
Borg, S.G., DePaolo, D.J., 1994. Laurentia, Australia, and Antarctica as a Late Proterozoic supercontinent: constraints from isotopic mapping. Geology 22, 307–310.
Bradley, D.C., 2008. Passive margins through earth history. Earth Sci. Rev. 91 (1—4), 1–26.
Brennan, D.T., Brian Mahoney, J., Li, Z.X., Link, P.K., Evans, N.J., Johnson, T.E., 2021a. Detrital zircon U-Pb and Hf signatures of Paleo-Mesoproterozoic strata in the Priest River region, northwestern USA: a record of Laurentia assembly and Nuna tenure. Precambrian Res. 367, 106445.
Brennan, D.T., Li, Z.X., Rankenburg, K., Evans, N., Link, P.K., Nordsvan, A.R., Kirkland, C.L., Mahoney, J.B., Johnson, T., McDonald, B.J., 2021. Recalibrating Rodinian rifting in the northwestern United States. Geology 49 (6), 617–622.
Bright, R., Amato, J., Denyszyn, S., Ernst, R., 2014. U-Pb geochronology of 1.1 Ga diabase in the southwestern United States: testing models for the origin of a post-Grenville large igneous province. Lithosphere 6 (3), 135–156. L335-1.
Brookfield, M.E., 1993. Neoproterozoic Laurentia-Australia fit. Geology 21, 683–686.
Brown, L.L., McEnroe, S.A., 2004. Palaeomagnetism of the Egersund-Ogna anorthosite, Rogaland, Norway, and the position of Fennoscandia in the Late Proterozoic. Geophys. J. Int. 158 (2), 479–488.
Brown, M., Johnson, T., 2019. Metamorphism and the evolution of subduction on Earth. Am. Mineral. 104 (8), 1065–1082.
Buchan, K.L., Ernst, R.E., 2019. Giant circumferential dyke swarms: catalogue and characteristics. In: Srivastava, R.K., Ernst, R.E., Peng, P. (Eds.), Dyke Swarms of the World:A Modern Perspective. Springer, pp. 1–44.
Buchan, K.L., Ernst, R.E., 2021. Plumbing systems of large igneous provinces (LIPs) on Earth and Venus: investigating the role of giant circumferential and radiating dyke swarms, coronae and novae, and mid-crustal intrusive complexes. Gondwana Res. 100, 25–43.
Buchan, K.L., Ernst, R.E., Bleeker, W., Davis, W.J., Villeneuve, M., van Breemen, O., Hamilton, M., Söderlund, U., 2010. Proterozoic Magmatic Events of the Slave Craton, Wopmay Orogen and Environs. Geological Survey of Canada Open File 5985.
Burke, K., Steinberger, B., Torsvik, T.H., Smethurst, M.A., 2008. Plume Generation zones at the margins of large Low Shear Velocity Provinces on the core-mantle boundary. Earth Planet. Sci. Lett. 265 (1—2), 49–60.
Bylund, G., 1985. Palaeomagnetism of middle Proterozoic basic intrusives in Central Sweden and the Fennoscandian apparent polar wander path. Precambrian Res. 28 (3—4), 283–310.
Bylund, G., 1992. Palaeomagnetism, mafic dykes and the Protogine Zone, southern Sweden. Tectonophysics 201 (1—2), 49–63.
Cai, Y., Pei, J., Zhang, S.-H., Tong, Y., Yang, Z., Zhao, Y., 2020. New paleomagnetic results from the ca. 1.68—1.63 Ga mafic dyke swarms in Western Shandong Province, Eastern China: implications for the reconstruction of the Columbia supercontinent. Precambrian Res. 337, 105531.
Campbell, I.H., Allen, C.M., 2008. Formation of supercontinents linked to increases in atmospheric oxygen. Nat. Geosci. 1 (8), 554–558.
Cao, X., Flament, N., Bodur, Ö.F., Müller, R.D., 2021. The evolution of basal mantle structure in response to supercontinent aggregation and dispersal. Sci. Rep. 11 (1), 22967.
Cawood, P.A., Hawkesworth, C.J., 2014. Earth's middle age. Geology 42 (6), 503–506.
Cawood, P.A., Hawkesworth, C.J., Pisarevsky, S.A., Dhuime, B., Capitanio, F.A., Nebel, O., 2018. Geological archive of the onset of plate tectonics. Philos. Trans. R. Soc. A Math. Phys. Eng. Sci. 376 (2132), 20170405.
Cawood, P.A., Strachan, R.A., Pisarevsky, S.A., Gladkochub, D.P., Murphy, J.B., 2016. Linking collisional and accretionary orogens during Rodinia assembly and breakup: implications for models of supercontinent cycles. Earth Planet. Sci. Lett. 449, 118–126.
Cawood, P.A., Wang, W., Zhao, T., Xu, Y., Mulder, J.A., Pisarevsky, S.A., Zhang, L., Gan, C., He, H., Liu, H., Qi, L., Wang, Y., Yao, J., Zhao, G., Zhou, M.-F., Zi, J.-W., 2020. Deconstructing South China and consequences for reconstructing Nuna and Rodinia. Earth Sci. Rev. 204, 103169.
Cawood, P.A., Wang, Y., Xu, Y., Zhao, G., 2013. Locating South China in Rodinia and Gondwana: a fragment of greater India lithosphere? Geology 41 (8), 903–906.
Chang, L., Zhang, S., Li, H., Xian, H., Wu, H., Yang, T., 2022. New paleomagnetic insights into the Neoproterozoic connection between South China and India and their position in Rodinia. Geophys. Res. Lett. 49 e2022GL098348.
Cheney, E.S., 1996. Sequence stratigraphy and plate tectonic significance of the Transvaal succession of southern Africa and its equivalent in Western Australia. Precambrian Res. 79 (1—2), 3–24.
Choudhary, B.R., Ernst, R.E., Xu, Y.-G., Evans, D.A.D., de Kock, M.O., Meert, J.G., Ruiz, A.S., Lima, G.A., 2019. Geochemical characterization of a reconstructed 1110 Ma Large Igneous Province. Precambrian Res. 332, 105382.
Coffin, M.F., Eldholm, O., 1994. Large igneous provinces: crustal structure, dimensions, and external consequences. Rev. Geophys. 32, 1–36.
Collins, A.S., 2006. Madagascar and the amalgamation of Central Gondwana. Gondwana Res. 9 (1), 3–16.
Condie, K.C., 2005. Earth as an Evolving Planetary System. Elsevier Academic Press.
Condie, K.C., Arndt, N., Davaille, A., Puetz, S.J., 2017. Zircon age peaks: production or preservation of continental crust? Geosphere 13 (2), 227–234.
Condie, K.C., Pisarevsky, S.A., Puetz, S.J., 2021. LIPs, orogens and supercontinents: the ongoing saga. Gondwana Res. 96, 105–121.
Conrad, C.P., Lithgow-Bertelloni, C., 2004. The temporal evolution of plate driving forces: Importance of "slab suction" versus "slab pull" during the Cenozoic. Journal of Geophysical Research-Solid Earth 109 (B10407).
Correa-Gomes, L., Oliveira, E., 2000. Radiating 1.0 Ga mafic dyke swarms of eastern Brazil and western Africa: evidence of post-assembly extension in the Rodinia supercontinent? Gondwana Res. 3 (3), 325–332.
Cox, D.M., Frost, C.D., Chamberlain, K.R., 2000. 2.01-Ga Kennedy dike swarm, southeastern Wyoming: record of a rifted margin along the southern Wyoming province. Rocky Mountain. Geology 35 (1), 7–30.
Cox, G.M., Halverson, G.P., Stevenson, R.K., Vokaty, M., Poirier, A., Kunzmann, M., Li, Z.-X., Denyszyn, S.W., Strauss, J.V., Macdonald, F.A., 2016. Continental flood basalt weathering as a trigger for Neoproterozoic Snowball Earth. Earth Planet. Sci. Lett. 446, 89–99.
Dalziel, I.W.D., 1991. Pacific margins of Laurentia and East Antarctica - Australia as a conjugate rift pair: evidence and implications for an Eocambrian supercontinent. Geology 19, 598–601.
Damm, V., Gendler, T., Gooskova, E., Khramov, A., Lewandowski, M., Nozharov, P., Pavlov, V., Petrova, G., Pisarevsky, S., Sokolov, S., 1997. Palaeomagnetic studies of Proterozoic rocks from the Lake Onega region, southeast Fennoscandian Shield. Geophys. J. Int. 129 (3), 518–530.
De Kock, M.O., Ernst, R., Söderlund, U., Jourdan, F., Hofmann, A., Le Gall, B., Bertrand, H., Chisonga, B.C., Beukes, N., Rajesh, H., 2014. Dykes of the 1.11 Ga Umkondo LIP, Southern Africa: clues to a complex plumbing system. Precambrian Res. 249, 129–143.
de Kock, M.O., Evans, D.A.D., Beukes, N.J., 2009. Validating the existence of Vaalbara in the Neoarchean. Precambrian Res. 174 (1), 145–154.

Denyszyn, S.W., Halls, H.C., Davis, D.W., Evans, D.A.D., 2009. Palaeomagnetism and U-Pb geochronology of Franklin dykes in high arctic Canada and Greenland: a revised age and paleomagnetic pole constraining block rotations in the Nares Strait region. Can. J. Earth Sci. 46 (9), 689–705.
Dhuime, B., Hawkesworth, C.J., Cawood, P.A., Storey, C.D., 2012. A change in the geodynamics of continental growth 3 billion years Ago. Science 335 (6074), 1334–1336.
Domeier, M., Torsvik, T.H., 2014. Plate tectonics in the late Paleozoic. Geosci. Front. 5 (3), 303–350.
Domeier, M., Torsvik, T.H., 2019. Full-plate modelling in pre-Jurassic time. Geol. Mag. 156 (2), 261–280.
Donskaya, T.V., 2020. Assembly of the Siberian Craton: constraints from Paleoproterozoic granitoids. Precambrian Res. 348, 105869.
Doucet, L.S., Li, Z.-X., Ernst, R.E., Kirscher, U., El Dien, H.G., Mitchell, R.N., 2020a. Coupled supercontinent–mantle plume events evidenced by oceanic plume record. Geology 48 (2), 159–163.
Doucet, L.S., Li, Z.-X., Gamal El Dien, H., Pourteau, A., Murphy, J.B., Collins, W.J., Mattielli, N., Olierook, H.K.H., Spencer, C.J., Mitchell, R.N., 2020b. Distinct formation history for deep-mantle domains reflected in geochemical differences. Nat. Geosci. 13 (7), 511–515.
Dziewonski, A.M., 1984. Mapping the lower mantle - determination of lateral heterogeneity in p-velocity up to degree and order-6. J. Geophys. Res. 89 (NB7), 5929–5952.
Dziewonski, A.M., Lekic, V., Romanowicz, B.A., 2010. Mantle Anchor Structure: an argument for bottom up tectonics. Earth Planet. Sci. Lett. 299 (1—2), 69–79.
Ernst, R.E., 2014. Large Igneous Provinces. In: Cambridge University Press, Cambridge, p. 653.
Ernst, R.E., Bell, K., 2010. Large igneous provinces (LIPs) and carbonatites. Mineral. Petrol. 98, 55–76.
Ernst, R.E., Bleeker, W., 2010. Large igneous provinces (LIPs), giant dyke swarms, and mantle plumes: significance for breakup events within Canada and adjacent regions from 2.5 Ga to the PresentThis article is one of a selection of papers published in this Special Issue on the the theme Lithoprobe—parameters, processes, and the evolution of a continent.Lithoprobe Contribution 1482. Geological Survey of Canada Contribution 20100072. Can. J. Earth Sci. 47 (5), 695–739.
Ernst, R.E., Bleeker, W., Söderlund, U., Kerr, A.C., 2013a. Large Igneous Provinces and supercontinents: toward completing the plate tectonic revolution. Lithos 174, 1–14.
Ernst, R.E., Bond, D.P.G., Zhang, S.-H., Buchan, K.L., Grasby, S.E., Youbi, N., El Bilali, H., Bekker, A., Doucet, L., 2021. Large Igneous Province record through time and implications for secular environmental changes and geological time-scale boundaries. In: Ernst, R.E., Dickson, A.J., Bekker, A. (Eds.), Large Igneous Provinces: A Driver of Global Environmental and Biotic Changes. AGU Geophysical Monograph, AGU, pp. 3–26.
Ernst, R.E., Buchan, K.L., 1997. Giant radiating dyke swarm: their use in identifying pre-Mesozoic large igneous province and mantle plumes. In: J.J.M.a.M.F. Coffin (Ed.), Large Igneous Provinces; Continental, Oceanic, and Planetary Flood Volcanism. Geophysical Monograph. American Geophysical Union, Washington, DC, pp. 297–333.
Ernst, R.E., Buchan, K.L., 2001. The use of mafic dike swarms in identifying and locating. In: Ernst, R.E., Buchan, K.L. (Eds.), Mantle Plumes: Their Identification through Time. Geological Society of America, Special Paper 352, pp. 247–265.
Ernst, R.E., Buchan, K.L., 2002. Maximum size and distribution in time and space of mantle plumes: evidence from large igneous provinces. J. Geodynam. 34, 309–342 [Erratum: J. Geodynamics, 2002, 34: 711-714].
Ernst, R.E., Buchan, K.L., 2003. Recognizing mantle plumes in the geological record. Annu. Rev. Earth Planet. Sci. 31, 469–523.
Ernst, R.E., Davies, D.R., Jowitt, S.M., Campbell, I.H., 2018. When do mantle plumes destroy diamonds? Earth Planet. Sci. Lett. 502, 244–252.
Ernst, R.E., Hamilton, M.A., Söderlund, U., Hanes, J.A., Gladkochub, D.P., Okrugin, A.V., Kolotilina, T., Mekhonoshin, A.S., Bleeker, W., LeCheminant, A.N., Buchan, K.L., Chamberlain, K.R., Didenko, A.N., 2016. Long-lived connection between southern Siberia and northern Laurentia in the Proterozoic. Nat. Geosci. 9 (6), 464–469.
Ernst, R.E., Pereira, E., Hamilton, M.A., Pisarevsky, S.A., Rodriques, J., Tassinari, C.C., Teixeira, W., Van-Dunem, V., 2013b. Mesoproterozoic intraplate magmatic 'barcode'record of the Angola portion of the Congo Craton: newly dated magmatic events at 1505 and 1110 Ma and implications for Nuna (Columbia) supercontinent reconstructions. Precambrian Res. 230, 103–118.
Ernst, R.E., Srivastava, R.K., 2008. India's place in the Proterozoic world: constraints from the Large Igneous Province (LIP) record. Indian dykes. In: Srivastava, R.K., Sivaji, Ch., Chalapathi Rao, N.V. (Eds.), Geochemistry, Geophysics, and Geochronology. Narosa Publishing House Pvt. Ltd, New Delhi, India, pp. 41–56.
Ernst, R.E., Wingate, M.T.D., Buchan, K.L., Li, Z.X., 2008b. Global record of 1600—700 Ma large Igneous Provinces (LIPs): implications for the reconstruction of the proposed Nuna (Columbia) and Rodinia supercontinents. Precambrian Res. 160 (1—2), 159–178.
Evans, D.A., 1998. True polar wander, a supercontinental legacy. Earth Planet. Sci. Lett. 157 (1—2), 1–8.
Evans, D.A.D., 2003. True polar wander and supercontinents. Tectonophysics 362, 303–320.
Evans, D.A.D., 2013. Reconstructing pre-Pangaean supercontinents. Geol. Soc. Am. Bull. 125 (11—12), 1735–1751.
Evans, D.A.D., 2021. Chapter 17 - Meso-Neoproterozoic Rodinia supercycle. In: Pesonen, L.J., Salminen, J., Elming, S.-Å., Evans, D.A.D., Veikkolainen, T. (Eds.), Ancient Supercontinents and the Paleogeography of Earth. Elsevier, pp. 549–576.
Evans, D.A., Li, Z.X., Kirschvink, J.L., Wingate, M.T., 2000. A high-quality mid-Neoproterozoic paleomagnetic pole from South China, with implications for ice ages and the breakup configuration of Rodinia. Precambrian Res. 100 (1—3), 313–334.
Evans, D.A.D., Li, Z.X., Murphy, J.B., 2016a. Four-dimensional context of Earth's supercontinents. In: Li, Z.X., Evans, D.A.D., Murphy, J.B. (Eds.), Supercontinent Cycles through Earth History. Geological Society, London, Special Publications, pp. 1–14.
Evans, D.A.D., Mitchell, R.N., 2011. Assembly and breakup of the core of Paleoproterozoic-Mesoproterozoic supercontinent Nuna. Geology 39 (5), 443–446.
Evans, D.A.D., Pisarevsky, S.A., 2008. Plate tectonics on early Earth? Weighing the paleomagnetic evidence. In: Condie, K.C., Pease, V. (Eds.), When Did Plate Tectonics Begin on Earth? Geological Society of America, Special Paper, pp. 249–263.
Evans, D.A.D., Trindade, R.I.F., Catelani, E.L., D'Agrella-Filho, M.S., Heaman, L.M., Oliveira, E.P., Söderlund, U., Ernst, R.E., Smirnov, A.V., Salminen, J.M., 2016b. Return to Rodinia? Moderate to high palaeolatitude of the São Francisco/Congo craton at 920 Ma. Geol. Soc. Lond., Spec. Publ. 424 (1), 167–190.
Evans, D.A.D., Veselovsky, R.V., Petrov, P.Y., Shatsillo, A.V., Pavlov, V.E., 2016c. Palaeomagnetism of Mesoproterozoic margins of the Anabar Shield: a hypothesised billion-year partnership of Siberia and northern Laurentia. Precambrian Res. 281, 639–655.
Evans, D.A.D., Pesonen, L.J., Eglington, B.M., Elming, S.-Å., Gong, Z., Li, Z.-X., McCausland, P.J., Meert, J.G., Mertanen, S., Pisarevsky, S.A., Pivarunas, A.F., Salminen, J., Swanson-Hysell, N.L., Torsvik, T.H., Trindade, R.I.F., Veikkolainen, T., Zhang, S., 2021. Chapter 19 – An expanding list of reliable paleomagnetic poles for Precambrian tectonic reconstructions., Ancient Supercontinents and the Paleogeography of Earth. In: Pesonen, L.J., Salminen, J., Elming, S.-Å., Evans, D.A.D., Veikkolainen, T. (Eds.), Ancient Supercontinents and the Paleogeography of Earth. Elsevier, pp. 605–639.
Eyster, A., Weiss, B.P., Karlstrom, K., Macdonald, F.A., 2020. Palaeomagnetism of the Chuar Group and evaluation of the late Tonian Laurentian apparent polar wander path with implications for the makeup and breakup of Rodinia. Bulletin 132 (3—4), 710–738.
Fahrig, W., 1987. The tectonic settings of continental mafic dyke swarms: failed arm and early passive margin. In: Halls, H.C., Fahrig, W.F. (Eds.), Mafic Dyke Swarms. Geological Association of Canada Special Paper 34, pp. 331–348.
Fan, H.-P., Zhu, W.-G., Li, Z.-X., 2020. Paleo- to Mesoproterozoic magmatic and tectonic evolution of the southwestern Yangtze Block, South China: new constraints from ca. 1.7—1.5 Ga mafic rocks in the Huili-Dongchuan area. Gondwana Res. 87, 248–262.
Fedotova, M., Khramov, A., Pisakin, B., Priyatkin, A., 1999. Early Proterozoic palaeomagnetism: new results from the intrusives and related rocks of the Karelian, Belomorian and Kola provinces, eastern Fennoscandian Shield. Geophys. J. Int. 137 (3), 691–712.
Forsyth, D., Uyeda, S., 1975. On the relative importance of the driving forces of plate motion. Geophys. J. Int. 43 (1), 163–200.
Fu, H., Zhang, S., Condon, D.J., Xian, H., 2022. Secular change of true polar wander over the past billion years. Sci.Adv. 8 (41), eabo2753.
Furlanetto, F., Thorkelson, D.J., Daniel Gibson, H., Marshall, D.D., Rainbird, R.H., Davis, W.J., Crowley, J.L., Vervoort, J.D., 2013. Late Paleoproterozoic terrane accretion in northwestern Canada and the case for circum-Columbian orogenesis. Precambrian Res. 224, 512–528.
Furlanetto, F., Thorkelson, D.J., Rainbird, R.H., Davis, W.J., Gibson, H.D., Marshall, D. D., 2016. The Paleoproterozoic Wernecke Supergroup of Yukon, Canada: Relationships to orogeny in northwestern Laurentia and basins in North America, East Australia, and China. Gondwana Res. 39, 14–40.
Gala, M.G., Symons, D.T.A., Palmer, H.C., 1995. In: Palaeomagnetism of the Jan Lake granite, Trans-Hudson orogen. Summary of Investigations 1995, Saskatchewan Geological Survey, Miscellaneous Report 95-4, pp. 145–152.
Gamal El Dien, H., Doucet, L.S., Li, Z.-X., 2019. Global geochemical fingerprinting of plume intensity suggests coupling with the supercontinent cycle. Nat. Commun. 10 (1), 5270.
Gamal El Dien, H., Doucet, L.S., Murphy, J.B., Li, Z.-X., 2020. Geochemical evidence for a widespread mantle re-enrichment 3.2 billion years ago: implications for global-scale plate tectonics. Sci. Rep. 10 (1), 9461.
Gibson, G.M., Hutton, L.J., Holzschuh, J., 2017. Basin inversion and supercontinent assembly as drivers of sediment-hosted Pb–Zn mineralization in the Mount Isa region, northern Australia. J. Geol. Soc. 174 (4), 773–786.
Gladkochub, D.P., Donskaya, T.V., Pisarevsky, S.A., Ernst, R.E., Söderlund, U., Kotov, A. B., Kovach, V.P., Okrugin, A.V., 2022. 1.79—1.75 Ga mafic magmatism of the Siberian craton and late Paleoproterozoic paleogeography. Precambrian Res. 370, 106557.
Gladkochub, D.P., Donskaya, T.V., Stanevich, A.M., Pisarevsky, S.A., Zhang, S., Motova, Z.L., Mazukabzov, A.M., Li, H., 2019. U-Pb detrital zircon geochronology and provenance of Neoproterozoic sedimentary rocks in southern Siberia: new insights into breakup of Rodinia and opening of Paleo-Asian Ocean. Gondwana Res. 65, 1–16.
Gladkochub, D.P., Pisarevsky, S.A., Donskaya, T.V., Ernst, R.E., Wingate, M.T.D., Söderlund, U., Mazukabzov, A.M., Sklyarov, E.V., Hamilton, M.A., Hanes, J.A., 2010. Proterozoic mafic magmatism in Siberian craton: an overview and implications for paleocontinental reconstruction. Precambrian Res. 183 (3), 660–668.
Godderis, Y., Donnadieu, Y., Nédélec, A., Dupré, B., Dessert, C., Grard, A., Ramstein, G., Francois, L.M., 2003. The Sturtian 'snowball' glaciation: fire and ice. Earth Planet. Sci. Lett. 211 (1—2), 1–12.
Goddéris, Y., Le Hir, G., Macouin, M., Donnadieu, Y., Hubert-Théou, L., Dera, G., Aretz, M., Fluteau, F., Li, Z.X., Halverson, G.P., 2017. Paleogeographic forcing of the strontium isotopic cycle in the Neoproterozoic. Gondwana Res. 42, 151–162.
Gold, T., 1955. Instability of Earth's axis of rotation. Nature 175, 526–529.

Goldberg, A.S., 2010. Dyke swarms as indicators of major extensional events in the 1.9—1.2 Ga Columbia supercontinent. J. Geodyn. 50 (3—4), 176–190.
Goldreich, P., Toomre, A., 1969. Some remarks on polar wandering. J. Geophys. Res. 74, 2555–2567.
Gong, Z., Evans, D.A.D., Youbi, N., Lahna, A.A., Söderlund, U., Malek, M.A., Wen, B., Jing, X., Ding, J., Boumehdi, M.A., Ernst, R.E., 2021. Reorienting the West African craton in Paleoproterozoic-Mesoproterozoic supercontinent Nuna. Geology 49 (10), 1171–1176.
Gumsley, A.P., Chamberlain, K.R., Bleeker, W., Söderlund, U., Kock, M.O.D., Larsson, E. R., Bekker, A., 2017. Timing and tempo of the Great Oxidation Event. Proc. Nat. Acad. Sci. 114 (8), 1811–1816.
Hamilton, M.A., Buchan, K.L., 2010. U-Pb geochronology of theWestern Channel Diabase, northwestern Laurentia:implications for a large 1.59Ga magmatic province, Laurentia's APWP and paleocontinental reconstructions of Laurentia, Baltica and Gawler Craton of southern Australia. Precambrian Res. 183, 463–473.
Hanson, R.E., Puckett Jr., R.E., Keller, G.R., Brueseke, M.E., Bulen, C.L., Mertzman, S.A., Finegan, S.A., McCleery, D.A., 2013. Intraplate magmatism related to opening of the southern Iapetus Ocean: Cambrian Wichita igneous province in the Southern Oklahoma rift zone. Lithos 174, 57–70.
Harlan, S.S., Geissman, J.W., 1998. Palaeomagnetism of the Middle Proterozoic Electra Lake Gabbro, Needle Mountains, southwestern Colorado. J. Geophys.Res.Solid Earth 103 (B7), 15497–15507.
Harlan, S.S., Geissman, J.W., Snee, L.W., 1997. In: Paleomagnetic and 40Ar/39Ar geochronologic data from Late Proterozoic mafic dikes and sills, Montana and Wyoming. United States Geological Survey Professional Paper, 1580, pp. 1–16.
Harlan, S.S., Geissman, J.W., Snee, L.W., 2008. Palaeomagnetism of Proterozoic mafic dikes from the Tobacco root Mountains, Southwest Montana. Precambrian Res. 163 (3—4), 239–264.
Harlan, S.S., Snee, L.W., Geissman, J.W., Brearley, A.J., 1994. Palaeomagnetism of the Middle Proterozoic Laramie anorthosite complex and Sherman Granite, southern Laramie Range, Wyoming and Colorado. J. Geophys. Res.Solid Earth 99 (B9), 17997–18020.
Harlan, S.S., Heaman, L., LeCheminant, A.N., Premo, W.R., 2003. Gunbarrel mafic magmatic event: a key 780 Ma time marker for Rodinia plate reconstructions. Geology 31 (12), 1053–1056.
Harrison, T.M., 2020. Hadean Earth. Springer. https://doi.org/10.1007/978-3-030-46687-9 ebook. 291 pp.
Hawkesworth, C., Cawood, P., Dhuime, B., 2013. Continental growth and the crustal record. Tectonophysics 609, 651–660.
Heaman, L.M., LeCheminant, A.N., Rainbird, R.H., 1992. Nature and timing of Franklin igneous events, Canada; implications for a late Proterozoic mantle plume and the break-up of Laurentia. Earth Planet. Sci. Lett. 109 (1—2), 117–131.
Hoffman, P.F., 1991. Did the breakout of Laurentia turn Gondwanaland inside-out? Science 252, 1409–1412.
Hoffman, P.F., 1997. Tectonic genealogy of North America. In: van der Pluijm, B.A., Marshak, S. (Eds.), Earth Structure: An Introduction to Structural Geology and Tectonics. McGraw-Hill, New York, pp. 459–464.
Hoffman, P.F., 2014. The Origin of Laurentia: Rae Craton as the backstop for proto-Laurentian amalgamation by slab suction. Geosci. Can. 41 (3), 313–320.
Hoffman, P.F., Abbot, D.S., Ashkenazy, Y., Benn, D.I., Brocks, J.J., Cohen, P.A., Cox, G. M., Creveling, J.R., Donnadieu, Y., Erwin, D.H., Fairchild, I.J., Ferreira, D., Goodman, J.C., Halverson, G.P., Jansen, M.F., Le Hir, G., Love, G.D., Macdonald, F. A., Maloof, A.C., Partin, C.A., Ramstein, G., Rose, B.E.J., Rose, C.V., Sadler, P.M., Tziperman, E., Voigt, A., Warren, S.G., 2017. Snowball Earth climate dynamics and Cryogenian geology-geobiology. Sci. Adv. 3 (11).
Hoffman, P.F., Kaufman, A.J., Halverson, G.P., Schrag, D.P., 1998. A Neoproterozoic snowball earth. Science 281 (5381), 1342–1346.
Holder, R.M., Viete, D.R., Brown, M., Johnson, T.E., 2019. Metamorphism and the evolution of plate tectonics. Nature 572 (7769), 378–381.
Hounslow, M.W., Domeier, M., Biggin, A.J., 2018. Subduction flux modulates the geomagnetic polarity reversal rate. Tectonophysics 742—743, 34–49.
Huang, C., Li, Z.X., Zheng, N., 2022. Will Earth's next supercontinent assemble through the closure of the Pacific Ocean? Natl. Sci. Rev. 9 (12), nwac205.
Jing, X.-Q., Yang, Z., Tong, Y., Han, Z., 2015. A revised paleomagnetic pole from the mid-Neoproterozoic Liantuo Formation in the Yangtze block and its paleogeographic implications. Precambrian Res. 268, 194–211.
Johnson, S.P., 2014. In: The birth of supercontinents and the Proterozoic assembly of Western Australia. Australasian Institute of Mining and Metallurgy, pp. 53–56.
Johnson, S.P., Sheppard, S., Rasmussen, B., Wingate, M.T.D., Kirkland, C.L., Muhling, J. R., Fletcher, I.R., Belousova, E.A., 2011. Two collisions, two sutures: punctuated pre-1950Ma assembly of the West Australian Craton during the Ophthalmian and Glenburgh Orogenies. Precambrian Res. 189 (3—4), 239–262.
Karlstrom, K.E., Harlan, S.S., Williams, M.L., McLelland, J., Geissman, J.W., Ahall, K.I., 1999. Refining Rodinia; geologic evidence for the Australia-Western U.S. Connection in the Proterozoic. GSA Today 9 (10), 1–7.
King, R.F., 1955. The remanent magnetism of artificially deposited sediments. Geophys. Suppl. Monthly Notices Roy.Astronom.Soc. 7 (3), 115–134.
Kirscher, U., Liu, Y., Li, Z.X., Mitchell, R.N., Pisarevsky, S.A., Denyszyn, S.W., Nordsvan, A., 2019. Palaeomagnetism of the Hart Dolerite (Kimberley, Western Australia) – a two-stage assembly of the supercontinent Nuna? Precambrian Res. 329, 170–181.
Kirscher, U., Mitchell, R.N., Liu, Y., Nordsvan, A.R., Cox, G.M., Pisarevsky, S.A., Wang, C., Wu, L., Murphy, J.B., Li, Z.-X., 2021. Paleomagnetic constraints on the duration of the Australia-Laurentia connection in the core of the Nuna supercontinent. Geology 49 (2), 174–179.
Kirschvink, J.L., 1992. Late Proterozoic low-latitude global glaciation: the snowball earth. In: Schopf, J.W., Klein, C. (Eds.), The Proterozoic Biosphere. Cambridge University Press, pp. 51–52.
Kirschvink, J.L., Ripperdan, R.L., Evans, D.A., 1997. Evidence for a large-scale reorganisation of Early Cambrian continental masses by inertial interchange true polar wander. Science 277, 541–545.
Knoll, A.H., 1991. End of the Proterozoic Eon. Sci. Am. 265 (4), 64–73.
Kodama, K.P., 2009. Simplification of the anisotropy-based inclination correction technique for magnetite- and haematite-bearing rocks: a case study for the Carboniferous Glenshaw and Mauch Chunk Formations,North America. Geophys. J. Int. 176 (2), 467–477.
Korenaga, J., 2021. Hadean geodynamics and the nature of early continental crust. Precambrian Res. 359, 106178.
Kroner, A., Cordani, U., 2003. African, southern indian and South American cratons were not part of the Rodinia supercontinent: evidence from field relationships and geochronology. Tectonophysics 375 (1—4), 325–352.
Kusky, T.M., Li, J., 2003. Paleoproterozoic tectonic evolution of the North China Craton. J. Asian Earth Sci. 22 (4), 383–397.
Kusky, T., Li, J., Santosh, M., 2007. The Paleoproterozoic North Hebei Orogen: North China craton's collisional suture with the Columbia supercontinent. Gondwana Res. 12 (1), 4–28.
Kusky, T.M., Polat, A., Windley, B.F., Burke, K.C., Dewey, J.F., Kidd, W.S.F., Maruyama, S., Wang, J.P., Deng, H., Wang, Z.S., Wang, C., Fu, D., Li, X.W., Peng, H. T., 2016. Insights into the tectonic evolution of the North China Craton through comparative tectonic analysis: a record of outward growth of Precambrian continents. Earth Sci. Rev. 162, 387–432.
Kusky, T., Windley, B.F., Polat, A., Wang, L., Ning, W., Zhong, Y., 2021. Archean dome-and-basin style structures form during growth and death of intraoceanic and continental margin arcs in accretionary orogens. Earth Sci. Rev. 220, 103725.
Lan, Z., Li, X.-H., Zhu, M., Zhang, Q., Li, Q.-L., 2015. Revisiting the Liantuo Formation in Yangtze Block, South China: SIMS U-Pb zircon age constraints and regional and global significance. Precambrian Res. 263, 123–141.
Le Vaillant, M., Barnes, S.J., Mole, D.R., Fiorentini, M.L., Laflamme, C., Denyszyn, S.W., Austin, J., Patterson, B., Godel, B., Hicks, J., 2020. Multidisciplinary study of a complex magmatic system: the Savannah Ni-Cu-Co Camp,Western Australia. Ore Geol. Rev. 117, 103292.
Li, W., Li, X., Li, Z.X., 2010. Ca. 850 Ma bimodal volcanic rocks in northeastern Jiangxi Province, South China: initial extension during the breakup of Rodinia? Am. J. Sci. 310 (9), 951–980.
Li, X.-H., Li, W.-X., Li, Z.X., Lo, C.-H., Wang, J., Ye, M.-F., Yang, Y.-H., 2009. Amalgamation between the Yangtze and Cathaysia Blocks in South China: constraints from SHRIMP U-Pb zircon ages, geochemistry and Nd–Hf isotopes of the Shuangxiwu volcanic rocks. Precambrian Res. 174 (1), 117–128.
Li, Z.X., Li, X., Kinny, P., Wang, J., 1999. The breakup of Rodinia: did it start with a mantle plume beneath South China? Earth Planet. Sci. Lett. 173 (3), 171–181.
Li, Z.X., Evans, D.A.D., 2011. Late Neoproterozoic 40° intraplate rotation within Australia allows for a tighter-fitting and longer-lasting Rodinia. Geology 39 (1), 39–42.
Li, Z.X., Evans, D.A.D., Halverson, G.P., 2013. Neoproterozoic glaciations in a revised global palaeogeography from the breakup of Rodinia to the assembly of Gondwanaland. Sediment. Geol. 294, 219–232.
Li, Z.X., Li, X., Kinny, P., Wang, J., Zhang, S., Zhou, H., 2003. Geochronology of Neoproterozoic syn-rift magmatism in the Yangtze Craton, South China and correlations with other continents: evidence for a mantle superplume that broke up Rodinia. Precambrian Res. 122 (1), 85–109.
Li, Z.X., Li, X.-H., Zhou, H., Kinny, P.D., 2002. Grenvillian continental collision in South China: new SHRIMP U-Pb zircon results and implications for the configuration of Rodinia. Geology 30 (2), 163–166.
Li, Z.X., Zhang, L., Powell, C.M., 1995. South China in Rodinia: part of the missing link between Australia-East Antarctica and Laurentia? Geology 23 (5), 407–410.
Li, Z.X., Bogdanova, S.V., Collins, A.S., Davidson, A., De Waele, B., Ernst, R.E., Fitzsimons, I.C.W., Fuck, R.A., Gladkochub, D.P., Jacobs, J., Karlstrom, K.E., Lu, S., Natapov, L.M., Pease, V., Pisarevsky, S.A., Thrane, K., Vernikovsky, V., 2008a. Assembly, configuration, and break-up history of Rodinia: a synthesis. Precambrian Res. 160 (1—2), 179–210.
Li, Z.X., Evans, D.A.D., Zhang, S., 2004. A 90° spin on Rodinia: possible causal links between the Neoproterozoic supercontinent, superplurne, true polar wander and low-latitude glaciation. Earth Planet. Sci. Lett. 220 (3—4), 409–421.
Li, Z.X., Li, X.H., Li, W.X., Ding, S., 2008b. Was Cathaysia part of Proterozoic Laurentia?–new data from Hainan Island, South China. Terra Nova 20 (2), 154–164.
Li, Z.X., Mitchell, R.N., Spencer, C.J., Ernst, R., Pisarevsky, S., Kirscher, U., Murphy, J.B., 2019. Decoding Earth's rhythms: modulation of supercontinent cycles by longer superocean episodes. Precambrian Res. 323, 1–5.
Li, Z.X., Powell, C.M., 2001. An outline of the palaeogeographic evolution of the Australasian region since the beginning of the Neoproterozoic. Earth Sci. Rev. 53 (3), 237–277.
Li, Z.X., Zhang, L., Powell, C.M., 1996. Positions of the East Asian cratons in the Neoproterozoic supercontinent Rodinia. Aust. J. Earth Sci. 43 (6), 593–604.
Li, Z.X., Zhong, S., 2009. Supercontinent-superplume coupling, true polar wander and plume mobility: plate dominance in whole-mantle tectonics. Phys.Earth Planet. Inter. 176 (3—4), 143–156.
Liu, Y., Li, Z.-X., Pisarevsky, S., Kirscher, U., Mitchell, R.N., Stark, J.C., 2019. Palaeomagnetism of the 1.89 Ga Boonadgin dykes of the Yilgarn Craton: possible connection with India. Precambrian Res. 329, 211–223.

Liu, Y., Mitchell, R.N., Brown, M., Johnson, T.E., Pisarevsky, S., 2022. Linking metamorphism and plate boundaries over the past 2 billion years. Geology 50 (5), 631–635.
Liu, Y., Mitchell, R.N., Li, Z.-X., Kirscher, U., Pisarevsky, S.A., Wang, C., 2021. Archean geodynamics: ephemeral supercontinents or long-lived supercratons. Geology 49 (7), 794–798.
Lu, G.M., Wang, W., Cawood, P.A., Ernst, R.E., Raveggi, M., Huang, S.F., Xue, E.K., 2020. Late Paleoproterozoic to Early Mesoproterozoic Mafic Magmatism in the SW Yangtze Block: Mantle Plumes Associated With Nuna Breakup? J. Geophys. Res. Solid Earth 125 (7) e2019JB019260.
Lu, K., Mitchell, R.N., Yang, C., Zhou, J.-L., Wu, L.-G., Wang, X.-C., Li, X.-H., 2022. Widespread magmatic provinces at the onset of the Sturtian snowball Earth. Earth Planet. Sci. Lett. 594, 117736.
Lu, S.N., Li, H.K., Zhang, C.L., Niu, G.H., 2008. Geological and geochronological evidence for the Precambrian evolution of the Tarim Craton and surrounding continental fragments. Precambrian Res. 160 (1—2), 94–107.
Lubnina, N., Pisarevsky, S., Söderlund, U., Nilsson, M., Sokolov, S., Khramov, A., Iosifidi, A., Ernst, R., Romanovskaya, M., Pisakin, B., 2012. In: New palaeomagnetic and geochronological data from the Ropruchey sill (Karelia, Russia): implications for late Palaeoproterozoic palaeogeography. Supercontinent Symposium, Helsinki, Finland, pp. 81–82.
Maloof, A.C., Halverson, G.P., Kirschvink, J.L., Schrag, D.P., Weiss, B.P., Hoffman, P.F., 2006. Combined paleomagnetic, isotopic, and stratigraphic evidence for true polar wander from the Neoproterozoic Akademikerbreen Group, Svalbard,Norway. Geol. Soc. Am. Bull. 118 (9—10), 1099–1124.
Martin, E.L., Spencer, C.J., Collins, W.J., Thomas, R.J., Macey, P.H., Roberts, N.M.W., 2020. The core of Rodinia formed by the juxtaposition of opposed retreating and advancing accretionary orogens. Earth Sci. Rev. 211, 103413.
Maruyama, S., 1994. Plume tectonics. J. Geol. Soc. Jpn. 100 (1), 24–49.
Matthews, K.J., Maloney, K.T., Zahirovic, S., Williams, S.E., Seton, M., Müller, R.D., 2016. Global plate boundary evolution and kinematics since the late Paleozoic. Glob. Planet. Chang. 146, 226–250.
McKenzie, D.P., Parker, R.L., 1967. The North Pacific: an example of tectonics on a sphere. Nature 216 (5122), 1276–1280.
McMenamin, M.A.S., McMenamin, D.L.S., 1990. The Emergence of Animals: The Cambrian Breakthrough. In: Colombia University Press, New York, p. 217.
Meert, J.G., 2002. Paleomagnetic evidence for a Paleo-Mesoproterozoic supercontinent Columbia. In: Santosh, M., John, J.W. Rogers (Eds.), Mesoproterozoic supercontinent. International Association for Gondwana Research. Osaka, Japan, 2002.
Meert, J.G., 2003. A synopsis of events related to the assembly of eastern Gondwana. Tectonophysics 362 (1—4), 1–40.
Meert, J.G., 2012. What's in a name? The Columbia (Paleopangaea/Nuna) supercontinent. Gondwana Res. 21 (4), 987–993.
Meert, J.G., Pivarunas, A.F., Evans, D.A.D., Pisarevsky, S.A., Pesonen, L.J., Li, Z.-X., Elming, S.-Å., Miller, S.R., Zhang, S., Salminen, J.M., 2020. The magnificent seven: a proposal for modest revision of the Van der Voo (1990) quality index. Tectonophysics 790, 228549.
Merdith, A.S., Collins, A.S., Williams, S.E., Pisarevsky, S., Foden, J.D., Archibald, D.B., Blades, M.L., Alessio, B.L., Armistead, S., Plavsa, D., Clark, C., Müller, R.D., 2017. A full-plate global reconstruction of the Neoproterozoic. Gondwana Res. 50, 84–134.
Merdith, A.S., Williams, S.E., Collins, A.S., Tetley, M.G., Mulder, J.A., Blades, M.L., Young, A., Armistead, S.E., Cannon, J., Zahirovic, S., Müller, R.D., 2021. Extending full-plate tectonic models into deep time: linking the Neoproterozoic and the Phanerozoic. Earth Sci. Rev. 214, 103477.
Mitchell, R.N., Cox, G.M., O'Rourke, J.G., Li, Z.-X., Spencer, C.J., Kirscher, U., Zhang, N., Murphy, J.B., Nordsvan, A., Asimow, P.D., 2018. Did Earth's first supercontinent form the inner core?, AGU Fall Meeting Abstracts. DI21B-0015.
Mitchell, R.N., Kilian, T.M., Evans, D.A.D., 2012. Supercontinent cycles and the calculation of absolute palaeolongitude in deep time. Nature 482 (7384), 208–211.
Mitchell, R.N., Zhang, N., Salminen, J., Liu, Y., Spencer, C.J., Steinberger, B., Murphy, J. B., Li, Z.-X., 2021. The supercontinent cycle. Nat.Rev.Earth Environ. 2 (5), 358–374.
Morgan, W.J., 1968. Rises, trenches, great faults, and crustal blocks. J. Geophys. Res. 73 (6), 1959–1982.
Moores, E.M., 1991. Southwest U.S.-East Antarctic (SWEAT) connection: a hypothesis. Geology 19, 425–428.
Moresi, L., Solomatov, V., 1998. Mantle convection with a brittle lithosphere: thoughts on the global tectonic styles of the Earth and Venus. Geophys. J. Int. 133 (3), 669–682.
Mulder, F.G., 1971. Paleomagnetic research in some parts of central and southern Sweden. Svenska, reproduktions AB (distr.), 56pp.
Müller, R.D., Cannon, J., Tetley, M., Williams, S.E., Cao, X., Flament, N., Bodur, Ö.F., Zahirovic, S., Merdith, A., 2022. A tectonic-rules based mantle reference frame since 1 billion years ago – implications for supercontinent cycles and plate-mantle system evolution. Solid Earth Discuss. 2022, 1–42.
Müller, R.D., Dutkiewicz, A., Seton, M., Gaina, C., 2013. Seawater chemistry driven by supercontinent assembly, breakup, and dispersal. Geology 41 (8), 907–910.
Müller, R.D., Seton, M., Zahirovic, S., Williams, S.E., Matthews, K.J., Wright, N.M., Shephard, G.E., Maloney, K.T., Barnett-Moore, N., Hosseinpour, M., Bower, D.J., Cannon, J., 2016. Ocean basin evolution and global-scale plate reorganisation events since Pangaea breakup. Annu. Rev. Earth Planet. Sci. 44 (1), 107–138.
Murphy, J.B., Nance, R.D., 2003. Do supercontinents introvert or extrovert?Sm-Nd isotope evidence. Geology (Boulder) 31 (10), 873–876.
Nance, R.D., Worsley, T.R., Moody, J.B., 1988. The supercontinent cycle. Sci. Am. 259, 44–52.
Niu, J., Li, Z.-X., Zhu, W., 2016. Palaeomagnetism and geochronology of mid-Neoproterozoic Yanbian dykes, South China: implications for a c. 820—800 Ma true polar wander event and the reconstruction of Rodinia. In: Li, Z.X., Evans, D.A.D., Murphy, J.B. (Eds.), Supercontinent Cycles through Earth History. Special Publications, pp. 191–211.
Nordsvan, A.R., Collins, W.J., Li, Z.-X., Spencer, C.J., Pourteau, A., Withnall, I.W., Betts, P.G., Volante, S., 2018. Laurentian crust in northeast Australia: implications for the assembly of the supercontinent Nuna. Geology 46 (3), 251–254.
O'Neill, C., Roberts, N.M.W., 2018. Lid tectonics – Preface. Geosci. Front. 9 (1), 1–2.
Park, J.K., Buchan, K.L., Harlan, S.S., 1995. A proposed giant radiating dyke swarm fragmented by the separation of Laurentia and Australia based on palaeomagnetism of ca.780 Ma mafic intrusions in western North America. Earth Planet. Sci. Lett. 132, 129–139.
Park, Y., Swanson-Hysell, N.L., Xian, H., Zhang, S., Condon, D.J., Fu, H., Macdonald, F. A., 2021. A consistently high-latitude South China from 820 to 780 Ma: implications for exclusion from Rodinia and the feasibility of large-scale true polar wander. <sb:contribution><sb:title>J. Geophys. Res. Solid</sb:title></sb:contribution><sb:host><sb:issue><sb:series><sb:title>Earth</sb:title></sb:series></sb:issue></sb:host> 126 (6), e2020JB021541.
Pavlov, V., Gallet, Y., 2010. Variations in geomagnetic reversal frequency during the Earth's middle age. Geochem. Geophys. Geosyst. 11 (1).
Pehrsson, S.J., Eglington, B.M., Evans, D.A.D., Huston, D., Reddy, S.M., 2016. Metallogeny and its link to orogenic style during the Nuna supercontinent cycle. Geol. Soc. Lond., Spec. Publ. 424 (1), 83–94.
Peng, P., Bleeker, W., Ernst, R.E., Söderlund, U., McNicoll, V., 2011. U-Pb baddeleyite ages, distribution and geochemistry of 925 Ma mafic dykes and 900 Ma sills in the North China craton: evidence for a Neoproterozoic mantle plume. Lithos 127 (1—2), 210–221.
Peng, P., Zhai, M.-G., Ernst, R.E., Guo, J.-H., Liu, F., Hu, B., 2008. A 1.78 Ga Large Igneous Province in the North China craton: the Xiong'er Volcanic Province and the North China Dyke Swarm. Lithos 101, 260–280.
Peng, P., Xu, H., Mitchell, R.N., Teixeira, W., Kirscher, U., Qin, Z., Oliveira, E.P., Girardi, V.A.V., Wang, C., Chemale, F., 2022. Earth's oldest hotspot track at ca. 1.8 Ga advected by a global subduction system. Earth Planet Sci Lett 585, 117530.
Pesonen, L.J., Evans, D.A., Veikkolainen, T., Salminen, J., Elming, S.-Å., 2021. In: Precambrian supercontinents and supercycles—an overview.Ancient Supercontinents and the Paleogeography of Earth, pp. 1–50.
Piper, J., 1992. Palaeomagnetism of the Almunge alkaline complex and Tuna dykes, Sweden: mid-Proterozoic palaeopoles from the Fennoscandian Shield. Geologiska Föreningen i Stockholm Förhandlingar 114 (3), 291–297.
Piper, J.D., Smith, R.L., 1980. Palaeomagnetism of the Jotnian lavas and sediments and post-Jotnian dolerites of Central Scandinavia. Geologiska Föreningen i Stockholm Förhandlingar 102 (2), 67–81.
Pisarevsky, S.A., Biswal, T.K., Wang, X.C., De Waele, B., Ernst, R.E., Söderlund, U., Tait, J.A., Ratre, K., Singh, Y.K., Cleve, M., 2013. Palaeomagnetic, geochronological and geochemical study of Mesoproterozoic Lakhna Dykes in the Bastar Craton, India: implications for the Mesoproterozoic supercontinent. Lithos 174, 125–143.
Pisarevsky, S.A., Elming, S.-Å., Pesonen, L.J., Li, Z.-X., 2014a. Mesoproterozoic paleogeography: supercontinent and beyond. Precambrian Res. 244, 207–225.
Pisarevsky, S.A., Gladkochub, D.P., Donskaia, T.V., 2021. Chapter 8 - Precambrian paleogeography of Siberia. In: Pesonen, L.J., Salminen, J., Elming, S.-Å., Evans, D.A. D., Veikkolainen, T. (Eds.), Ancient Supercontinents and the Paleogeography of Earth. Elsevier, pp. 263–275.
Pisarevsky, S.A., Li, Z.X., Tetley, M.G., Liu, Y., Beardmore, J., 2022. An updated internet-based Global Paleomagnetic Database. Earth-Sci. Rev. 235, 104258.
Pisarevsky, S.A., Li, Z., Wingate, M., Tohver, E., 2012. In: Palaeomagnetism of the 1210 Ma Gnowangerup-Fraser dyke swarm, Western Australia, EGU General Assembly Conference Abstracts, p. 4049.
Pisarevsky, S.A., Wingate, M.T.D., Harris, L.B., 2003a. Late Mesoproterozoic (ca 1.2 Ga) palaeomagnetism of the Albany-Fraser orogen: no pre-Rodinia Australia-Laurentia connection. Geophys. J. Int. 155, F6–F11.
Pisarevsky, S.A., Wingate, M.T.D., Li, Z.-X., Wang, X.-C., Tohver, E., Kirkland, C.L., 2014b. Age and palaeomagnetism of the 1210Ma Gnowangerup-Fraser dyke swarm, Western Australia, and implications for late Mesoproterozoic paleogeography. Precambrian Res. 246, 1–15.
Pisarevsky, S.A., Wingate, M.T.D., Powell, C.M., Johnson, S., Evans, D.A.D., 2003b. Models of Rodinia assembly and fragmentation. In: Yoshida, M., Windley, B.F., Dasgupta, S. (Eds.), Proterozoic East Gondwana: Supercontinent Assembly and Breakup. Geol. Soc. London Spec. Pub. 206, pp. 35–55.
Pourteau, A., Smit, M.A., Li, Z.X., Collins, W.J., Nordsvan, A.R., Volante, S., Li, J., 2018. 1.6 Ga crustal thickening along the final Nuna suture. Geology 46 (11), 959–962.
Powell, C.M., Preiss, W., Gatehouse, C., Krapez, B., Li, Z.X., 1994. South Australian record of a Rodinian epicontinental basin and its mid-Neoproterozoic breakup (~ 700 Ma) to form the Palaeo-Pacific Ocean. Tectonophysics 237 (3), 113–140.
Pu, J.P., Bowring, S.A., Ramezani, J., Myrow, P., Raub, T.D., Landing, E., Mills, A., Hodgin, E., Macdonald, F.A., 2016. Dodging snowballs: geochronology of the Gaskiers glaciation and the first appearance of the Ediacaran biota. Geology 44 (11), 955–958.
Pu, J.P., Macdonald, F.A., Schmitz, M.D., Rainbird, R.H., Bleeker, W., Peak, B.A., Flowers, R.M., Hoffman, P.F., Rioux, M., Hamilton, M.A., 2022. Emplacement of the Franklin large igneous province and initiation of the Sturtian Snowball Earth. Sci. Adv. 8 (47), eadc9430.
Preiss, W.V., 2000. The Adelaide Geosyncline of South Australia and its significance in Neoproterozoic continental reconstruction. Precambrian Res. 100, 21–63.

Priyatkina, N., Ernst, R.E., Khudoley, A.K., 2020. A preliminary reassessment of the Siberian cratonic basement with new U-Pb-Hf detrital zircon data. Precambrian Res. 340, 105645.
Rainbird, R.H., Stern, R.A., Khudoley, A.K., Kropachev, A.P., Heaman, L.M., Sukhorukov, V.I., 1998. U-Pb geochronology of Riphean sandstone and gabbro from Southeast Siberia and its bearing on the Laurentia-Siberia connection. Earth Planet. Sci. Lett. 164 (3), 409–420.
Robert, B., Domeier, M., Jakob, J., 2020. Iapetan oceans: an analog of Tethys? Geology 48 (9), 929–933.
Rogers, C., Kamo, S., Söderlund, U., Hamilton, M., Ernst, R.E., Cousens, B., Harlan, S., Wade, C., Thorkelson, D., 2018. Geochemistry and U-Pb geochronology of 1590 and 1550 Ma mafic dyke swarms of western Laurentia: Mantle plume magmatism shared with Australia. Lithos 314, 216–235.
Rogers, J.J.W., Santosh, M., 2002. Configuration of Columbia, a mesoproterozoic supercontinent. Gondwana Res. 5 (1), 5–22.
Ross, G.M., 1991. Tectonic setting of the Windermere Supergroup revisited. Geology 19, 1125–1128.
Salminen, J.M., Klein, R., Mertanen, S., Pesonen, L.J., Fröjdö, S., Mänttäri, I., Eklund, O., 2016. Palaeomagnetism and U-Pb geochronology of c. 1570 Ma intrusives from Åland archipelago, SW Finland–implications for Nuna. Geol. Soc. Lond., Spec. Publ. 424 (1), 95–118.
Schmitt, R.D.S., Fragoso, R.D.A., Collins, A.S., 2018. Suturing Gondwana in the Cambrian: the Orogenic Events of the Final Amalgamation. In: Siegesmund, S., Basei, M.A.S., Oyhantçabal, P., Oriolo, S. (Eds.), Geology of Southwest Gondwana. Springer International Publishing, Cham.
Seton, M., Müller, R.D., Zahirovic, S., Gaina, C., Torsvik, T., Shephard, G., Talsma, A., Gurnis, M., Turner, M., Maus, S., Chandler, M., 2012. Global continental and ocean basin reconstructions since 200Ma. Earth Sci. Rev. 113 (3—4), 212–270.
Shu, L.-S., Faure, M., Yu, J.-H., Jahn, B.-M., 2011. Geochronological and geochemical features of the Cathaysia block (South China): new evidence for the Neoproterozoic breakup of Rodinia. Precambrian Res. 187 (3—4), 263–276.
Silveira, E., Söderlund, U., Oliveira, E., Ernst, R., Leal, A.M., 2013. First precise U-Pb baddeleyite ages of 1500 Ma mafic dykes from the São Francisco Craton, Brazil, and tectonic implications. Lithos 174, 144–156.
Smirnov, A.V., Evans, D.A.D., Ernst, R.E., Söderlund, U., Li, Z.X., 2013. Trading partners: tectonic ancestry of southern Africa and Western Australia, in Archean supercratons Vaalbara and Zimgarn. Precambrian Res. 224, 11–22.
Söderlund, U., Elming, S.-Å., Ernst, R.E., Schissel, D., 2006. The Central Scandinavian Dolerite Group – pronounced hotspot activity or back-arc magmatism? Constraints from U-Pb baddeleyite geochronology and Hf isotopic data. Precambrian Res. 150, 136–152.
Söderlund, U., Isachsen, C.E., Bylund, G., Heaman, L.M., Jonathan Patchett, P., Vervoort, J.D., Andersson, U.B., 2005. U-Pb baddeleyite ages and Hf, Nd isotope chemistry constraining repeated mafic magmatism in the Fennoscandian Shield from 1.6 to 0.9 Ga. Contrib. Mineral. Petrol. 150 (2), 174–194.
Söderlund, U., Patchett, P.J., Vervoort, J.D., Isachsen, C.E., 2004. The 176Lu decay constant determined by Lu–Hf and U-Pb isotope systematics of Precambrian mafic intrusions. Earth Planet. Sci. Lett. 219 (3—4), 311–324.
Stark, J.C., Wang, X.-C., Denyszyn, S.W., Li, Z.-X., Rasmussen, B., Zi, J.-W., Sheppard, S., Liu, Y., 2019. Newly identified 1.89 Ga mafic dyke swarm in the Archean Yilgarn Craton, Western Australia suggests a connection with India. Precambrian Res. 329, 156–169.
Steinberger, B., Torsvik, T.H., 2008. Absolute plate motions and true polar wander in the absence of hotspot tracks. Nature 452 (7187), 620–623.
Su, W., Li, H., Huff, W., Ettensohn, F., Zhang, S., Zhou, H., Wan, Y., 2010. SHRIMP U-Pb dating for a K-bentonite bed in the Tieling Formation, north China. Chinese Sci. Bull. 55 (29), 3312–3323.
Summers, M., Hall, R., Hughes, D., Nesbitt, R., Snyder, G., 1995. The Tony Ridge zoned ultramafic dyke, Wyoming, USA: preliminary geochemical results. In: Baer, G., Heimann, A. (Eds.), Physics and Chemistry of Dykes. Balkema, Rotterdam, pp. 193–204.
Swanson-Hysell, N.L., 2021. Chapter 4 - the Precambrian paleogeography of Laurentia. In: Pesonen, L.J., Salminen, J., Elming, S.-Å., Evans, D.A.D., Veikkolainen, T. (Eds.), Ancient Supercontinents and the Paleogeography of Earth. Elsevier, pp. 109–153.
Swanson-Hysell, N.L., Avery, M.S., Zhang, Y., Hodgin, E.B., Sherwood, R.J., Apen, F.E., Boerboom, T.J., Keller, C.B., Cottle, J.M., 2021. The Paleogeography of Laurentia in its early years: new constraints from the Paleoproterozoic East-Central Minnesota Batholith. Tectonics 40 (5), e2021TC006751.
Tauxe, L., Kent, D.V., 2004. A simplified statistical model for the geomagnetic field and the detection of shallow bias in paleomagnetic inclinations: was the ancient magnetic field dipolar? In: Channell, J.E.T., Kent, D., Lowrie, W., Meert, J.G. (Eds.), Timescales of the Paleomagnetic Field. Geophysical Monograph. AGU, Washington, DC, pp. 101–117.
Teixeira, W., Hamilton, M.A., Girardi, V.A., Faleiros, F.M., Ernst, R.E., 2019. U-Pb baddeleyite ages of key dyke swarms in the Amazonian Craton (Carajás/Rio Maria and Rio Apa areas): tectonic implications for events at 1880, 1110 Ma, 535 Ma and 200 Ma. Precambrian Res. 329, 138–155.
Thorkelson, D.J., Laughton, J.R., 2016. Paleoproterozoic closure of an Australia-Laurentia seaway revealed by megaclasts of an obducted volcanic arc in Yukon, Canada. Gondwana Res. 33, 115–133.
Thorkelson, D.J., Mortensen, J.K., Creaser, R.A., Davidson, G.J., Abbott, J.G., 2001. Early Proterozoic magmatism in Yukon, Canada: constraints on the evolution of northwestern Laurentia. Can. J. Earth Sci. 38 (10), 1479–1494.
Torsvik, T.H., 2019. Earth history: a journey in time and space from base to top. Tectonophysics 760, 297–313.
Torsvik, T.H., Carter, L.M., Ashwal, L.D., Bhushan, S.K., Pandit, M.K., Jamtveit, B., 2001. Rodinia refined or obscured: palaeomagnetism of the Malani Igneous Suite (NW India). Precambrian Res. 108 (3—4), 319–333.
Torsvik, T.H., Müller, R.D., Voo, R.V.D., Steinberger, B., Gaina, C., 2008. Global plate motion frames: toward a unified model. Rev. Geophys. 46 (3), RG3004.
Torsvik, T.H., Steinberger, B., Ashwal, L.D., Doubrovine, P.V., Trønnes, R.G., Polat, A., 2016. Earth evolution and dynamics—a tribute to Kevin Burke. Can. J. Earth Sci. 53 (11), 1073–1087.
Torsvik, T.H., Steinberger, B., Cocks, L.R.M., Burke, K., 2008b. Longitude: linking Earth's ancient surface to its deep interior. Earth Planet. Sci. Lett. 276 (3—4), 273–282.
Torsvik, T.H., van der Voo, R., Doubrovine, P.V., Burke, K., Steinberger, B., Ashwal, L.D., Trønnes, R.G., Webb, S.J., Bull, A.L., 2014. Deep mantle structure as a reference frame for movements in and on the Earth. Proc. Natl. Acad. Sci. 111 (24), 8735–8740.
Torsvik, T.H., Van der Voo, R., Preeden, U., Mac Niocaill, C., Steinberger, B., Doubrovine, P.V., van Hinsbergen, D.J.J., Domeier, M., Gaina, C., Tohver, E., Meert, J.G., McCausland, P.J.A., Cocks, L.R.M., 2012. Phanerozoic polar wander, palaeogeography and dynamics. Earth Sci. Rev. 114 (3—4), 325–368.
Tucker, R.D., Roig, J.Y., Moine, B., Delor, C., Peters, S.G., 2014. A geological synthesis of the Precambrian shield in Madagascar. J. Afr. Earth Sci. 94, 9–30.
Turnbull, R.E., Schwartz, J.J., Fiorentini, M.L., Jongens, R., Evans, N.J., Ludwig, T., McDonald, B.J., Klepeis, K.A., 2021. A hidden Rodinian lithospheric keel beneath Zealandia, Earth's newly recognized continent. Geology 49 (8), 1009–1014.
van der Hilst, R.D., 2004. Changing views on Earth's deep mantle. Science 306 (5697), 817–818.
van der Hilst, R.D., Widiyantoro, S., Engdahl, E.R., 1997. Evidence for deep mantle circulation from global tomography. Nature (London) 386 (6625), 578–584.
Van der Voo, R., 1990. The reliability of paleomagnetic data. Tectonophysics 184 (1), 1–9.
Van der Voo, R., 1994. True polar wander during the middle Paleozoic? Earth PlanetSci. Lett. 122, 239–243.
Verbaas, J., Thorkelson, D.J., Crowley, J., Davis, W.J., Foster, D.A., Gibson, H.D., Marshall, D.D., Milidragovic, D., 2018. A sedimentary overlap assemblage links Australia to northwestern Laurentia at 1.6 Ga. Precambrian Res. 305, 19–39.
Volante, S., Collins, W.J., Pourteau, A., Li, Z.-X., Li, J., Nordsvan, A.R., 2020a. Structural evolution of a 1.6 Ga orogeny related to the final assembly of the supercontinent Nuna. Tectonics 39 (10), e2020TC006162.
Volante, S., Pourteau, A., Collins, W.J., Blereau, E., Li, Z.-X., Smit, M., Evans, N.J., Nordsvan, A.R., Spencer, C.J., McDonald, B.J., Li, J., Günter, C., 2020b. Multiple P-T–d–t paths reveal the evolution of the final Nuna assembly in Northeast Australia. J. Metamorph. Geol. 38 (6), 593–627.
Walderhaug, H.J., Torsvik, T.H., Halvorsen, E., 2007. The Egersund dykes (SW Norway): a robust Early Ediacaran (Vendian) palaeomagnetic pole from Baltica. Geophys. J. Int. 168 (3), 935–948.
Wang, C., Li, Z.-X., Peng, P., Pisarevsky, S., Liu, Y., Kirscher, U., Nordsvan, A., 2019. Long-lived connection between the North China and North Australian cratons in supercontinent Nuna: paleomagnetic and geological constraints. Sci. Bull. 64 (13), 873–876.
Wang, C., Mitchell, R.N., Murphy, J.B., Peng, P., Spencer, C.J., 2021. The role of megacontinents in the supercontinent cycle. Geology 49 (4), 402–406.
Wang, C., Peng, P., Li, Z.-X., Pisarevsky, S., Denyszyn, S., Liu, Y., Gamal El Dien, H., Su, X., 2020a. The 1.24—1.21 Ga Licheng large Igneous Province in the North China Craton: implications for paleogeographic reconstruction. <sb:contribution><sb:title>J. Geophys. Res. Solid</sb:title></sb:contribution><sb:host><sb:issue><sb:series><sb:title>Earth</sb:title></sb:series></sb:issue></sb:host> 125 (4), e2019JB019005.
Wang, J., Li, Z.X., 2003. History of Neoproterozoic rift basins in South China: implications for Rodinia break-up. Precambrian Res. 122 (1—4), 141–158.
Wang, X.-C., Wilde, S.A., Li, Z.-X., Li, S., Li, L., 2020b. Do Supercontinent-superplume cycles control the growth and evolution of continental crust? J. Earth Sci. 31 (6), 1142–1169.
Wang, X.C., Li, X.H., Li, W.X., Li, Z.X., 2007. Ca. 825 Ma komatiitic basalts in South China: first evidence for > 1500 degrees C mantle melts by a Rodinian mantle plume. Geology 35 (12), 1103–1106.
Wen, B., Evans, D.A.D., Li, Y.-X., 2017. Neoproterozoic paleogeography of the Tarim Block: an extended or alternative "missing-link" model for Rodinia? Earth Planet. Sci. Lett. 458, 92–106.
Wen, B., Evans, D.A.D., Wang, C., Li, Y.-X., Jing, X., 2018. A positive test for the Greater Tarim Block at the heart of Rodinia: mega-dextral suturing of supercontinent assembly. Geology 46 (8), 687–690.
Williams, H., Hoffman, P.F., Lewry, J.F., Monger, J.W.H., Rivers, T., 1991. Anatomy of North America: thematic portrayals of the continent. Tectonophysics 187, 117–134.
Williams, S.E., Müller, R.D., Landgrebe, T.C., Whittaker, J.M., 2012. An open-source software environment for visualizing and refining plate tectonic reconstructions using high-resolution geological and geophysical data sets. GSA Today 22 (4/5), 4–9.
Windley, B.F., Kusky, T., Polat, A., 2021. Onset of plate tectonics by the Eoarchean. Precambrian Res. 352, 105980.
Wingate, M.T.D., Giddings, J.W., 2000. Age and palaeomagnetism of the Mundine well dyke swarm, Western Australia: implications for an Australia-Laurentia connection at 755 Ma. Precambrian Res. 100, 335–357.
Wingate, M.T.D., Pirajno, F., Morris, P.A., 2004. Warakurna large igneous province: a new Mesoproterozoic large igneous province in west-Central Australia. Geology 32 (2), 105–108.
Wingate, M.T.D., Pisarevsky, S.A., Evans, D.A.D., 2002. Rodinia connections between Australia and Laurentia: no SWEAT, no AUSWUS? Terra Nova 14 (2), 121–128.

Worsley, T.R., Kidder, D.L., 1991. First-order coupling of paleogeography and Co2, with global surface-temperature and its latitudinal contrast. Geology 19 (12), 1161–1164.
Wu, C., Wang, G., Zhou, Z., Haproff, P.J., Zuza, A.V., Liu, W., 2022. Paleoproterozoic plate tectonics recorded in the Northern Margin Orogen, North China Craton. Geochem. Geophys. Geosyst. 23 (11), e2022GC010662.
Wu, H., 2005. New paleomagnetic results from Mesoproterozoic successions in Jixian area, North China Block, and their implications for paleocontinental reconstructions. PhD Thesi. China University of Geosciences, Beijing, 133pp.
Wu, H., Zhang, S., Li, Z.-X., Li, H., Dong, J., 2005. New paleomagnetic results from the Yangzhuang Formation of the Jixian System, North China, and tectonic implications. Chin. Sci. Bull. 50 (14), 1483–1489.
Wu, L., Murphy, J.B., Quesada, C., Li, Z.-X., Waldron, J.W.F., Williams, S., Pisarevsky, S., Collins, W.J., 2021. The amalgamation of Pangaea: paleomagnetic and geological observations revisited. GSA Bull. 133 (3—4), 625–646.
Xia, B., Zhang, L., Du, Z., Xu, B., 2019. Petrology and age of Precambrian Aksu blueschist, NW China. Precambrian Res. 326, 295–311.
Yao, W., Li, Z.-X., Li, W.-X., Li, X.-H., 2017. Proterozoic tectonics of Hainan Island in supercontinent cycles: new insights from geochronological and isotopic results. Precambrian Res. 290, 86–100.
Yao, W.-H., Li, Z.-X., Li, W.-X., Li, X.-H., Yang, J.-H., 2014. From Rodinia to Gondwanaland: a tale of detrital zircon provenance analyses from the southern Nanhua Basin, South China. Am. J. Sci. 314 (1), 278–313.
Yong, W., Zhang, L., Hall, C.M., Mukasa, S.B., Essene, E.J., 2013. The 40Ar/39Ar and Rb–Sr chronology of the Precambrian Aksu blueschists in western China. J. Asian Earth Sci. 63, 197–205.
Youbi, N., Ernst, R.E., Mitchell, R.N., Boumehdi, M.A., El Moume, W., Lahna, A.A., Bensalah, M.K., Söderlund, U., Doblas, M., Tassinari, C.C.G., 2021. Preliminary Appraisal of a Correlation Between Glaciations and Large Igneous Provinces Over the Past 720 Million Years, Large Igneous Provinces. In: Ernst, R.E., Dickson, A.J., Bekker, A. (Eds.), American Geophysical Union Geophysical Monograph Series, pp. 169–190.
Zahirovic, S., Müller, R.D., Seton, M., Flament, N., 2015. Tectonic speed limits from plate kinematic reconstructions. Earth Planet. Sci. Lett. 418, 40–52.
Zegers, T.E., De, W.M.J., Dann, J., White, S.H., 1998. Vaalbara, Earth's oldest assembled continent? A combined structural. Terra Nova 10 (5), 250–259.
Zhang, N., Zhong, S., 2011. Heat fluxes at the Earth's surface and core-mantle boundary since Pangaea formation and their implications for the geomagnetic superchrons. Earth Planet. Sci. Lett. 306 (3—4), 205–216.
Zhang, N., Zhong, S., Leng, W., Li, Z.-X., 2010. A model for the evolution of the Earth's mantle structure since the Early Paleozoic. J. Geophys.Res.Solid Earth 115 (B6), B06401.
Zhang, S.-H., Ernst, R.E., Yang, Z., Zhou, Z., Pei, J., Zhao, Y., 2022. Spatial distribution of 1.4-1.3 Ga LIPs and carbonatite-related REE deposits: evidence for large-scale continental rifting in the Columbia (Nuna) supercontinent. Earth Planet. Sci. Lett. 597, 117815.
Zhang, S., Evans, D.A.D., Li, H., Wu, H., Jiang, G., Dong, J., Zhao, Q., Raub, T.D., Yang, T., 2013. Palaeomagnetism of the late Cryogenian Nantuo Formation and paleogeographic implications for the South China Block. J. Asian Earth Sci. 72, 164–177.
Zhang, S., Li, Z.-X., Evans, D.A.D., Wu, H., Li, H., Dong, J., 2012a. Pre-Rodinia supercontinent Nuna shaping up: a global synthesis with new paleomagnetic results from North China. Earth Planet. Sci. Lett. 353—354, 145–155.
Zhang, S.-H., Zhao, Y., Li, X.-H., Ernst, R.E., Yang, Z.-Y., 2017. The 1.33—1.30 Ga Yanliao large igneous province in the North China Craton: implications for reconstruction of the Nuna (Columbia) supercontinent, and specifically with the North Australian Craton. Earth Planet. Sci. Lett. 465, 112–125.
Zhang, S.-H., Zhao, Y., Santosh, M., 2012b. Mid-Mesoproterozoic bimodal magmatic rocks in the northern North China Craton: implications for magmatism related to breakup of the Columbia supercontinent. Precambrian Res. 222—223, 339–367.
Zhao, G., Cawood, P.A., Wilde, S.A., Sun, M., 2002. Review of global 2.1-1.8 Ga orogens; implications for a pre-Rodinia supercontinent. Earth Sci. Rev. 59 (1—4), 125–162.
Zhao, J.X., Malcolm, M.T., Korsch, R.J., 1994. Characterisation of a plume-related ~ 800 Ma magmatic event and its implications for basin formation in Central-Southern Australia. Earth Planet. Sci. Lett. 121, 349–367.
Zhong, S., Zhang, N., Li, Z.-X., Roberts, J.H., 2007. Supercontinent cycles, true polar wander, and very long-wavelength mantle convection. Earth Planet. Sci. Lett. 261 (3), 551–564.
Zhou, Z., Chen, P., 1990. Biostratigraphy and Geological Evolution of Tarim. In: Science Press, Beijing, p. 366.
Zhu, Z., Campbell, I.H., Allen, C.M., Brocks, J.J., Chen, B., 2022. The temporal distribution of Earth's supermountains and their potential link to the rise of atmospheric oxygen and biological evolution. Earth Planet. Sci. Lett. 580, 117391.
Zou, H., Li, Q.-L., Bagas, L., Wang, X.-C., Chen, A.-Q., Li, X.-H., 2021. A Neoproterozoic low-δ18O magmatic ring around South China: implications for configuration and breakup of Rodinia supercontinent. Earth Planet. Sci. Lett. 575, 117196.